VYSOKÉ UČENÍ TECHNICKÉ V BRNĚ
BRNO UNIVERSITY OF TECHNOLOGY

FAKULTA STROJNÍHO INŽENÝRSTVÍ
LETECKÝ ÚSTAV

FACULTY OF MECHANICAL ENGINEERING
INSTITUTE OF AEROSPACE ENGINEERING

UNMANNED AERIAL SYSTEM DESIGN COMPETITION

BEZPILOTNÍ SYSTÉM PRO LETECKOU KONSTRUKČNÍ SOUTĚŽ

BAKALÁŘSKÁ PRÁCE
BACHELOR´S THESIS

AUTOR PRÁCE — MATĚJ MALINOWSKI
AUTHOR

VEDOUCÍ PRÁCE — Ing. JAN PEJCHAR
SUPERVISOR

BRNO 2015

Vysoké učení technické v Brně, Fakulta strojního inženýrství

Letecký ústav
Akademický rok: 2014/2015

ZADÁNÍ BAKALÁŘSKÉ PRÁCE

student(ka): Matěj Malinowski

který/která studuje v **bakalářském studijním programu**

obor: **Základy strojního inženýrství (2341R006)**

Ředitel ústavu Vám v souladu se zákonem č.111/1998 o vysokých školách a se Studijním a zkušebním řádem VUT v Brně určuje následující téma bakalářské práce:

Bezpilotní systém pro leteckou konstrukční soutěž

v anglickém jazyce:

Unmanned Aerial System design competition

Stručná charakteristika problematiky úkolu:

Pro zahraniční studentskou soutěž z leteckého prostředí navrhněte bezpilotní letoun splňující předepsané kvalifikační podmínky. Při návrhy zohledněte požadavky na vysoké výkony a manévrovatelnost stroje, schopnost nést platící zatížení a vypouštět další bezpilotní prostředky v definovaném polygonu.

Cíle bakalářské práce:

Předmětem této práce je:
1) vyberat vhodnou studentskou soutež z leteckého prostředí
2) vytvořit přehled koncepcí letounů schopných splnit zadání soutěže
3) vybrat optimální variantu
4) zpracovat její konstrukční návrh s ohledem na dostupné technologie

Seznam odborné literatury:

[1] Jane´s: All the Worldś Aircraft (všech vydání)
[2] Torenbeek, E.: Synthesis of Subsonic Airplane Design, Delft University Pres, 1976
[3] Roskam, J.: Airplane Design (Parts), The University of Kansas, 1989

Vedoucí bakalářské práce: Ing. Jan Pejchar

Termín odevzdání bakalářské práce je stanoven časovým plánem akademického roku 2014/2015.

V Brně, dne 18.11.2014

L.S.

doc. Ing. Jaroslav Juračka, Ph.D. Ředitel ústavu	prof. RNDr. Miroslav Doupovec, CSc., dr. h. c. Děkan fakulty

ABSTRACT

This bachelor thesis deals with a design process of small unmanned aerial vehicle intended for Air Cargo Challenge 2015 competition. The thesis is organized according to the development process. The initial conceptual design is followed by the choice of appropriate shape of the airplane and its airfoils. Calculation of flight performance, maximum takeoff weight and aircraft balance follows. The final part of the thesis describes structure of the aircraft and prediction of the payload dependence on the air density.

KEY WORDS

Unmanned Aerial System, design, competition, Unmanned Aerial Vehicle, aerodynamic, flight performance, payload

ABSTRAKT

Bakalářská práce se zabývá návrhem malého bezpilotního letounu určeného pro soutěž Air Cargo Challenge 2015. Práce je uspořádána dle postupu vývojových prací. Na prvotní koncepční návrh navazuje volba vhodného tvaru letounu a jeho profiláže. Následuje výpočet letových výkonů, maximální vzletové hmotnosti a centráže letounu. Poslední část práce se zabývá konstrukcí letounu a je provedena analýza závislosti užitečného zatížení na hustotě vzduchu.

KLÍČOVÁ SLOVA

bezpilotní letecký systém, návrh, soutěž, bezpilotní letoun, aerodynamický, letové výkony, užitečné zatížení

BIBLIOGRAPHIC CITATION

MALINOWSKI, M. *Unmanned aerial system design competition*. Brno: Brno University of Technology, Faculty of Mechanical Engineering, 2015. 103 p. Supervised by Ing. Jan Pejchar.

STATEMENT OF AUTHENTICITY

I, Matěj Malinowski, hereby declare that I worked out this bachelor's thesis independently under the supervision of this bachelor's thesis supervisor Ing. Jan Pejchar. I also hereby declare that all professional literature and other information sources, which were used during the creation of this thesis, are properly cited and listed in the bibliography.

In Brno:_____ Author's signature:_____

ACKNOWLEDGMENT

At this point, I would like to thank my bachelor's thesis supervisor Ing. Jan Pejchar for his valuable advice during the work at this thesis. I would also like to thank him and other members of Institute of Aerospace Engineering at Faculty of Mechanical Engineering of Brno University of Technology for trusting in me and members of the development team and for the provision of the opportunity to be implemented in the practical project, which brought me a lot of valuable experience.

CONTENTS

1 INTRODUCTION

This bachelor's thesis describes the design process of unmanned aerial vehicle (further stated UAV) newly developed by the students of Faculty of Mechanical Engineering at Brno University of Technology. The student team and UAV will fight for victory in the competition Air Cargo Challenge 2015, which will be held in August in Stuttgart, Germany. Bachelor's thesis describes considerations taken into account during the conceptual design of UAV, aerodynamical design and basic flight performance calculations of UAV, mass and balance analysis, basic structural design and payload prediction in regards to the air density.

A part of the thesis, which describes the first conceptual design, includes arrangement of aerodynamic surfaces, undercarriage type and propulsion system selection. The aerodynamic design part of the thesis consists of the wing and empennage shape and airfoils selection. Next part of this section describes the fuselage shape development and selection, which is followed by the control surfaces design. The final part of aerodynamic design consists of aircraft polar and longitudinal stability calculation. The aerodynamic design is followed by the flight performance calculations. The part describing the flight performance consists of the evaluation of horizontal flight characteristic speeds, climbing capabilities of the aircraft, the calculation of limit turns diagrams and evaluation of takeoff ground roll distance and time. The flight performance evaluation is followed by the mass and balance analysis. That part of thesis stands for description of individual parts masses and their centres of gravity determination. After all individual masses were defined, centre of gravity of the aircraft was calculated. The structural design part describes individual components composition and gives the overview of the aircraft structure as the whole. The final part of the thesis, which is named payload prediction, includes the description of the process, which led to the determination of the payload weight dependence on the air density.

2 ACC COMPETITION

Air Cargo Challenge competition was established in 2003 by the APAE (Portuguese Association of Aeronautics and Space) and was inspired by the North American DBF (design-build-fly) aircraft university competitions. Since then, the competition has been held every two years. Since 2007, many of the European countries have taken part in it. [19]

From the beginning, Air Cargo Challenge was intended to awake a passion for aviation and airplane design among students of technical universities.

2.1 Aim of ACC 2015 competition

The Air Cargo Challenge allows students to get closer to the practical engineering and actively participate in the design process of new unmanned aerial vehicle (further mentioned as UAV). Strict regulations as well as the time deadlines are given and there is also highly competitive environment within teams from all over the world, which participating in the competition.

Air Cargo Challenge 2015 competition aim differs from aim of previous competition years. This time, teams have to design UAV which have to transport maximum payload on the maximum possible distance within given time frame. Last competition year, task was bit of

easier, because there was no distance task. UAV had only to take-off, make a go around and land safely.

- **UAV competition flight mission:**

The flight mission for which was UAV designed is described by the regulations document which was issued by the ACC 2015 organizing committee. The idea of the given competition flight mission profile is evident from the figure 2.1 which is listed below.

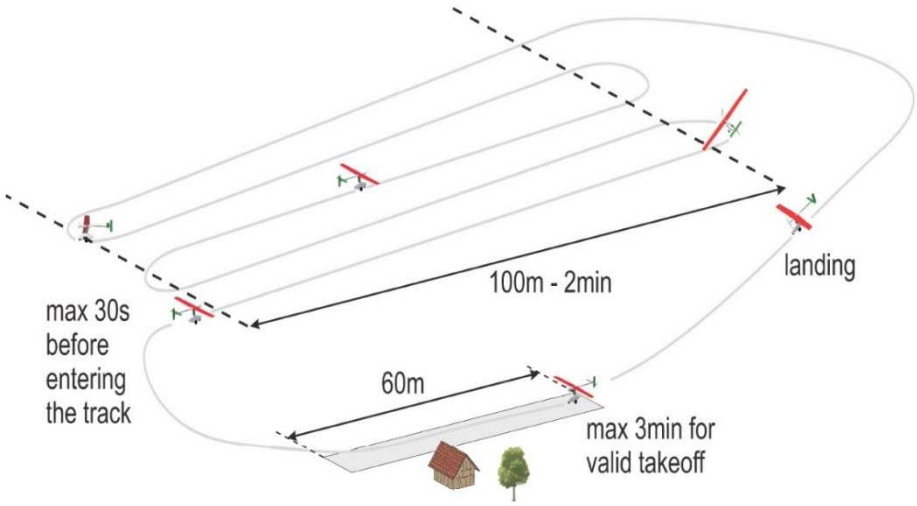

Fig. 2.1 Competition flight mission profile idea [19]

2.2 BUT Chicken Wings university team

In the competition as well as in the practice, it is necessary to create new, highly valuable designs. Because of that, BUT Chicken Wings team was established. The diversity of the individual team members' interests increases the overall ability of the team to design a new competitive UAV. Team members are:

- **Matěj Malinowski - Team leader**

The student of the third year of bachelor's study programme Fundamentals of Mechanical Engineering at the Brno University of Technology. During the design process he focuses on concept creation, aerodynamical design, flight performance calculation, mass and balance calculation, payload prediction, and structural design and cooperates with other team members on particular structural design aspects, marketing and sponsoring tasks.

- **Jan Jílek – Composites specialist**

The student of the third year of bachelor's study programme Fundamentals of Mechanical Engineering at the Brno University of Technology. During the design process he focuses on the challenges associated with the design of UAV composite structures. He also participates in the 3D CAD models creation.

- **Bc. Michal Kubo – Strength calculations**

The student of the first year of master's study programme Aircraft design at Brno University of Technology. He focuses on the strength calculations of the wing, 3D CAD modes creation and conceptual design of selected structural nodes.

- **Ondřej Kövér – Manufacturing specialist**

The student of the third year of bachelor's study programme Fundamentals of Mechanical Engineering at the Brno University of Technology. Because of his experience with the production of Ellipse Spirit aircraft parts, he focuses on the manufacturing process of UAV. This includes the question of moulds creation and selection of its material, and also preparation of moulds for the manufacturing process. He will also participate in the production of UAV individual parts.

- **Ing. Filip Sklenář – Competition pilot**

The student of doctoral study programme Aircraft Design and Air Transportation at the Brno University of Technology. The main task of this team member is piloting of UAV at the competition and preparation for this task.

- **Michaela Hánová – Marketing specialist**

The student of the second year of bachelor's study programme Fundamentals of Mechanical Engineering at the Brno University of Technology. She focuses on the marketing communication with companies which were addressed in context of sponsors finding. She also monitors the technical development of UAV to be capable of effective communication with potential project partners.

3 ACC 2015 TECHNICAL REGULATIONS

Technical requirements for the newly developed UAV are enshrined in the competition regulations. The main technical requirements and limitations, which are set by the ACC organising committee follows. [19]

- **Aircraft configuration:**

Any aircraft configuration is acceptable except rotary wing or lighter than air configuration. Externally assisted take-off is prohibited. It means, that energy needed for take-off must come from propulsion battery pack on-board the UAV. The only acceptable propulsion of UAV is an electric motor, which is described below.

- **Motor:**

AXI Gold 2826/10 electric motor has to be used for the UAV propulsion. Only one engine is allowed for the UAV propulsion. Any type of electronic speed control (ESC) system could be used. Open mounting is recommended for good cooling of engine.

- **Batteries:**

Any type of Lithium based battery (LiPo, LiFe, LiIon) is allowed. Batteries with up to 3 cells in series could be used. The product of maximum continuous discharge rate times the capacity has to be at least 45A. The main battery parameters, which are voltage, capacity and maximal charge and discharge rate have to be identified on the battery.

- **Propeller:**

There is a possibility to use many different types of devices generating thrust. Shrouded propellers, multiple and single propeller and ducted fans are allowed. However, if the propeller

is used, the only allowed type is APC 13x7 inches Sport propeller (manufacturer Product Code LP 13070). The propeller must be properly secured using a spinner or security screw.

- **Transmission:**

Types of allowed transmissions are transmission gears, chains or propeller shafts, but only if the rotation ratio between the propeller and motor remains 1:1.

- **Aircraft dimensions:**

Aircraft dimensions are restricted so that the assembled plane has to fit in square of 2,5 m edge while standing on its landing gear.

- **Cargo bay:**

The cargo bay, which is intended for the payload placement has to have minimal internal dimensions of 160 x 80 x 80 mm (Fig. 3.1).

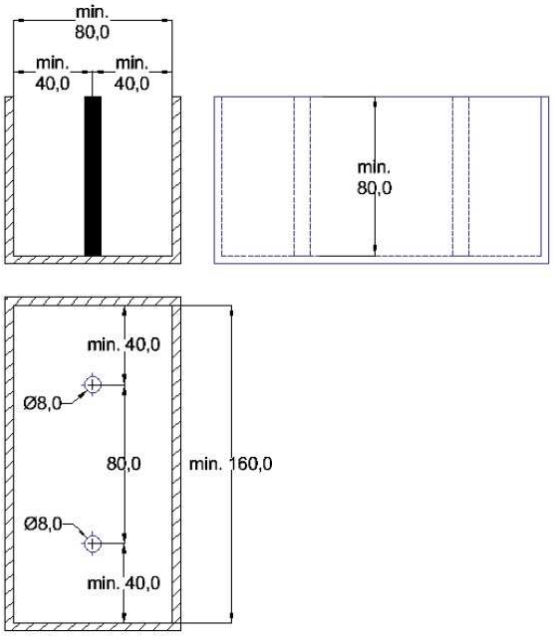

Fig. 3.1 Minimal internal dimensions of the cargo bay [19]

However, the internal dimensions may be larger for making sure, that the foam control box, which will be used during dimensional inspection will fit into the cargo bay. The cargo bay has to contain a payload mounting.

- **Payload:**

The payload, which will be consisted of an amount of steel plates (Fig. 3.2), must be secured against the movement under normal loads (taxiing, flight, and landing). The payload may be carried inside or outside the plane. Payload mustn't affect the structural stability of the UAV. It mustn't have much influence on the UAV centre of gravity position.

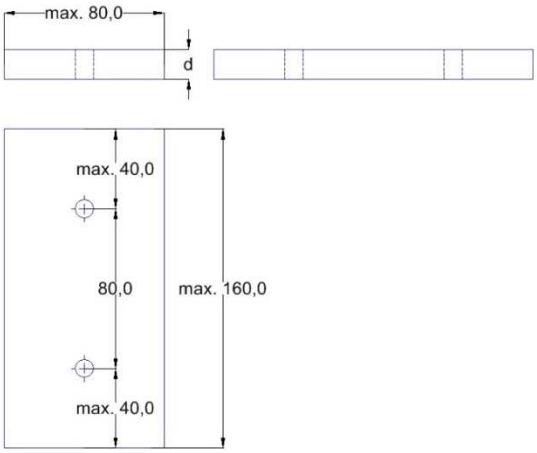

Fig. 3.2 Payload in form of steel plate [19]

- **Transportation box:**

All teams have to use a transportation box for transports of UAV. Minimal internal dimensions could be seen in figure 3.3.

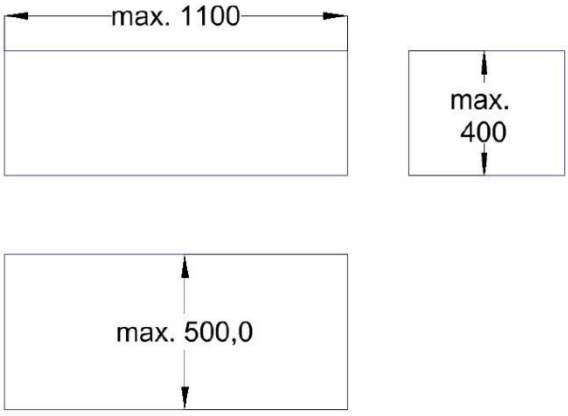

Fig. 3.3 UAV mandatory transportation box [19]

All structural parts of UAV and its electronics (wing, tail, fuselage, landing gear, electric motor, propeller, batteries …) have to fit into a transportation box at one time.

- **Aircraft identification:**

The aircraft must have unique identification symbols, which should be team number and name of the university. Logos of sponsors are allowed, too. Wings and the fuselage of the aircraft have to be identified by the team number written in clear figures of at least 10 cm height. The team number must be clearly visible at least on top and bottom of each wing half and on both fuselage sides. University name (if applicable) should be placed on the fuselage or the wing in clearly readable form. Initials of the university should be used, if they are unique and recognizable.

- **Radio requirements and control system:**

It is highly recommended to use 2,4 GHz radio control system. An independent battery pack for RX is mandatory. It has to have a minimum capacity of 600 mAh. Competition flight will be performed independently on weather conditions, thus electronic equipment have to be placed

taking this fact into account. Servos have to withstand aerodynamical loads, which could occurs. The usage of autopilot or control assistance systems (gyroscope, any artificial stabilizing systems) is strongly prohibited. Mixing abilities may be used. However, no input of sensors into aircraft control is allowed. Sensors for monitoring of such parameters as controlling voltage of RX battery, battery temperature, temperature of electric motor etc. are allowed.

4 CONCEPT OF NEW UAV

The conception of UAV comes from the Air Cargo Challenge 2015 competition flight mission. First prerequisite for success in the competition is creation of concept of a plane with relatively high maximum take-off weight and rigid construction, which can withstand high loads during fast flight in turns and which has also good potential to resist to aeroelastic phenomena.

- **Relative position of wing and fuselage:**

There were three possible options of the wing – fuselage configuration. Namely a high wing, mid wing and low wing configuration (Fig. 4.1). Advantages and disadvantages of each configuration are mentioned in the table 4.1 below.

Configuration	High wing	Mid wing	Low wing
Advantages	High maximum lift coefficient $C_{Lmax.}$	Low interference drag between fuselage and wing and maneuverability.	Low weight of landing gear and good load transfer through aircraft structure.
Disadvantages	Higher landing gear weight when attached to the wing.	Wing goes through fuselage, which limits the payload placement.	High interference drag without proper aerodynamic filets.

Tab. 4.1 Advantages and disadvantages of a different wing to fuselage relative positions

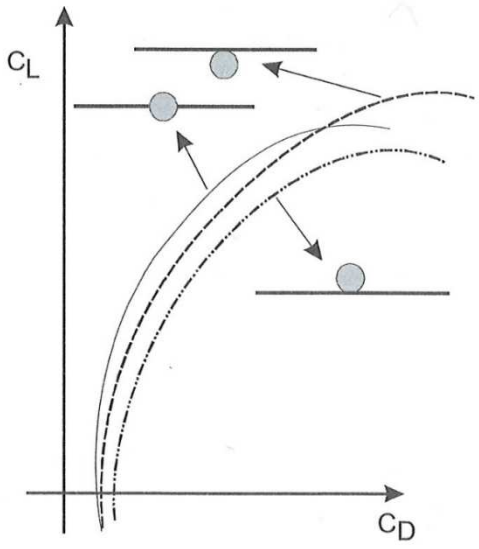

Fig. 4.1 Wing to fuselage relative position [5]

Finally the low wing configuration was chosen. The main reason for this choice was technological requirements and best load transfer through the important design nodes.

- **Relative position of wing and horizontal tail:**

The horizontal tail relative position against the wing was chosen as the conventional conception. It means horizontal stabiliser and elevator is positioned behind the wing of UAV (Fig. 4.2).

Fig. 4.2 Relative position of horizontal tail and wing [18]

- **Relative position of horizontal and vertical tail:**

The relative position of horizontal and vertical tail, which was chosen, could be seen in the figure 4.3, letter *a* below. This configuration provides relatively small vertical stabiliser and rudder area shaded by the elevator wake during the flight near the stall.

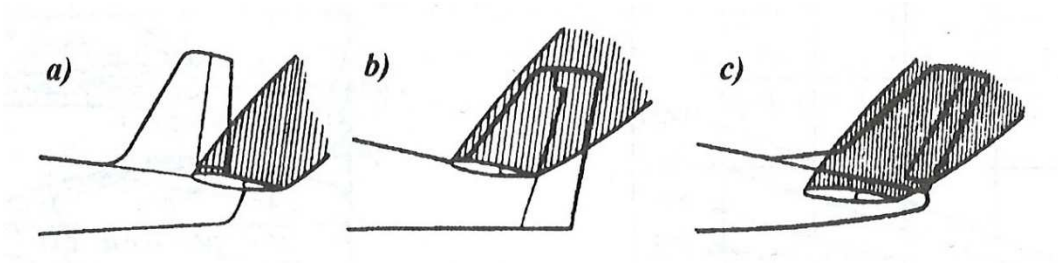

Fig. 4.3 Relative position of horizontal and vertical tail [7]

- **Landing gear:**

The conventional landing gear type (Fig. 4.4), which is non retractable was chosen. The main landing gear utilizes solid spring type of shock absorber. The tail landing gear will utilize tailskid. The table of advantages and disadvantages of landing gear configuration follows.

Configuration	Non retractable tail wheel type landing gear with solid spring shock absorber
Advantages	Low weight, simplicity, reliability, taxi and landing load distribution directly to the main wing spar (landing gear attachment point).
Disadvantages	Higher aerodynamic drag than retractable landing gear.

Tab. 4.2 Advantages and disadvantages of chosen landing gear

Fig. 4.4 Landing gear type [14]

- **Propulsion system:**

AXI 2826/10 brushless electric motor (Fig. 4.5) has to be used by all teams participating in the competition. Beyond the regulations it is possible to use optional radial mount for this type of engine. This mount consists of a mounting flange, propeller adaptor, securing collar and additional screws [17]. AXI 2826/10 electric motor characteristics are available in appendix A.1, Fig. A1.1.

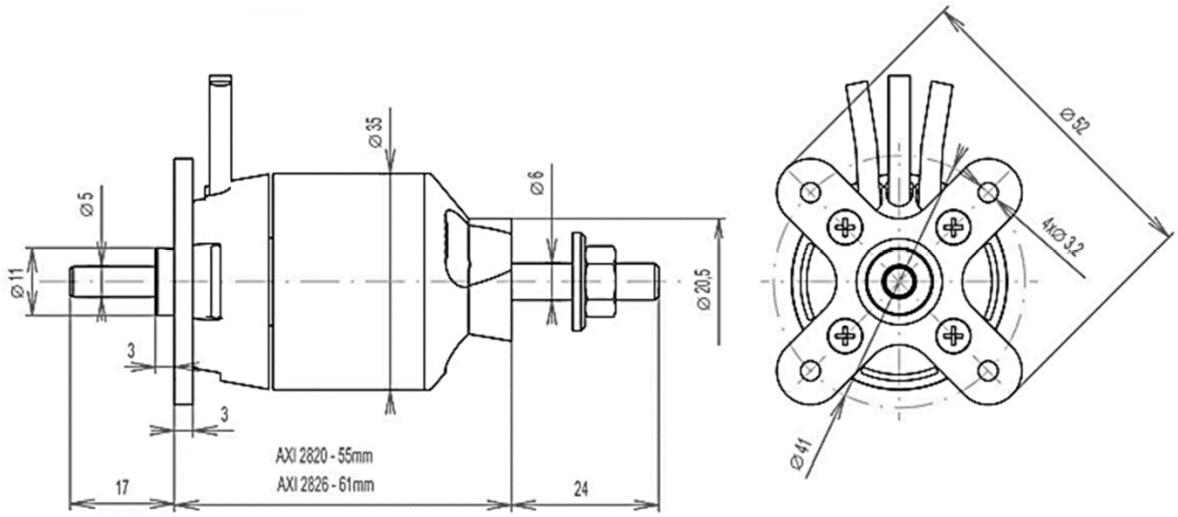

Fig. 4.5 AXI 2826/10 motor drawing [17]

The mandatory type of propeller is APC 13x7 inches Sport propeller. The main reason for usage of the same propeller for all UAVs involved in the competition is to achieve comparable propulsion system characteristics for all teams.

- **Primary structure composition:**

Primary structure of aircraft is going to be made mainly of composite materials.

Part	Part description
Wing covering	Carbon and glass fibre reinforced composite sandwich with core made of Rohacell
Wing spar web	Carbon fibre reinforced composite sandwich with core made of Rohacell
Wing spar flanges	Thicker carbon fabric reinforced composite
Empennage	Composition same as in the case of the wing
Fuselage	Thin carbon and glass reinforced composite shell

Tab. 4.3 Primary structure composition

Detailed structure composition is described in chapter 8.

5 AERODYNAMIC DESIGN

The main objective of this chapter is to define the aerodynamic shape of the UAV, its rough aerodynamic polar and to calculate the longitudinal stability.

5.1 Expected properties of environment

An important difference in the aerodynamic process compared to the classical approach lies in the calculation for the environment expected at the competition area. This approach was chosen because the aircraft is designed especially for the competition and there is an effort to achieve maximum possible performance even under the worst possible conditions. Expected properties of the air were based on the historical data of the ambient air temperature and pressure at the Stuttgart airport (ICAO code EDDS) area in the last five years (2010 – 2014) in the August.

Period	Maximum air temperature [˚C]	Minimum sea level air pressure [hPa]
1.7.2010 – 31.8.2010	34	1006
1.7.2011 – 31.8.2011	34	1003
1.7.2012 – 31.8.2012	35	1004
1.7.2013 – 31.8.2013	34	1005
1.7.2014 – 31.8.2014	33	1005

Tab. 5.1 Air properties extremes at EDDS [23]

The worst expected conditions could occur when the maximum temperature and minimum possible air pressure combines, which led to the thinnest air and lower thrust generated by the propulsion system compared to the ideal international standard atmosphere. The calculation of air properties in table 5.3 was done with following input parameters.

Property of air	Designation	Value	Unit
Air temperature	T	308,15	K
Air pressure	p	100 000	Pa
Specific gas constant	r	287,06	$J \cdot kg^{-1} \cdot K^{-1}$
Reference dynamic viscosity	μ_0	$1{,}716 \cdot 10^{-5}$	Pa·s
Reference temperature	T_0	273,15	K
Sutherland's constant [1]	T_S	110,4	K
Heat capacity ratio	κ	1,4	-

Tab. 5.2 Input parameters for calculation of air properties

The formulas for calculation of air density:

$$p \cdot V = m \cdot r \cdot T \tag{5.1}$$

$$\rho = \frac{p}{r \cdot T} \tag{5.2}$$

Dynamic viscosity of air was calculated using Sutherland's law:

$$\mu = \mu_0 \cdot \left(\frac{T}{T_0}\right)^{3/2} \cdot \frac{T_0 + T_S}{T + T_S} \tag{5.3}$$ [1]

The formula for calculation of air kinematic viscosity:

$$\nu = \frac{\mu}{\rho} \tag{5.4}$$ [1]

The formula for calculation of speed of sound:

$$a = \sqrt{\kappa \cdot r \cdot T} \tag{5.5}$$ [1]

Property of air	Designation	Value	Unit
Density	ρ	1,130	$kg \cdot m^{-3}$
Dynamic viscosity	μ	$1{,}88431 \cdot 10^{-5}$	Pa·s
Kinematic viscosity	ν	$1{,}66705 \cdot 10^{-5}$	$m^2 \cdot s^{-1}$
Speed of sound	a	351,910	$m \cdot s^{-1}$

Tab. 5.3 Calculated air properties

5.2 Wing aerodynamic design

The main objective of wing aerodynamic design is the definition of the airfoils, and of the wing geometry. Preliminary planform of the wing could be seen in the figure 5.1 below. First conceptual sketch of FabricK UAV could be seen in the appendix A.1, figure A1.2.

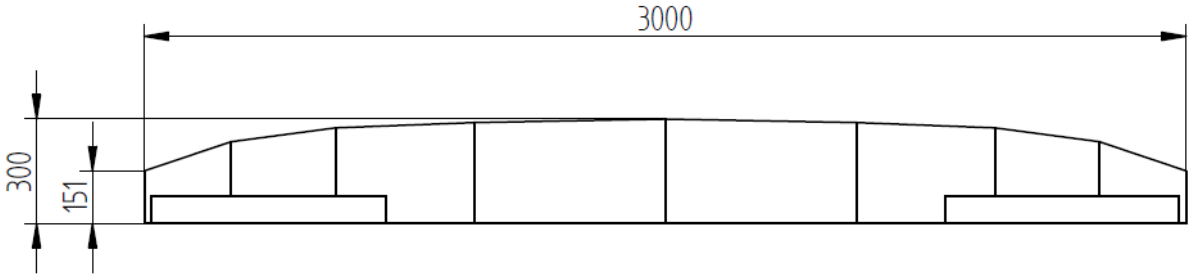

Fig. 5.1 Preliminary planform of the wing

- **Airfoil selection:**

Requirements of airfoil properties was a low drag coefficient, high maximum lift coefficient, sufficient airfoil thickness (strength requirements) and good airfoil characteristics during the stall. CAL 1215j, S1210 and SD7062 airfoils was considered. SD7062 was chosen from the remaining two airfoils (Fig. 5.2) because of its high maximal lift coefficient C_{Lmax} and low drag at low lift coefficient area in the polar graphs compared to S1210 (Fig. 5.3).

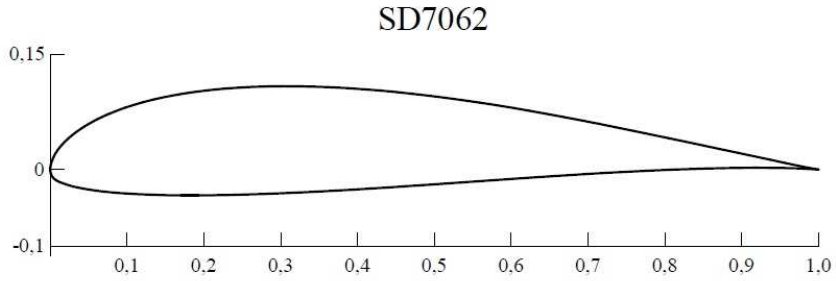

Fig. 5.2 SD 7062 Airfoil

Property	Value [%]	Location at chord [%]
Maximum thickness	14	25,5
Maximum chamber	3,5	38,8

Tab. 5.4 SD 7062 airfoil geometrical characteristics

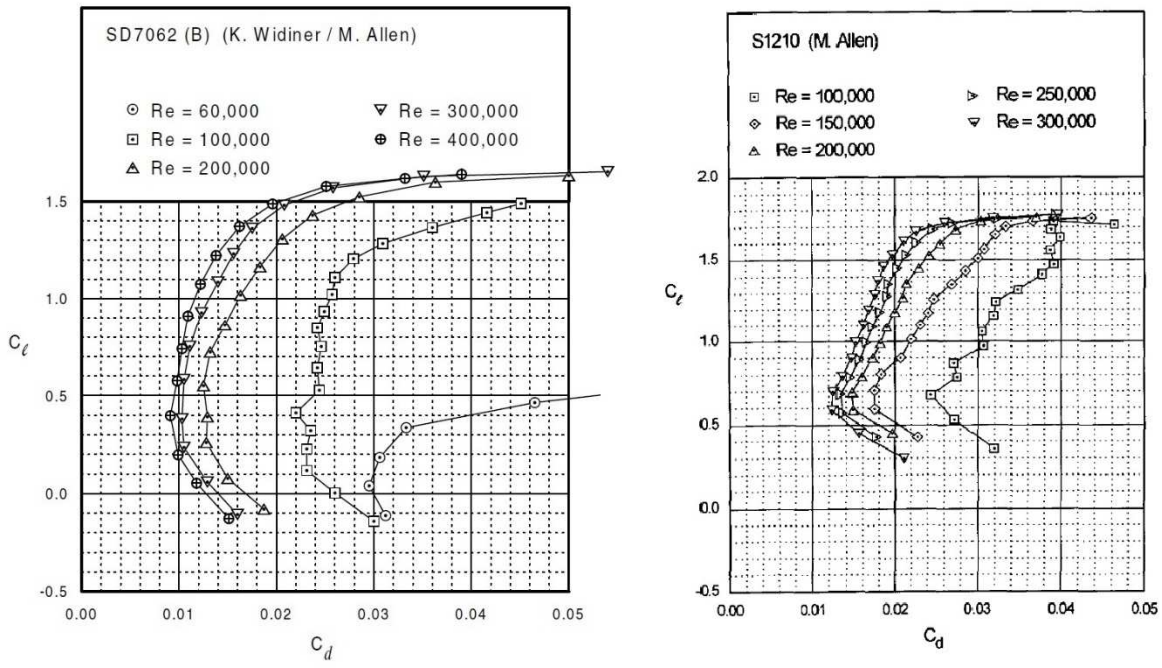

Fig. 5.3 Comparison of SD7062 and S1210 aerodynamic polars [6], [8]

SD7062 airfoil was simulated in XFLR5 aerodynamic simulation software. Polar and lift curves were created for Reynolds numbers from 10 000 to 1 000 000 that means for airfoil chord 300 mm speed range of 0,556 to 55,567 m/s. The angle of attack range was defined from -20 to 20 degrees. Aerodynamic polars and lift curves could be seen in figures 5.4 and 5.5. For clear arrangement polar and lift curves are not displayed for all simulated Reynolds numbers. Obtained data was used for further simulation of UAV wing.

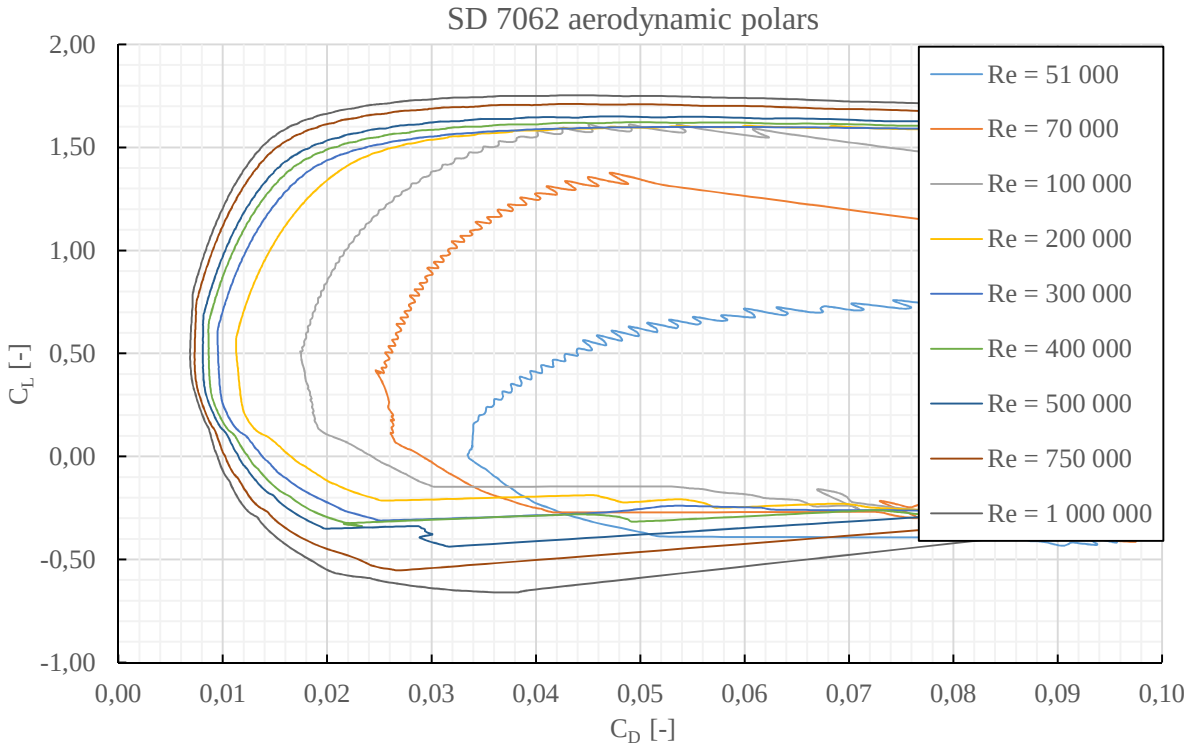

Fig. 5.4 SD7062 aerodynamic polars (XFLR 5)

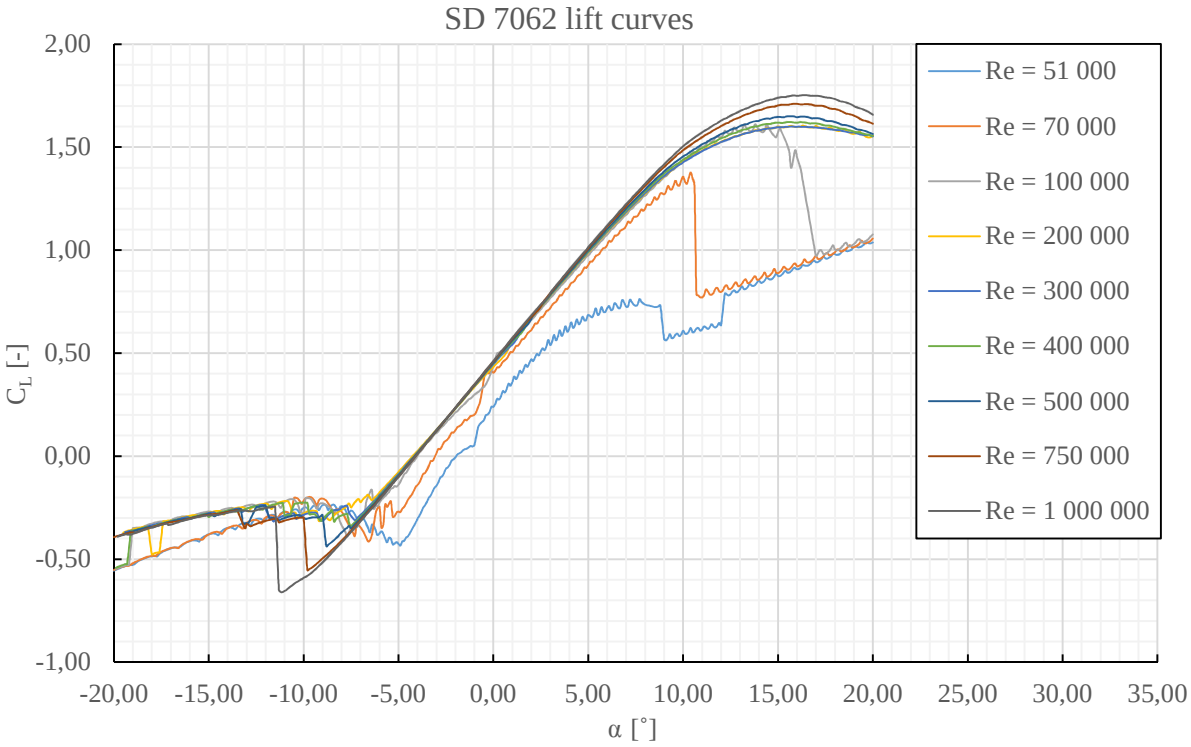

Fig. 5.5 SD7062 lift curves (XFLR 5)

- **Maximum wing lift coefficient estimation:**

The maximum wing lift coefficient was obtained by lowering of airfoil maximum lift coefficient at Reynolds number of 225 000, which is Reynolds number of root airfoil and free stream velocity of 12,5 m/s. Maximum airfoil lift coefficient at this Reynolds number is 1,6. For calculation of wing area, maximum lift coefficient of wing was considered to be 1,55.

$$C_{Lmax} = 1{,}55$$

- **Maximum takeoff weight determination:**

The maximum takeoff weight was estimated taking into account the weight of radio controlled aircraft models (Tab. 5.5) similar to the aircraft, which has to be designed. Next factor taken into account was the maximum payload weight of airplanes of ACC competition in year 2013 (Tab. 5.6).

Aircraft	Wingspan [m]	Weight [kg]
ASW 28 GFK [21]	4,090	4,000
Moswey 4 [16]	3,900	5,000
Duo Discuss GFK [22]	3,070	3,000
DG 303 GFK [22]	3,300	3,750
DG 600 GFK [22]	3,200	1,600
ASW 28 GFK [22]	3,000	2,500

Tab. 5.5 Composite radio controlled models weights

Team	Predicted payload [kg]	Actual payload [kg]
AKAModell Stuttgart e.V.	12,840	12,050
Tsinghua University	10,840	12,070
Beihang Aeromodelling Team 1	10,200	10,000
HUSZ Vulture	13,100	9,040
Beihang Aeromodelling Team 2	10,200	8,000
High Flyers	13,020	8,020

Tab. 5.6 ACC 2013 aircrafts predicted and actual payload [12]

Taking into account the change of flight mission compared to the year 2013, which is now more focused on the speed of aircraft, maximum takeoff weight was estimated to be between weights of classical radio controlled model and payload weight of ACC 2013 aircrafts. Whereas the new aircraft is considered not to utilize high lifting devices on the wing (flaps), the conservative approach was chosen and maximum takeoff weight was in the first estimation defined to be following.

$$m_{MTOW} = 9{,}5\ kg$$

- **Maximum lift-off speed determination:**

Maximum lift-off speed V_{LOF} desired was defined to be:

$$V_{LOF} = 12{,}5\ m/s$$

In the initial phase of design, this speed was estimated as input parameter for further calculations. Lift-off speed and stall speed are in relation defined by the following equation.

$$V_{LOF} = 1{,}15 \cdot V_S \tag{5.6}$$

Usually, the lift-off speed is defined to be 1,1 times stall speed. [2]

Above mentioned modification was made to rise the takeoff speed as all simulations made in XFLR5 could be affected by some simulation errors. Rising of lift-off speed reducing the risk of stall during takeoff.

- **Wing area determination:**

UAV wing area calculation is performed for take-off parameters in the moment of lift-off when UAV weight is just balanced by the wing lift. The initial proposal of wing area calculation is based on basic equation for wing lift calculation.

$$L = \frac{1}{2} \cdot \rho \cdot V^2 \cdot S \cdot C_L \tag{5.7}$$

Where for wing area calculation:

$$V = V_S = \frac{V_{LOF}}{1{,}15} \tag{5.8}$$

$$S = S_W \tag{5.9}$$

$$C_L = C_{Lmax} \tag{5.10}$$

$$L = m_{MTOW} \cdot g \tag{5.11}$$

After substitution to the equation 5.7:

$$m_{MTOW} \cdot g = \frac{1}{2} \cdot \rho \cdot \left(\frac{V_{LOF}}{1{,}15}\right)^2 \cdot S_W \cdot C_{Lmax} \tag{5.12}$$

Wing area S_W expression from equation 5.12:

$$S_W = \frac{1{,}15^2 \cdot 2 \cdot m_{MTOW} \cdot g}{\rho \cdot {V_{LOF}}^2 \cdot C_{Lmax}} \tag{5.13}$$

And finally after input parameters were substituted in equation 5.13 wing area S_W was calculated to be:

$$S_W = 0{,}9\ m^2$$

- **Wing geometry:**

Aspect ratio of the wing could be calculated using the equation 5.14 below.

$$AR = \frac{{l_W}^2}{S_W} \tag{5.14}$$ [5]

Maximum wingspan of competition UAV is limited by the square of 2,5 m x 2,5 m dimension. It means, that maximal theoretical wingspan is:

$$l_{Wmt} = \sqrt{2{,}5^2 + 2{,}5^2} = 3{,}5\ m \tag{5.15}$$

After consideration, that wing tip chord is not zero, maximum wingspan was chosen to be 3m with possibility to increase wingspan by the wingtip extensions intended for induced drag reduction.

$$l_W = 3\ m$$

After substitution into equation 5.14:

$$AR = 10$$

Next important parameter, which has to be chosen is wing dihedral angle. This angle is positive in case when wing tips are directed upwards (Fig. 5.6).

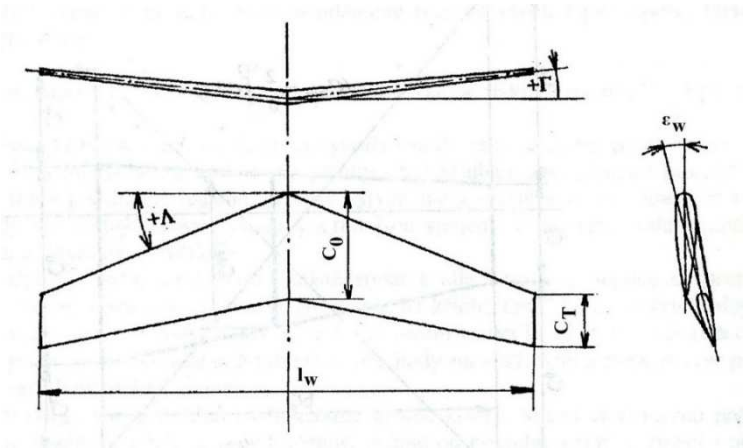

Fig. 5.6 Wing geometry description [1]

Dihedral angle is important in matter of the lateral static stability of the UAV. Usually, positive dihedral angle is chosen in case of low wing planes, because it would provide natural transversal stability of the aircraft and no artificial stabilisation system is required.

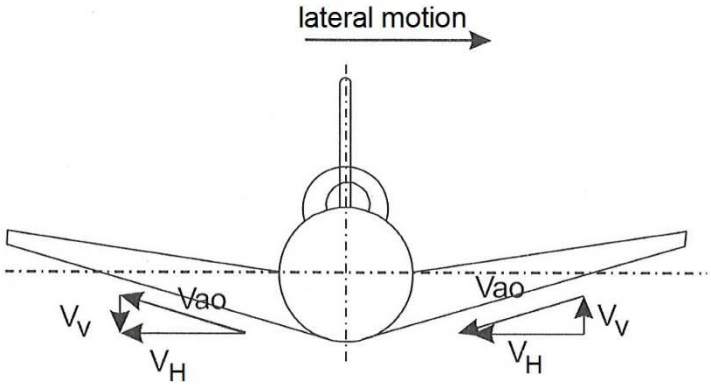

Fig. 5.7 Lateral stability principle [5]

When the sideslip of the aircraft occurs (Fig. 5.7), the lift on the forward wing (in direction of sideslip) increases while lift on the opposite wing decreases. This phenomenon causes stabilising banking torque, which has tendency to lower the bank angle of the aircraft and thus the sideslip.

In case of the newly designed competition UAV, the dihedral angle was chosen to be positive with value of 5 degrees.

$$\Gamma = 5°$$

- **Wing planform geometry:**

Firstly the multi segmented trapezoidal wing design was considered, but further in the design process, in regards to the manufacturing technology chosen, semi-elliptical wing planform was chosen. The wing planform can be seen in the figure 5.8 below.

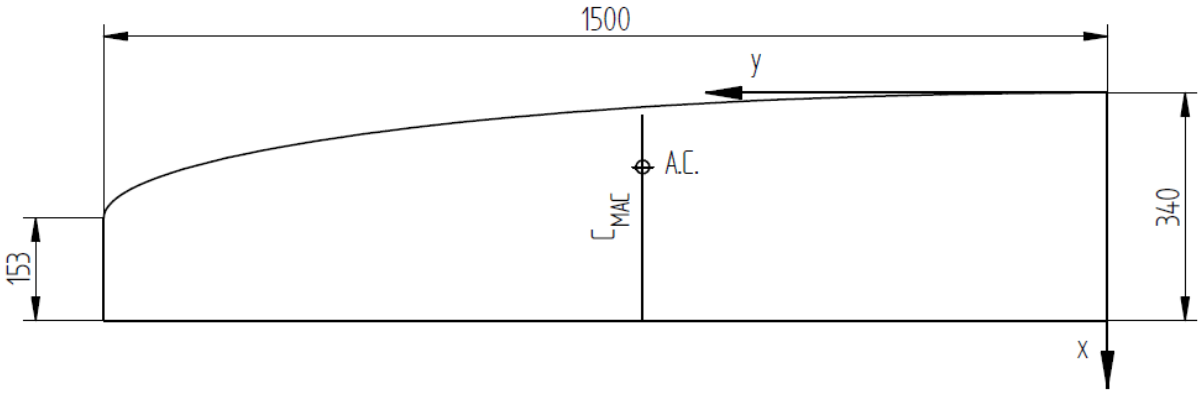

Fig. 5.8 Wing planform

The aspect ratio of the wing, which was calculated in the chapter before has to be recalculated, because wing area S_W in not exactly 0,9 m^2, but a bit smaller. New wing area S_W has value of 0,89961 m^2.

$$AR = 10{,}004$$

There is also little increase in the lift-off speed V_{LOF}. The calculation was performed using equation 6.7.

$$V_{LOF} = 12{,}506\ m/s$$

Because of safety, wing was finally geometrical twisted. Twisting starts at the y coordinate 500 mm, measured from the longitudinal axis of UAV and ends at the y coordinate 1500 mm, which is wing tip. The wing tip airfoil is twisted to minus three degrees relative to the airfoil located at the y coordinate 500 mm.

$$\varepsilon_w = -3^{\circ}$$

- **Mean aerodynamic chord calculation:**

The mean aerodynamic chord (further stated as MAC) is defined as a chord value for the equivalent rectangular wing planform [13]. The position of the MAC in matter of wingspan and its longitudinal position is important. Equations for calculation of these parameters [19]:

$$c_{MAC} = \frac{2}{S}\int_0^{l_W/2} c^2(y)\ dy \qquad \text{[20] (5.16)}$$

$$x_{MAC} = \frac{2}{S}\int_0^{l_W/2} c(y)\cdot x(y)\ dy \qquad \text{[20] (5.17)}$$

$$y_{MAC} = \frac{2}{S}\int_0^{l_W/2} c(y)\cdot y\ dy \qquad \text{[20] (5.18)}$$

For calculation of above mentioned parameters, equation of chord value dependence on the spanwise position y (eq. 5.19) is needed same as dependence of the leading edge x coordinate on the y position (eq. 5.20).

$$c(y) = \sqrt{\frac{a^2\cdot b^2 - y^2\cdot b^2}{a^2}} + k \qquad (5.19)$$

$$x(y) = b - \sqrt{\frac{a^2\cdot b^2 - y^2\cdot b^2}{a^2}} \qquad (5.20)$$

Explanation of unknowns in equations 5.19 and 5.20:

Unknown explanation	Designation	Value	Unit
Half of wing span	a	1,500	m
Wing root minus wing tip chord	b	0,187	m
Wing tip chord value	k	0,153	m
Spanwise position	y	-	m

Tab. 5.7 Mean aerodynamic chord calculation unknowns

After integration of above mentioned equations (5.16 – 5.18) final value of c_{MAC}, x_{MAC} and y_{MAC} was found.

$$c_{MAC} = 305{,}680\ mm$$
$$x_{MAC} = 34{,}321\ mm$$
$$y_{MAC} = 694{,}469\ mm$$

- **Summary information on the wing geometry:**

The table, which contains summary information of the wing design parameters, is shown below.

Parameter	Designation	Value	Unit
Area	S_W	0,89961	m^2
Wingspan	l_W	3000	mm
Aspect ratio	AR_W	10,004	-
Root chord	c_{0W}	340	mm
Tip chord	c_{TW}	153	mm
Dihedral angle	Γ_W	5	°
Washout angle	ε_w	3	°
Mean aerodynamic chord	c_{MAC}	305,680	mm

Tab. 5.8 Design parameters of wing

5.3 Empennage aerodynamic design

The empennage is mainly intended for the stabilisation of the UAV in flight and for providing of good maneuverability. The main source for the design of the empennage of the UAV is statistical values obtained and verified by the operation of the aircrafts already in use.

- **Horizontal and vertical tailplane airfoil selection:**

Airfoil selection for UAV tailplane was reduced to the symmetrical airfoils. The decision was between two NACA symmetrical airfoils. Namely between NACA 0010 and NACA 0012 airfoils. After pros and cons considerations were done it was decided to use NACA 0010 airfoil (Fig. 5.9).

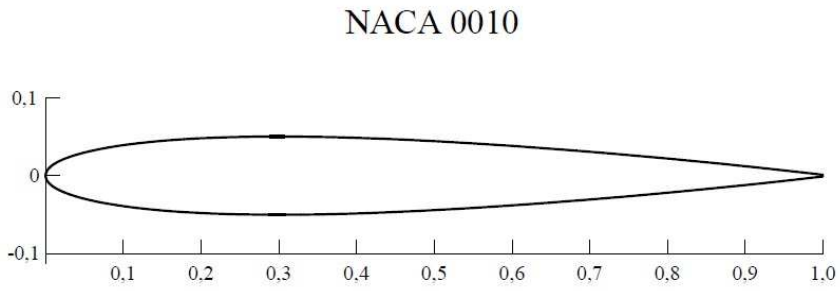

Fig. 5.9 NACA 0010 Airfoil

The main reason for choosing of NACA 0010 is its lower drag coefficient in comparison to the NACA 0012. Lower drag coefficient is consequence of thinner airfoil (10% compared to 12%). However thinner NACA 0010 airfoil has lower construction height.

- **Horizontal tail plane aerodynamic design:**

Most design parameters of horizontal tailplane is defined by the statistical data of the similar type of the aircraft. For the new UAV design, statistical data was taken from literature, which focuses on the design of full scale airplanes. Statistical data is available in the table 5.9 below.

Parameter	Designation	Range	Unit
Relative area	$\overline{S_H} = S_H/S_W$	0,22±0,044	1
Aspect ratio	AR_H	4,5±0,74	1
Dihedral angle	Γ_H	0	°
Root airfoil thickness	$\overline{b_{0H}}$	12-15	%
Tip airfoil thickness	$\overline{b_{TH}}$	10	%
Horizontal tail volume	A_H	0,68±0,23	1

Tab. 5.9 Horizontal tailplane design parameters statistical data [7]

After a few design iterations, the horizontal tailplane geometry was defined, which results in its following parameters.

Parameter	Designation	Value	Unit
Area	S_H	0,16611	m^2
Span	l_H	850	mm
Aspect ratio	AR_H	4,34962	-
Root chord	c_{0H}	226	mm
Tip chord	c_{TH}	83,5	mm
Dihedral angle	Γ_H	0	°

Tab. 5.10 Design parameters of horizontal tailplane

Horizontal tailplane planform can be seen at the figure 5.10 below.

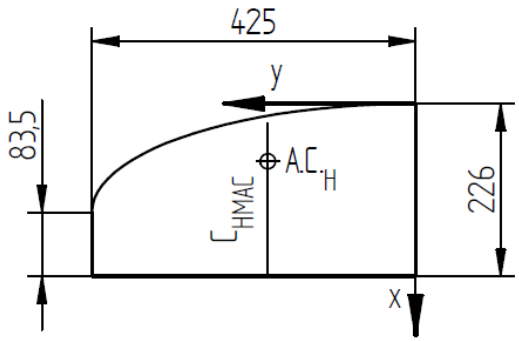

Fig 5.10 Horizontal tailplane planform

The next important step is to define horizontal tailplane arm. The horizontal tailplane arm is the length value measured between quarter point of a wing and horizontal tail MAC projected to the planform of the UAV (Fig. 5.11).

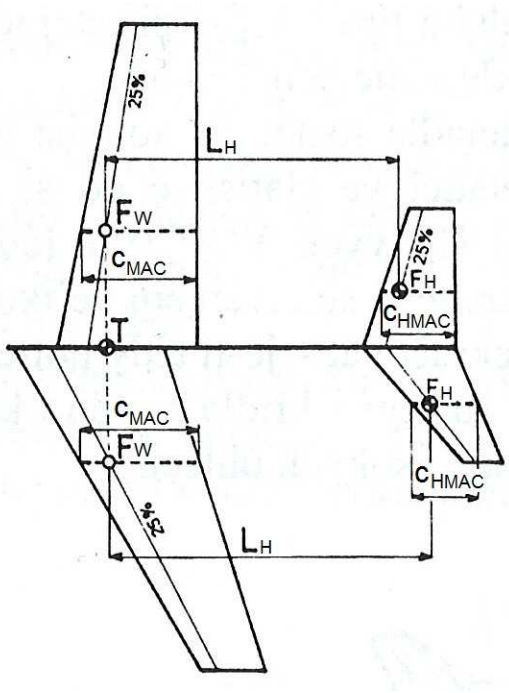

Fig. 5.11 Horizontal tailplane arm definition [7]

Due to the limited length of the UAV, which is given by the 2,5m x 2,5m square mentioned in the section 6.1, arm of the horizontal tailplane was finally defined to be 1,175 m.

$$L_H = 1{,}175\ m$$

The result of the equation for calculation of horizontal tailplane volume, which is in the following form, has to be within desired limits mentioned in the table 5.8.

$$A_H = \frac{S_H \cdot L_H}{S_W \cdot c_{MAC}} \qquad [7]\ (5.21)$$

And finally after substitution.

$$A_H = 0{,}70976$$

This value of horizontal tailplane volume is within desired limits. After the volume calculation, it was important to calculate horizontal tailplane MAC and position of the MAC in the longitudinal direction and its position in the span direction. After integration of the equations 5.16 to 5.18 with substituting of unknowns by the values of the horizontal tailplane, results are following.

$$c_{HMAC} = 200{,}596\ mm$$
$$x_{HMAC} = 25{,}404\ mm$$
$$y_{HMAC} = 194{,}102\ mm$$

- **Vertical tailplane aerodynamic design:**

Design parameters of vertical tailplane is also defined by the statistical data.

Parameter	Designation	Range	Unit
Relative area	$\overline{S_V} = S_V/S_W$	0,170±0,04	1
Aspect ratio	AR_V	1,33±0,27	1
MAC airfoil thickness	$\overline{b_{H_{MAC}}}$	10,5±2,2	%
Vertical tail volume	A_V	0,0686±0,016	1

Tab. 5.11 Vertical tailplane design parameters statistical data [7]

After a few design iterations, vertical tailplane geometry was defined, which results in its following parameters.

Parameter	Designation	Value	Unit
Area	S_V	0,10066	m^2
Span	l_V	400	mm
Aspect ratio	AR_V	1,58951	-
Root chord	c_{0V}	289	mm
Tip chord	c_{TV}	115	mm

Tab. 5.12 Design parameters of vertical tailplane

The planform of the vertical tailplane is similar to that of the horizontal tailplane. However, there is one difference in the geometry of the leading and trailing edge. Trailing edge of the vertical tailplane is deflected 8 degrees back and leading edge points are also deflected backwards.

Vertical tailplane planform can be seen at the figure 5.12.

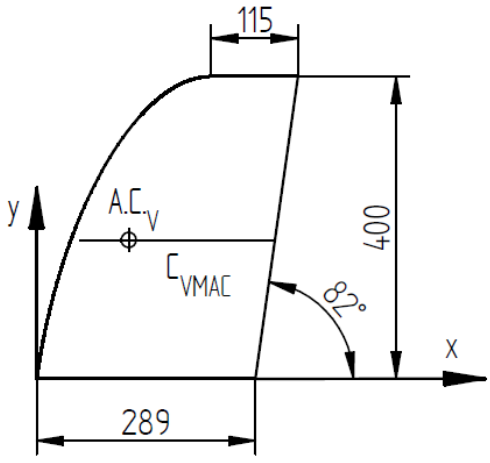

Fig. 5.12 Vertical tailplane planform

The vertical tailplane arm is the length value measured between quarter point of wing and vertical tail MAC projected to the planform of the UAV (Fig. 5.13).

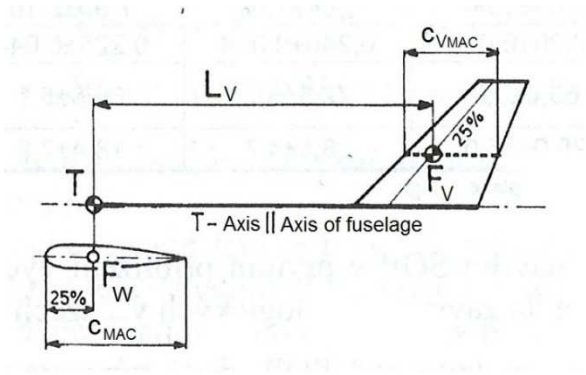

Fig. 5.13 Vertical tailplane arm definition [7]

Because of the desired offset of the horizontal tailplane against vertical one, the arm of the vertical tailplane was finally defined to be 1,100 m.

$$L_V = 1{,}100\ m$$

The equation for calculation of vertical tail volume is very similar to equation 5.21.

$$A_V = \frac{S_V \cdot L_V}{S_W \cdot l_W} \qquad \text{[7] (5.22)}$$

And finally after substitution.

$$A_V = 0{,}04103$$

The value of the vertical tail volume isn't within limits mentioned in table 5.10. However, this value is within limits given by another source. According to the airspace.cz webpage, which focuses on the airplane RC models design, vertical tailplane volume has to be within following limits.

$$0{,}020 < A_V < 0{,}039 \qquad \text{[11] (5.23)}$$

The result is, that the value of the vertical tail volume is between lowest value mentioned in table 5.10 and highest value mentioned in equation 5.23. Calculation of vertical tailplane MAC and position of the MAC in the longitudinal direction and its position in the vertical tail span direction follows.

The equation of leading edge x coordinate is given without derivation and has the following form.

$$x(y) = b - \sqrt{\frac{a^2 \cdot b^2 - y^2 \cdot b^2}{a^2}} + \tan\xi \cdot y \qquad (5.24)$$

Explanation of unknowns in equations 5.24:

Unknown explanation	Designation	Value	Unit
Vertical tailplane span	a	0,400	m
Vertical tail root minus tip chord	b	0,174	m
Vertical tail tip chord value	k	0,115	m
Spanwise position	y	-	m

Tab. 5.13 Mean aerodynamic chord calculation unknowns

After integration of the equations 5.16 to 5.18 with substituting of unknowns by the values of the vertical tailplane, results are as follows.

$$c_{VMAC} = 257{,}653\, mm$$
$$x_{VMAC} = 57{,}148\, mm$$
$$y_{VMAC} = 183{,}582\, mm$$

5.4 Fuselage aerodynamic design

The main purpose of the fuselage is the placement of UAV systems and payload and is required to have drag as low as possible. The minimal drag of the fuselage can be observed in the glider planes category (Fig. 5.14, letter f), where all ways to reduce drag are used to the maximum extent possible. Because of this, a glider like fuselage was proposed as an optimal variant for UAV fuselage design.

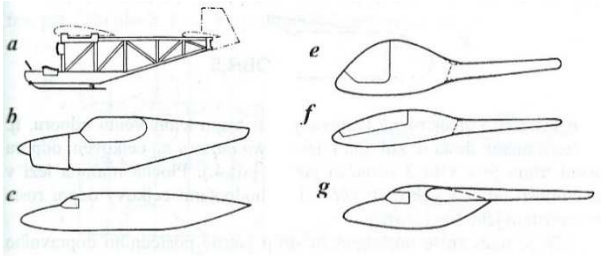

Fig. 5.14 Usual fuselage shapes [7]

First design version of the fuselage could be seen in the figure 5.15. It is evident, that shape of fuselage was defined with changes in shape to be as smooth as possible. In the first concept sketch, the payload bay is embedded to the wing structure, to maximally limit the frontal area of the fuselage. This solution has also impact on the wetted area reduction.

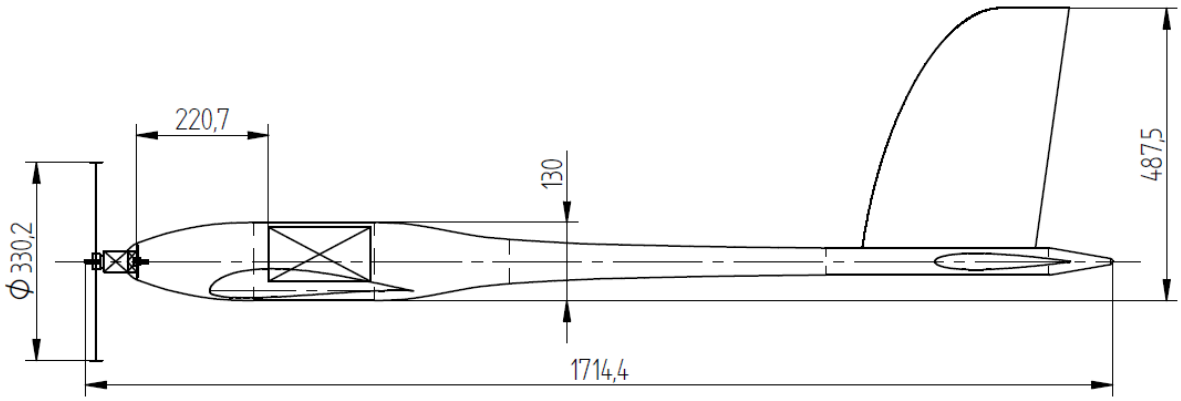

Fig. 5.15 Fuselage version 1

Due to the structural design difficulties of the wing to fuselage attachment node arising from the embedded payload bay, it was decided to simplify this construction node by moving the payload bay above the wing structure. New fuselage concept could be seen in the figure 5.16.

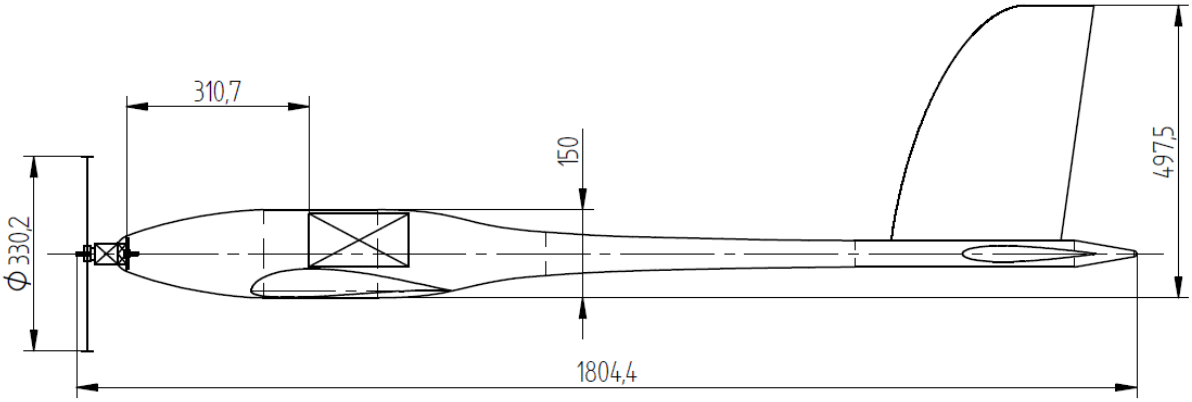

Fig. 5.16 Fuselage version 2

5.5 Control surfaces design

Control surfaces design focuses on determination of control surfaces type, its dimensions and area.

- **Ailerons:**

The function principle lies in changing of the lift distribution (Fig. 5.17) on the wing causing a banking moment in direction, that wing half with aileron deflected up moves downwards.

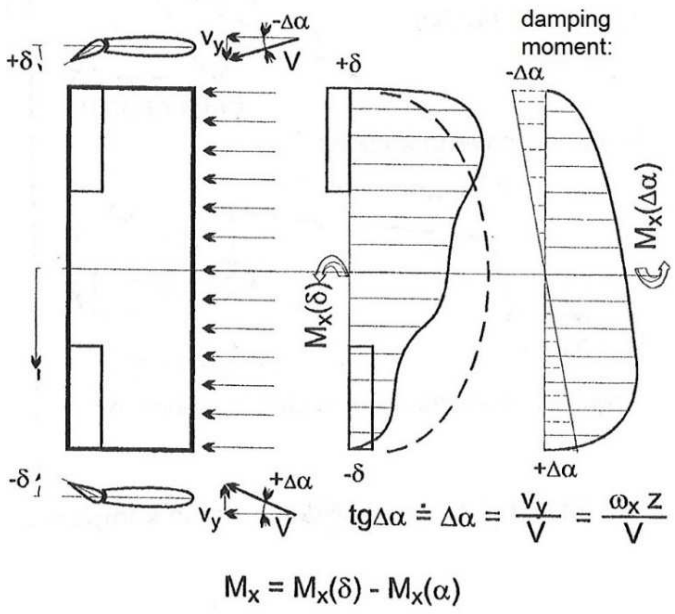

Fig. 5.17 Ailerons function principle [9]

Other phenomenon which occurs when using ailerons is additional yaw moment generation. It is possible to eliminate this parasite moment by differentiation of ailerons deflection or by the usage of Friese ailerons (Fig. 5.18). The differentiation of ailerons deflection will be chosen as it is not difficult to provide difference of deflections by the ailerons servomotors programing.

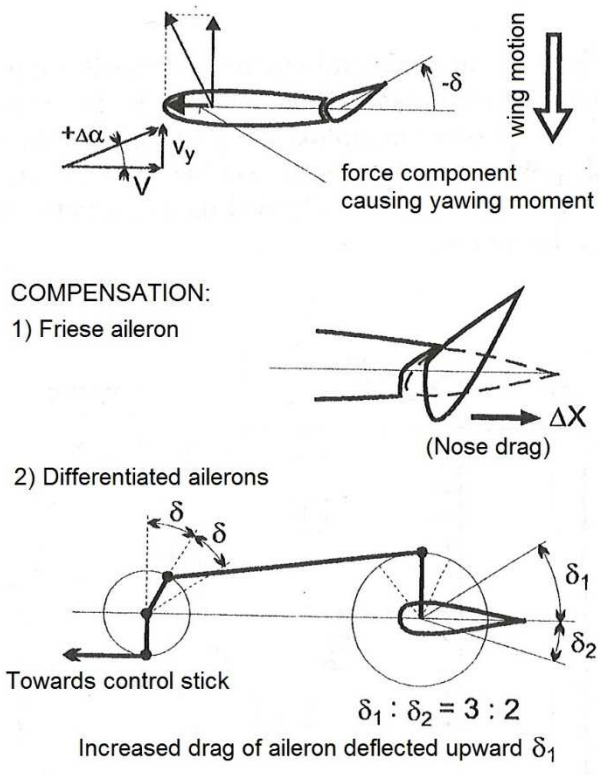

Fig. 5.18 Friese and differentiated ailerons [10]

In case of newly designed UAV, ailerons were designed to have parameters mentioned in table 5.14 which can be seen below.

Parameter	Designation	Value	Unit
Aileron length	l_A	675	mm
Aileron depth	c_A	79	mm
Aileron area	S_A	53325	mm^2
Relative ailerons area	$\overline{S_A}$	0,11855	-
Position of aileron axis - % c_{MAC}	A_{ax}	0,74156	%
Aileron deflection	δ_A	$-30/+20$	°

Tab. 5.14 Ailerons design parameters

The detail of aileron of left half of the wing can be seen in the figure 5.19.

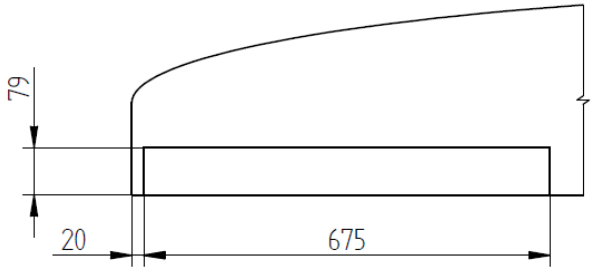

Fig. 5.19 Aileron geometry

- **Rudder:**

The design parameters of the rudder, which are referred in the table 5.15 was chosen. Rudder deflection can be adjusted according to the UAV flight properties observed during the test flights.

Parameter	Designation	Value	Unit
Rudder length	l_R	385,5	mm
Rudder depth	c_R	86,5	mm
Rudder area	S_R	33345,75	mm^2
Relative rudder area	$\overline{S_R}$	0,33126	-
Position of rudder axis - % c_{VMAC}	R_{ax}	0,66428	%
Rudder deflection	δ_R	± 30	°

Tab. 5.15 Rudder design parameters

The detail of rudder geometry can be seen in figure 5.20.

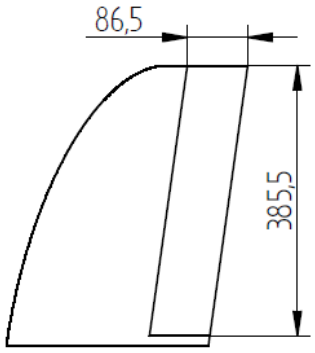

Fig. 5.20 Rudder geometry

- **Elevator:**

The elevator of the all flying type was chosen. This arrangement provides very good manoeuvrability and also good longitudinal trimming capability. As the all flying elevator is not usual within slow flying aircrafts and UAVs, design parameters are given without deeper analysis.

The main design parameters of the elevator are mentioned in the table 5.16. The elevator deflection can be adjusted according to the UAV flight properties observed during test flights.

Parameter	Designation	Value	Unit
Elevator length	l_E	791	mm
Elevator area	S_E	152779,20	mm^2
Relative elevator area	$\overline{S_E}$	0,91977	-
Position of elevator axis - % c_{VMAC}	E_{ax}	20	%
Elevator deflection	δ_E	$-12/+9$	°

Tab. 5.16 Elevator design parameters

Geometry of the elevator can be seen in the figure 5.21 located on the following page.

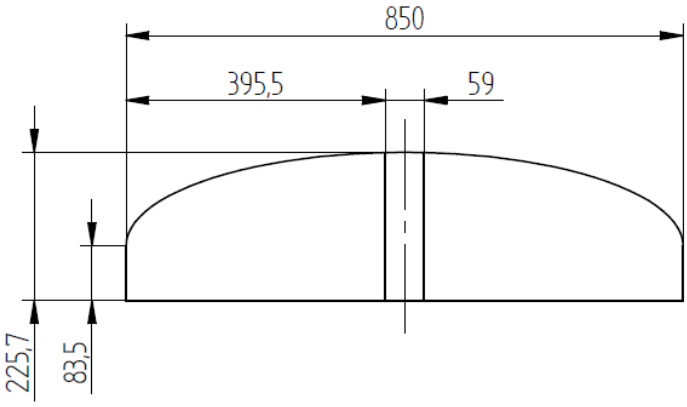

Fig. 5.21 Elevator geometry

5.6 UAV aerodynamic polar calculation

UAV polar curve was obtained for simplified configuration. Main simplification consist in the zero wing and elevator angle of incidence. Next simplification is not considering effect of the faster air stream behind propeller.

- **Wing polar:**

The wing aerodynamic polar was determined using the simulation software XFLR5. Total two polar curves were created. One for the level flight analysis and one for the flight in steady turn.

The polar for the level flight was created using the constant lift analysis, where mass of the airplane defined was 9,5 kg (Fig. 5.22).

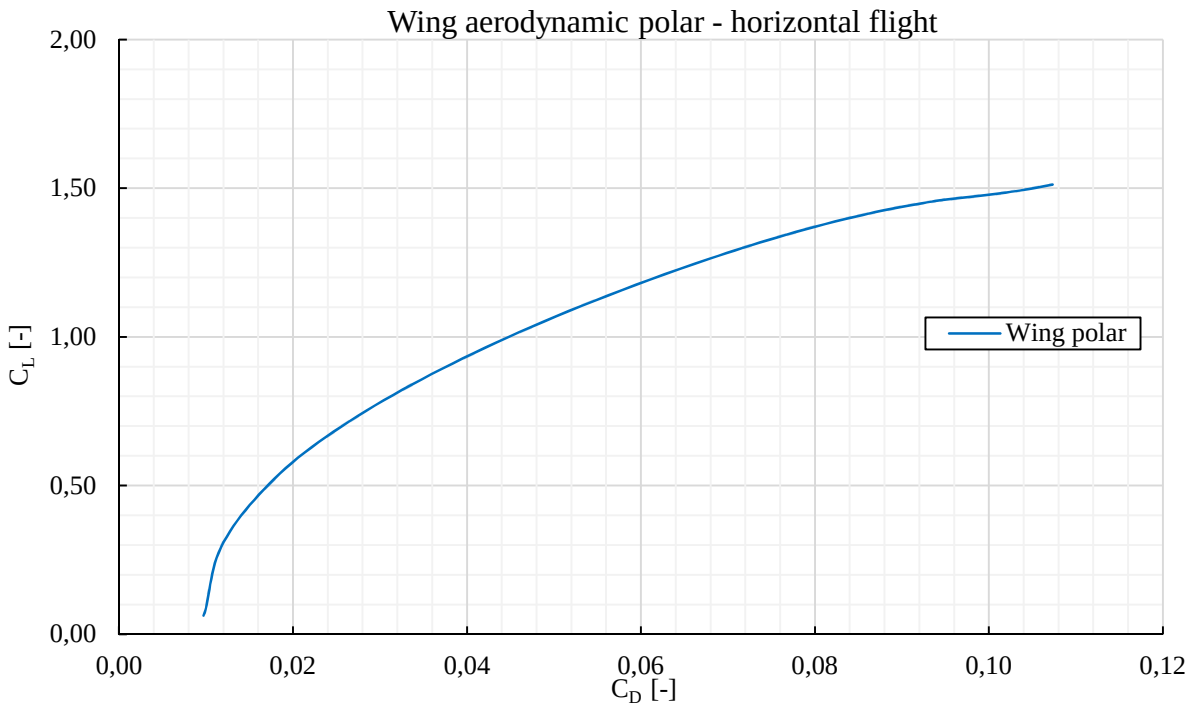

Fig. 5.22 Wing horizontal flight polar

The polar curve intended for turning flight analysis was created using constant speed analysis type, where the speed of the UAV defined was 25,9 m/s (Fig. 5.23).

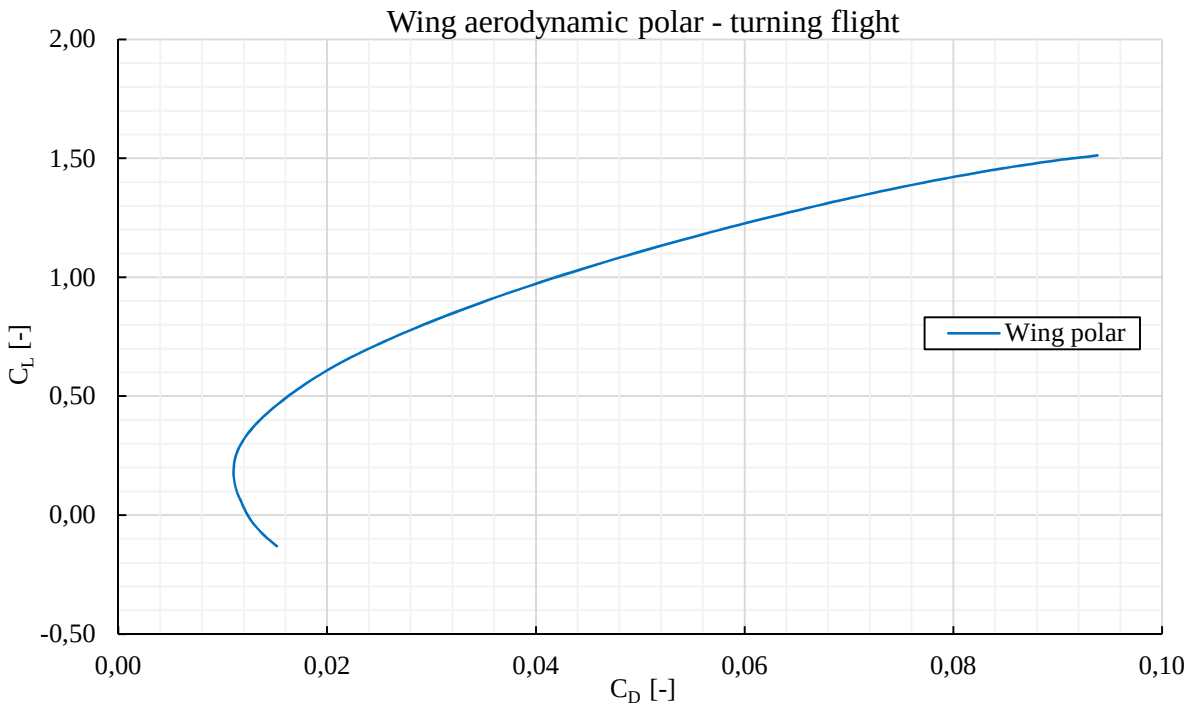

Fig. 5.23 Wing turning flight polar

- **Wing and tail polar:**

The analysis was performed including only the wing and horizontal tail followed by analysis including the wing, horizontal tail and also vertical tail (Fig. 5.24, Fig. 5.25). Software does not calculate the interference drag between the horizontal and vertical tail. Hence it was needed to calculate contribution of interference additionally.

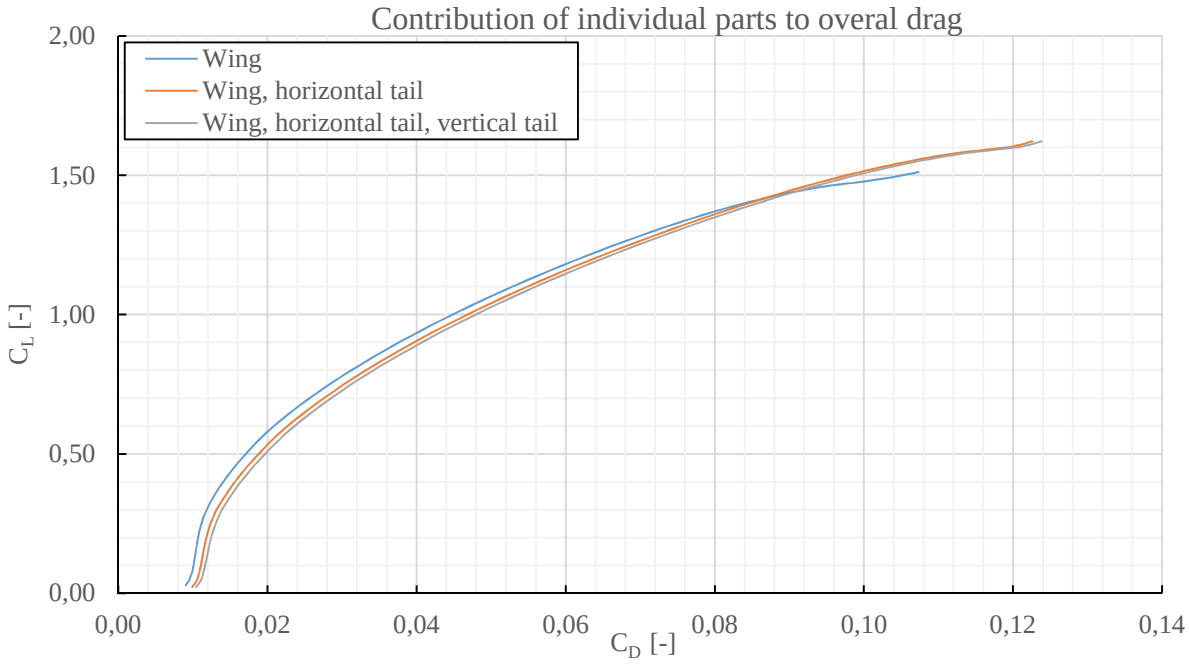

Fig. 5.24 Contribution of individual parts to overall drag in horizontal flight

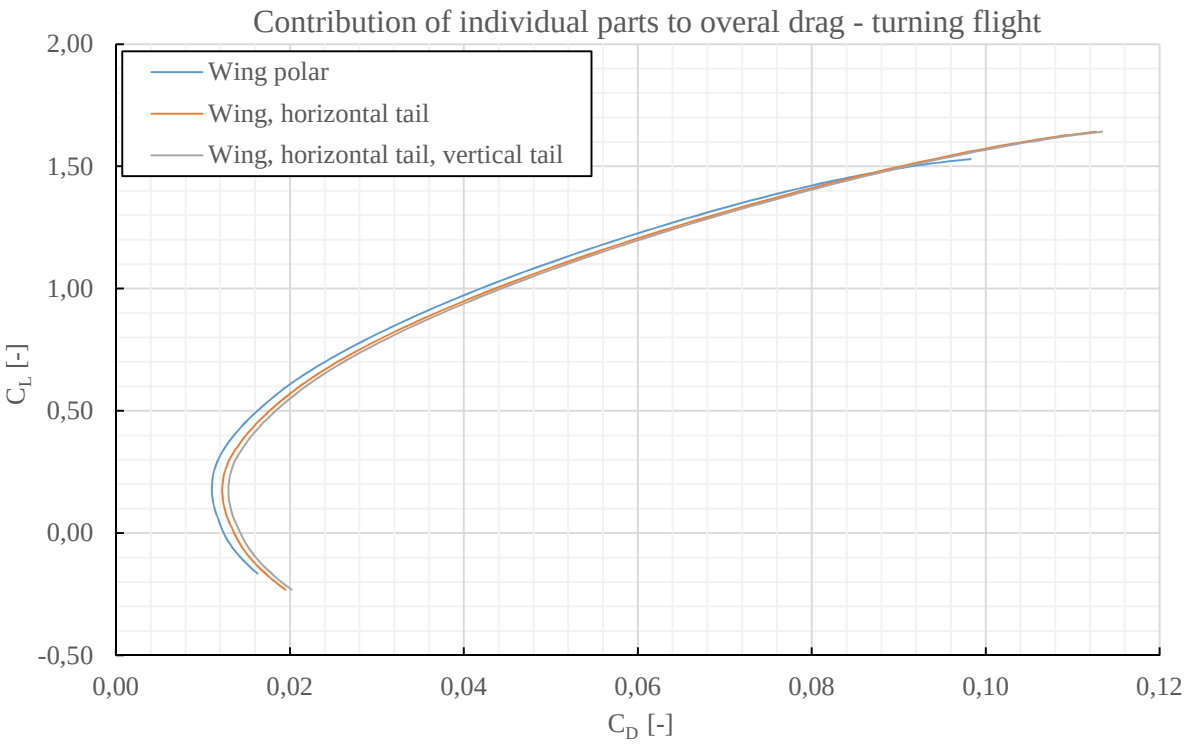

Fig. 5.25 Contribution of individual parts to overall drag in turning flight

- **Parasite drag calculation:**

The drag of all parts other than wing was calculated using data obtained by the procedure mentioned above and by the usage of empirical formulas. [4]

The calculation of the parasite drag for angle of attack of one degree ($\alpha = 1°$) and the analysis of constant lift type (horizontal flight) is described below. This angle of attack was chosen for outlining of calculation method. The resulting data after decomposition of total lift and drag to individual parts is in the table 5.17.

Parameter	Designation	Value	Unit
Angle of attack	α	1	°
Wing lift coefficient	C_{LW}	0,363789	-
Wing drag coefficient	C_{DW}	0,013159	-
Horizontal tail lift coefficient	C_{LH}	-0,010826	-
Horizontal tail drag coefficient	C_{DH}	0,001265	-
Vertical tail drag coefficient	C_{DV}	0,000762	-

Tab. 5.17 Aerodynamic coefficients for parasite drag calculation

Determination of other important UAV parts drag follows. Parts, which were taken into account, are fuselage, landing gear shock absorber and undercarriage wheels. Fuselage drag coefficient was calculated using equation 5.25.

$$C_{DF} = \frac{C_R}{2}\left(1 + 2\overline{d_F}\right) \qquad \text{[4] (5.25)}$$

$$\overline{d_F} = \frac{d_{Fmax}}{l_F} \quad \text{[4] (5.26)}$$

Symbol C_R stands for aerodynamic drag of the flat plate parallel with stream velocity vector and with Reynolds number equivalent to that of fuselage (see appendix A.2, Fig. A2.1). Fuselage Reynolds number was calculated for the reference speed of 25 m/s.

$$Re_F = \frac{V_{inf} \cdot l_F}{\nu} \quad (5.27)$$

Resulting fuselage drag coefficient is:

$$C_{DF} = 0{,}003701$$

Landing gear shock absorber drag coefficient was calculated as the drag coefficient of a flat plate placed in stream with velocity vector parallel to the plate. Reynolds number was calculated for the width of shock absorber and velocity of stream same as in the case of fuselage. The shock absorber drag coefficient is:

$$C_{DSa} = 0{,}049922$$

Landing gear wheel drag coefficient was obtained from literature [4].

$$C_{DWh} = 0{,}25$$

Reference area of fuselage as well as reference area of shock absorber is its wetted area. Reference area of landing gear wheel is its frontal area.

$$S_{DF} = 0{,}421649\ m^2$$
$$S_{DSa} = 0{,}006743\ m^2$$
$$S_{DWh} = 0{,}002175\ m^2$$

Formula intended for determination of parasite drag [4].

$$C_{DP} = F_i \cdot \left(C_{DH} + C_{DV} + C_{DF} \cdot \frac{S_{DF}}{S_W} + C_{DSa} \cdot \frac{S_{DSa}}{S_W} + C_{DSa} \cdot \frac{2 \cdot S_{DWh}}{S_W} \right) \quad (5.28)$$

Where F_i is increasing coefficient, which have to be used to take interference drag into account. For usual aeroplane models the coefficient has value of 1,1 [4]:

$$F_i = 1{,}1$$

After substitution into equation 5.28 parasite drag coefficient is:

$$C_{DP} = 0{,}005879$$

Lift coefficient and drag coefficient of the UAV is calculated using equations 5.29 and 5.30.

$$C_L = C_{LW} + C_{LH} \quad (5.29)$$

$$C_D = C_{DW} + C_{DP} \quad (5.30)$$

Resulting aerodynamic coefficients:

$$C_L = 0{,}352963$$

$$C_D = 0{,}019038$$

This procedure was used for calculation of lift and drag coefficients of UAV in the angle of attack range from -2,6 to 13,8 degrees in case of constant lift analysis and in the range of -5 to 13,8 degrees in case of constant speed analysis type (see appendix A.3, Tab. A3.3). Resulting polar graphs for horizontal flight (Fig. 5.26) and for turning flight (Fig. 5.27) can be seen lower.

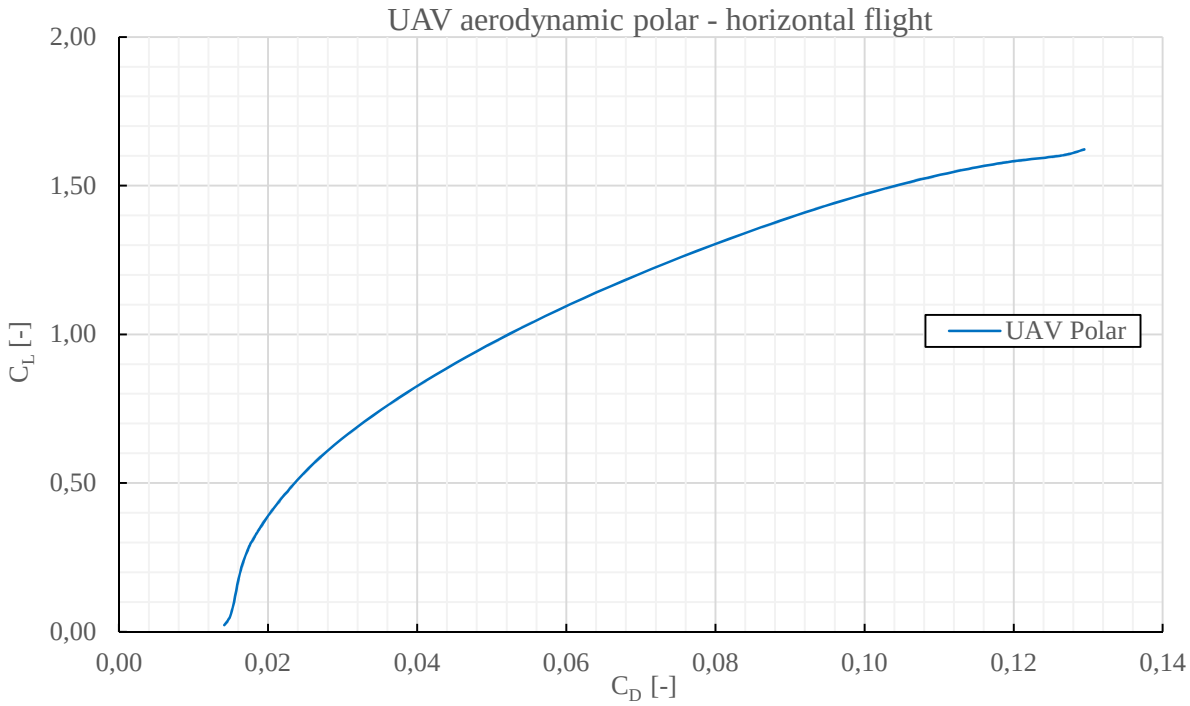

Fig. 5.26 UAV horizontal flight polar

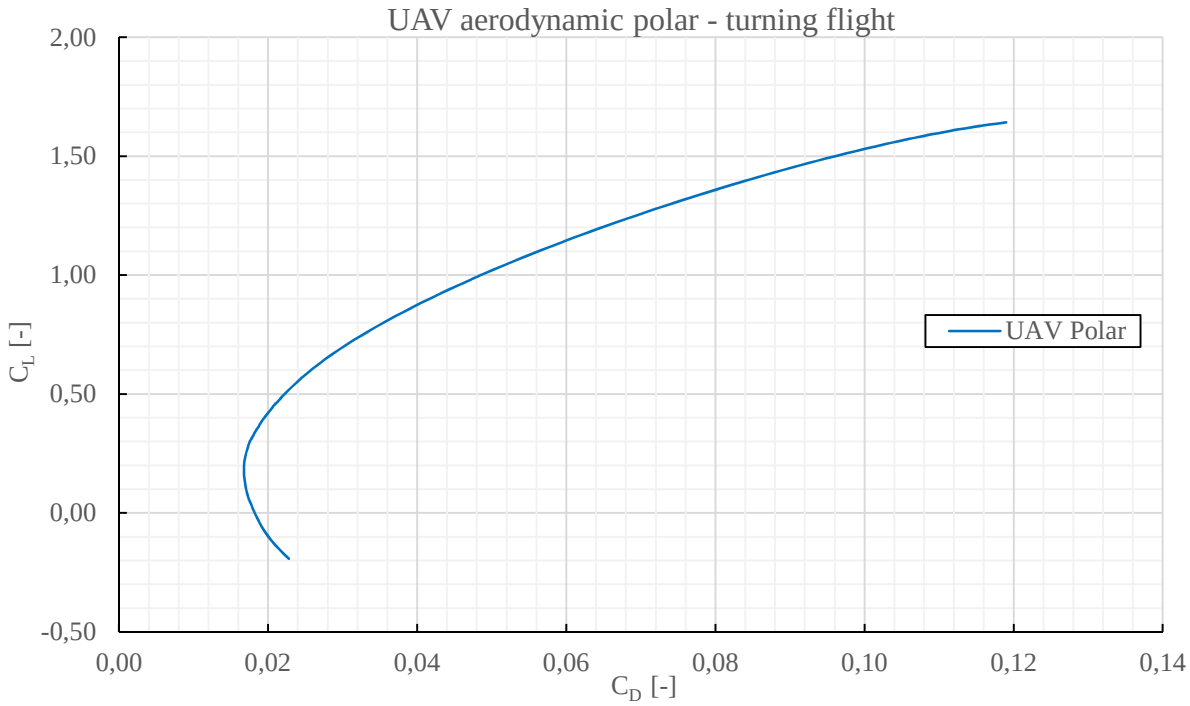

Fig. 5.27 UAV turning flight polar

All calculations and simulations, which led to the UAV horizontal flight and turning flight polar curves calculation, are affected by calculation and simulation errors. For example,

increase of the fuselage drag, when affected by the faster stream behind propeller could be even more than 1,5 times the drag value of fuselage not affected by faster stream. [4] Because of the calculation errors and simplifications mentioned at the beginning of this chapter, it is necessary to look at the results in this chapter as the results used for preliminary design of UAV.

5.7 Longitudinal stability calculation

The first step when considering longitudinal stability was to determine UAV aerodynamic centre. The second step was the definition of desired centre of gravity location and the consequent adjustment angle. The relative position of UAV aerodynamic centre and centre of gravity is extremely important to ensure longitudinal stability.

- **Aerodynamic centre calculation:**

The first assumption in the aerodynamic centre determination process was, that the aerodynamic centre of wing is approximately in the quarter of wing mean aerodynamic chord. The impact of the fuselage, landing gear and other parts are not taken into account. Because of that only the influence of the horizontal tail, which is most significant will be taken into account. Aerodynamic centre relative position on wing mean aerodynamic chord could be calculated using equation 5.31.

$$\overline{x_F} = 0{,}25 + \Delta\overline{x_{FH}} \qquad \text{[4] (5.31)}$$

Where the influence of horizontal tail on the aerodynamic centre position:

$$\Delta\overline{x_{FH}} = \frac{a_H}{a} \cdot A_H \cdot (1 - D) \qquad \text{[4] (5.32)}$$

Or similar equation:

$$\Delta\overline{x_{FH}} = \frac{a_H}{a} \cdot k_H \cdot A_H \cdot \left(1 - \frac{\partial\varepsilon}{\partial\alpha}\right) \qquad \text{[3] (5.33)}$$

However, equation 5.32 was used because $\frac{\partial\varepsilon}{\partial\alpha}$ and k_H members of the equation could not be determined using methods available in the design process used in this thesis. Other members of equation were calculated using the equations below.

$$a = a_H \cdot \left[1 + \frac{a_H}{a_W} \cdot \frac{S_H}{S_W} \cdot (1 - D)\right] \qquad \text{[4] (5.34)}$$

$$D = \frac{a_W \cdot (1 + \tau)}{\pi \cdot AR} \cdot \left[2 + \frac{1}{16} \cdot \left(\frac{l_W}{L_H}\right)^2\right] \qquad \text{[4] (5.35)}$$

Lift curve slopes a_H and a_W were determined from lift curves data of the wing and horizontal tail (see appendix A.3, Tab. A3.1). Coefficient τ has value of zero in case of elliptical wing. [4] After substitution to above mentioned equations, results are:

$$D = 0{,}349568$$

$$a = 5{,}543239\ rad^{-1}$$

$$\Delta\overline{x_{FH}} = 0{,}337724$$

And finally after substitution to the equation 5.31:

$$\overline{x_F} = 0{,}587724$$

- **Centre of gravity and adjustment angle calculation:**

The centre of gravity of the UAV has to be located in front of its aerodynamic centre to provide static longitudinal stability (Fig. 5.28).

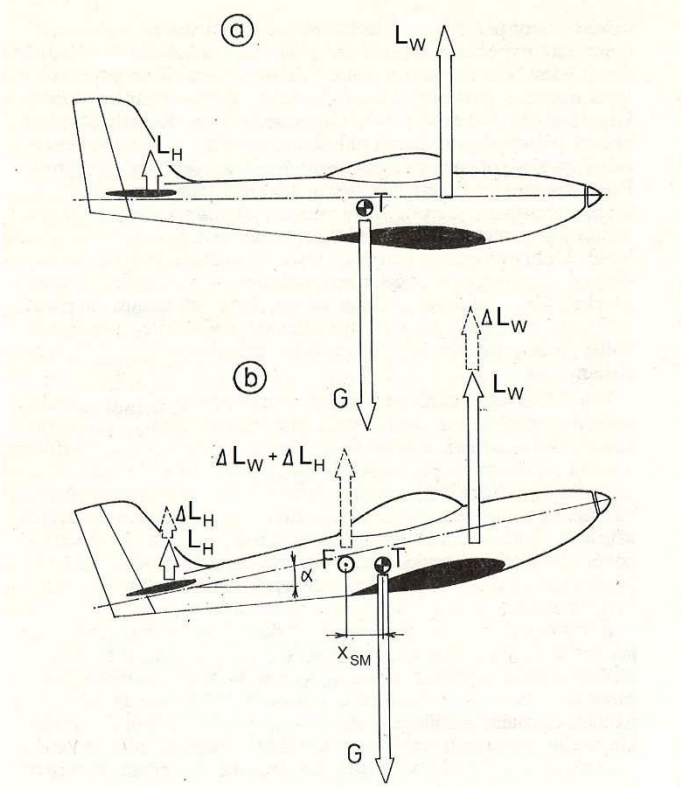

Fig. 5.28 Relative position of A.S. and C.G. and static longitudinal stability principle [4]

The difference between the position of the aerodynamic centre and centre of gravity is called a static margin. For conventional airplane models the static margin has usually value of ten percent of wing MAC [4]. It means that:

$$\overline{x_{SM}} = \overline{x_F} - \overline{x_{CG}} = 0{,}1$$

This leads to:

$$\overline{x_{CG}} = 0{,}487724$$

This value represents desired centre of gravity relative location on the MAC, which has to be achieved by a proper distribution of individual mass groups of the UAV.

The horizontal tail lift coefficient needed for compensation of pitching moment has to be determined using equation 5.37. The calculation of this parameter is related to a certain defined speed. Speed of 25 m/s was chosen as reference speed for this calculation.

$$m_{z0_W} + C_{LW} \cdot (\overline{x_{CG}} - 0{,}25) - C_{LH} \cdot A_H + C_{LH} \cdot \frac{S_H}{S_W} (\overline{x_{CG}} - 0{,}25) = 0 \qquad [4]\ (5.36)$$

After expression of the C_{LH}:

$$C_{LH} = \frac{m_{z0_W} + C_{LW} \cdot (\overline{x_{CG}} - 0{,}25)}{A_H - \frac{S_H}{S_W}(\overline{x_{CG}} - 0{,}25)} \qquad [4]\ (5.37)$$

In the next step m_{z0_W}, which is wing moment coefficient related to quarter point of the wing MAC and wing lift coefficient C_{LW} has to be defined. Wing lift coefficient was in first iteration calculated from the lift and mass equilibrium equation (eq. 5.7).

$$C_{LW1} = 0{,}293266$$

From lift curve of the wing (Fig. 5.29), angle of attack corresponding to above mentioned wing lift coefficient was found.

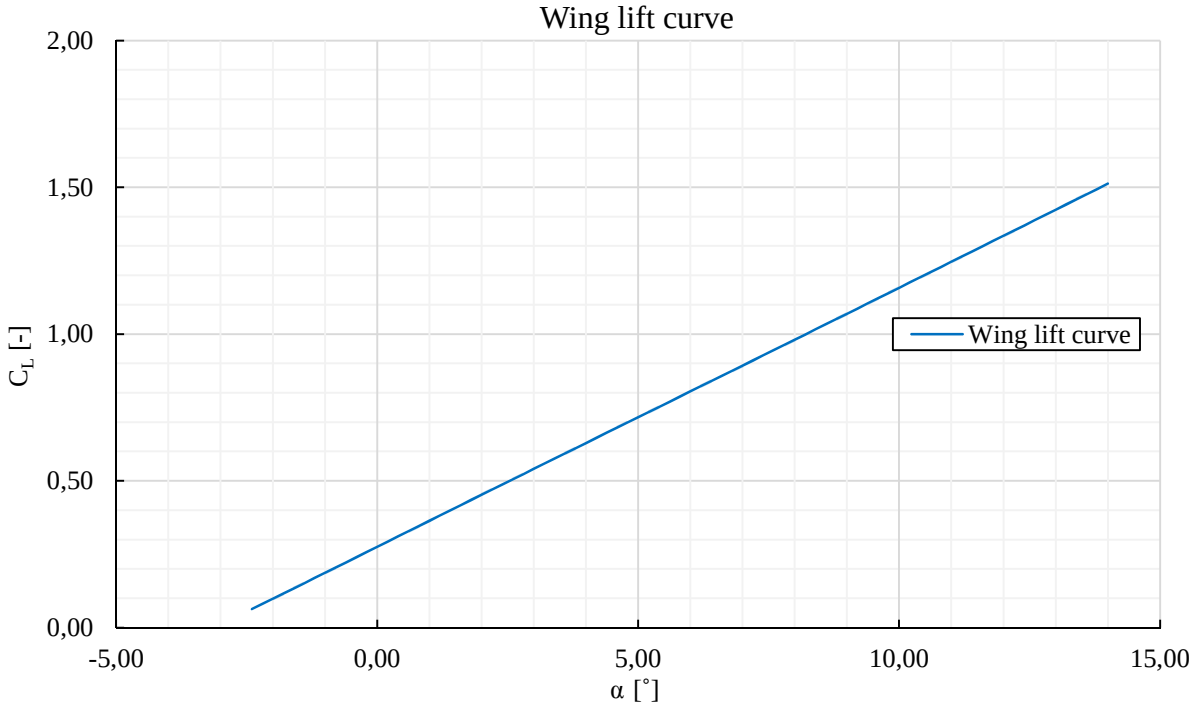

Fig. 5.29 Lift curve of wing

Angle of attack of wing for lift coefficient 0,293266 is:

$$\alpha_{W1} = 0{,}204°$$

Wing moment coefficient m_{z0_W} has to be found from the moment curve (Fig. 5.30). Tabular data of wing moment curve could be seen in appendix A.3, table A3.2.

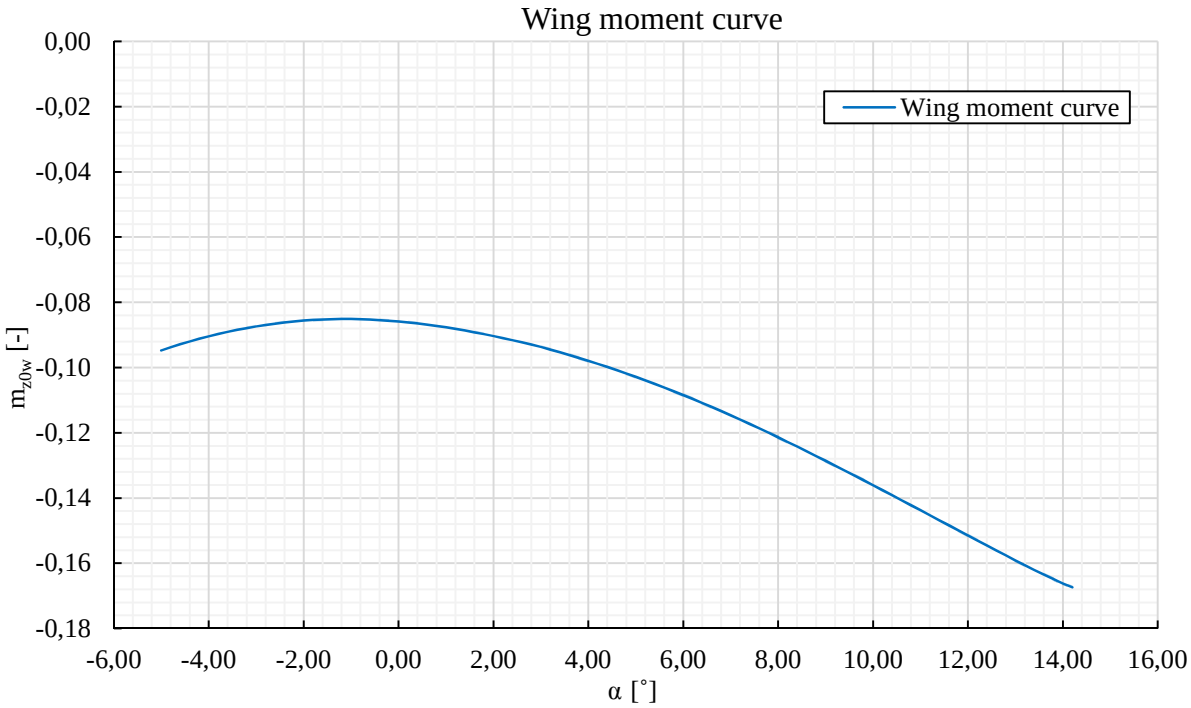

Fig. 5.30 Moment curve of wing

Moment coefficient of wing at lift coefficient of 0,293266 is:

$$m_{z0_{W}1} = -0{,}08620$$

And after substitution to equation 5.37:

$$C_{LH1} = -0{,}024756$$

Negative lift coefficient of horizontal tail implies that lift generated by this part will decrease overall lift of the UAV. Because of that, horizontal tail lift coefficient has to be calculated again for higher value of wing lift coefficient. Wing lift coefficient has to be increased by the following value.

$$\Delta C_{LW1} = -C_{LH1} \cdot \frac{S_H}{S_W} \tag{5.38}$$

After substitution the result is:

$$\Delta C_{LW1} = 0{,}004571$$

This value has to be added to lift coefficient 0,293266. Lift coefficient for second iteration is:

$$C_{LW2} = 0{,}297837$$

Calculation mentioned above was performed again with following results:

$$\alpha_{W2} = 0{,}258°$$
$$m_{z0_{W}2} = -0{,}08625$$
$$C_{LH2} = -0{,}023199$$
$$\Delta C_{LW2} = 0{,}004283$$

The resulting lift coefficient of wing after second iteration is:

$$C_{LW2r} = 0{,}297837 - 0{,}004283 = 0{,}293554$$

This wing lift coefficient has following difference from the coefficient, which is needed.

$$\Delta C_{LW2r} = C_{LW2r} - C_{LW1} \tag{5.39}$$
$$\Delta C_{LW2r} = 0{,}293554 - 0{,}293266 = 0{,}000288$$

This difference has to be subtracted from C_{LW2} and results for third and final iteration is then:

$$C_{LW3} = 0{,}297550$$
$$\alpha_{W3} = 0{,}255°$$
$$m_{z0_{W3}} = -0{,}0862$$
$$C_{LH3} = -0{,}023301$$
$$\Delta C_{LW3} = 0{,}004302$$

The resulting lift coefficient of wing after final iteration is:

$$C_{LW3r} = 0{,}297550 - 0{,}004302 = 0{,}293248$$

The difference between this lift coefficient and needed one is $1{,}8 \cdot 10^{-5}$. It is important to find horizontal tail angle of attack corresponding to its lift coefficient equal to C_{LH3}. After analysis of horizontal tail lift curve (Fig. 5.31), the horizontal tail angle of attack has to be following.

$$\alpha_H = -0{,}345°$$

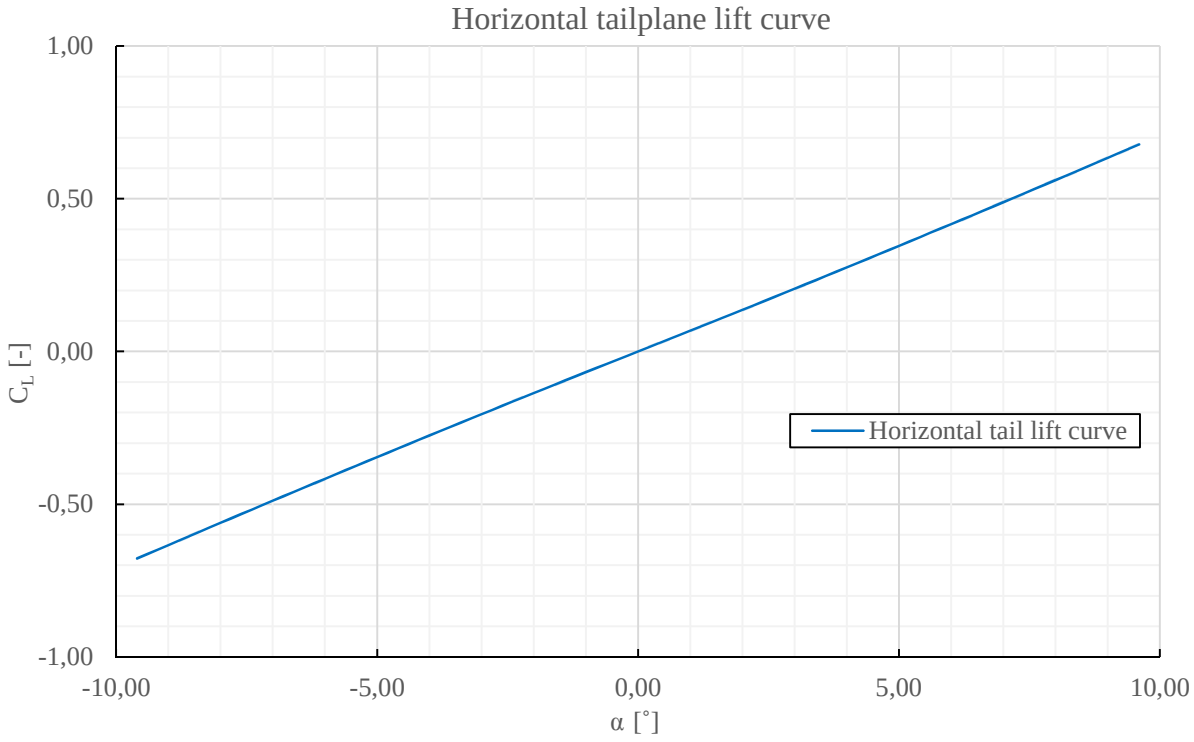

Fig. 5.31 Horizontal tailplane lift curve

The horizontal tail lift coefficient was calculated, the wing and horizontal tail angle of incidence (Fig 5.32) has to be determined. Also the adjustment angle has to be defined. This parameters are important for a proper placement of the wing and horizontal tail in relation to the fuselage longitudinal axis. It is desirable to set an angle between the fuselage longitudinal axis and wing so that at desired flight speed, fuselage longitudinal axis is parallel with the free stream velocity. The horizontal tail angle of incidence is than set to achieve moment equilibrium at desired speed.

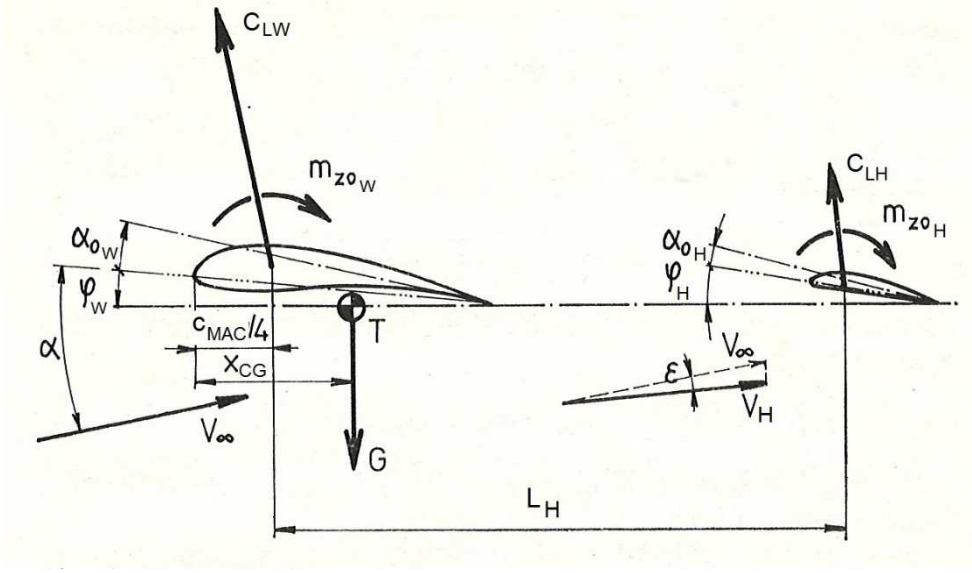

Fig. 5.32 Angles of incidence of wing and horizontal tail [4]

Downwash angle at the position of horizontal tail:

$$\varepsilon = \frac{C_{LW} \cdot (1+\tau)}{\pi \cdot AR} \cdot \left[2 + \frac{1}{16} \cdot \left(\frac{l_W}{L_H}\right)^2\right] \qquad \text{[4] (5.40)}$$

After substitution:

$$\varepsilon = 0{,}022792\ rad$$

$$\varepsilon = 1{,}305859°$$

The wing angle of incidence was chosen to be 0,255˚, so that the fuselage longitudinal axis is set to the angle of attack equal zero during flight at 25 m/s.

$$\varphi_W = 0{,}255°$$

Adjustment angle:

$$\varphi = \alpha_W - \alpha_H - \varepsilon \qquad \text{[4] (5.41)}$$

After substitution:

$$\varphi = -0{,}707°$$

The horizontal tail angle of incidence is then calculated using equation 5.42.

$$\varphi_H = \varphi_W - \varphi \qquad \text{[4] (5.42)}$$

Which results in:

$$\varphi_H = 0{,}961°$$

6 FLIGHT PERFORMANCE

This chapter describes the determination of flight performance of newly designed UAV. Each subsection focuses on a particular key flight regime.

6.1 Level flight

During horizontal flight, the balance between the force of gravity and lift, the same as between thrust and drag, has to be achieved. This is evident form the figure 6.1 below.

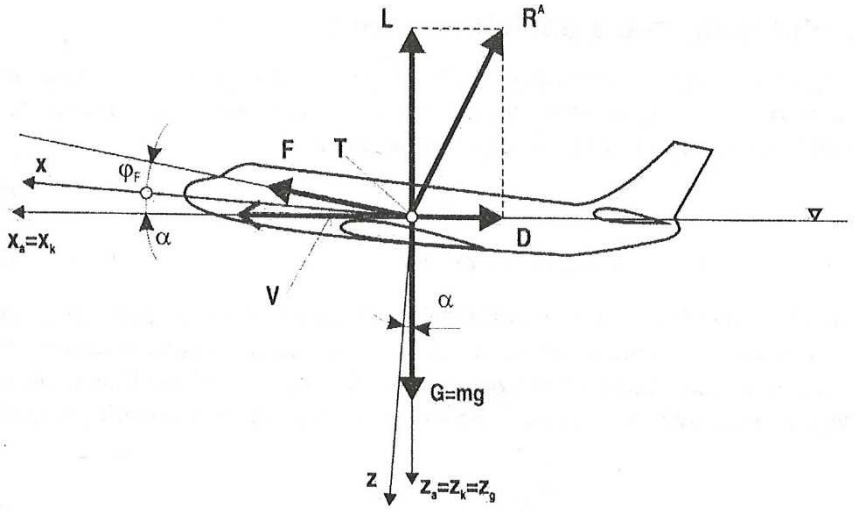

Fig. 6.1 Force equilibrium in steady turn [2]

When simplification lying in thinking of the small angle of attack α and small thrust vector incidence angle φ_F is taken into account, the equilibrium of forces is expressed by the equilibrium equations 6.1 and 6.2, which are valid for steady horizontal flight [2].

$$F - D = 0 \qquad [2]\ (6.1)$$

$$L - G = 0 \qquad [2]\ (6.2)$$

For analysis of horizontal flight, it is necessary to obtain curves of usable and required thrust and power.

During the calculation of UAV performance, the first step was the creation of a usable thrust curve. The principle of usable thrust curve creation lies in thinking of equilibrium between the electric motor moment and the moment of the propeller caused by drag of propeller blades during its rotation. Calculated data are included in appendix A.4, table A4.1. Usable thrust curve is not smooth, because it is based on the data obtained from the manufacturer of the electric motor and of the propeller, which could contain some measurement errors. Same problem occurs in the figure 6.3, which contains usable power curve.

The required thrust curve was created using following procedure. Airflow speed was determined by the speed expression from the equation of lift and the weight equilibrium.

$$V = \sqrt{\frac{2 \cdot m \cdot g}{\rho \cdot S_W \cdot C_L}} \tag{6.3}$$

After level flight speed for one angle of attack is calculated, it is possible to calculate drag for the same angle of attack.

$$D = \frac{1}{2} \cdot \rho \cdot V^2 \cdot S_W \cdot C_D \qquad \text{[5] (6.4)}$$

After the calculation of the drag, one point of required thrust curve is created. By this process, it is possible to obtain drag values for desired speed range (see appendix A.4, Tab. A4.2). This drag values corresponds to required thrust.

$$D = F_R \tag{6.5}$$

Required and usable thrust curves can be seen in the figure 6.2 below.

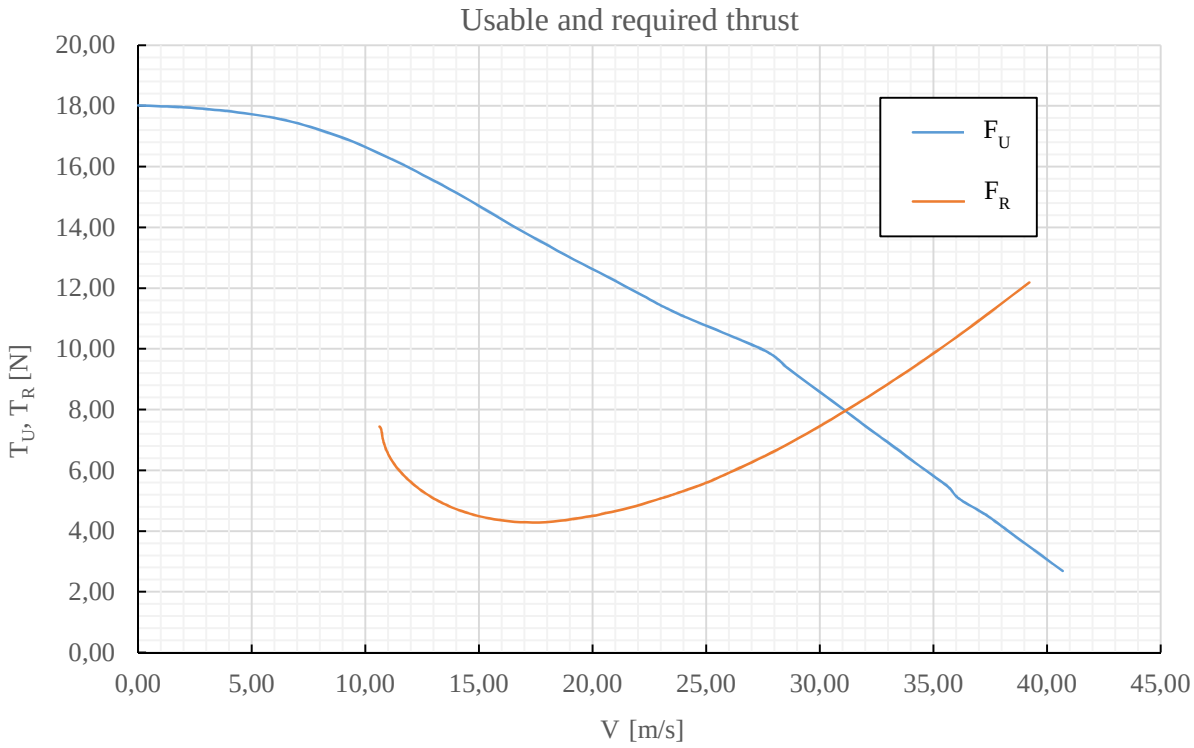

Fig. 6.2 Usable and required thrust curves

Required and usable power curves were determined using following equations.

$$P_U = F_U \cdot V \qquad \text{[2] (6.6)}$$

$$P_R = F_R \cdot V \qquad \text{[2] (6.7)}$$

The table of required and usable power values for speed range same as in case of thrust are included in appendix A.4, table A4.3. Curves of required and usable power can be seen in the figure 6.3 on next page.

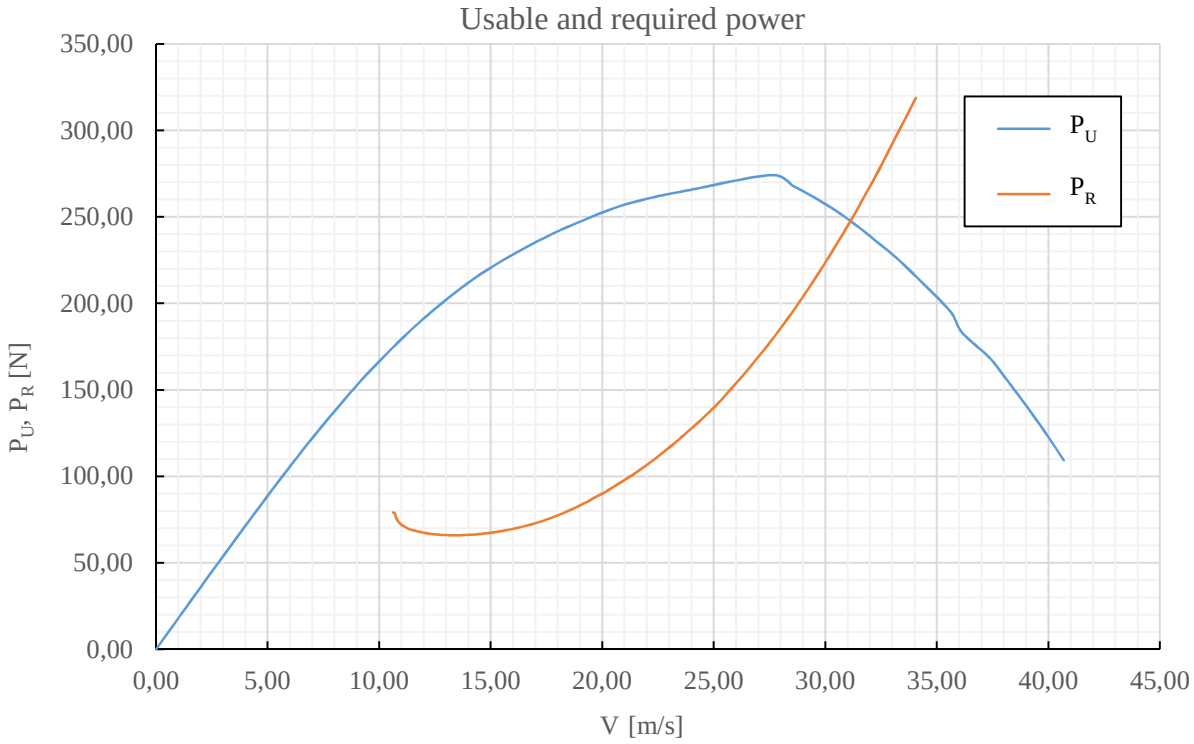

Fig. 6.3 Usable and required power curves

The identification of the characteristic speeds of horizontal flight follows. Optimal flight speed, economic flight speed, cruise speed and maximum speed of UAV will be determined. This characteristic speeds can be seen in the figure 6.4 below.

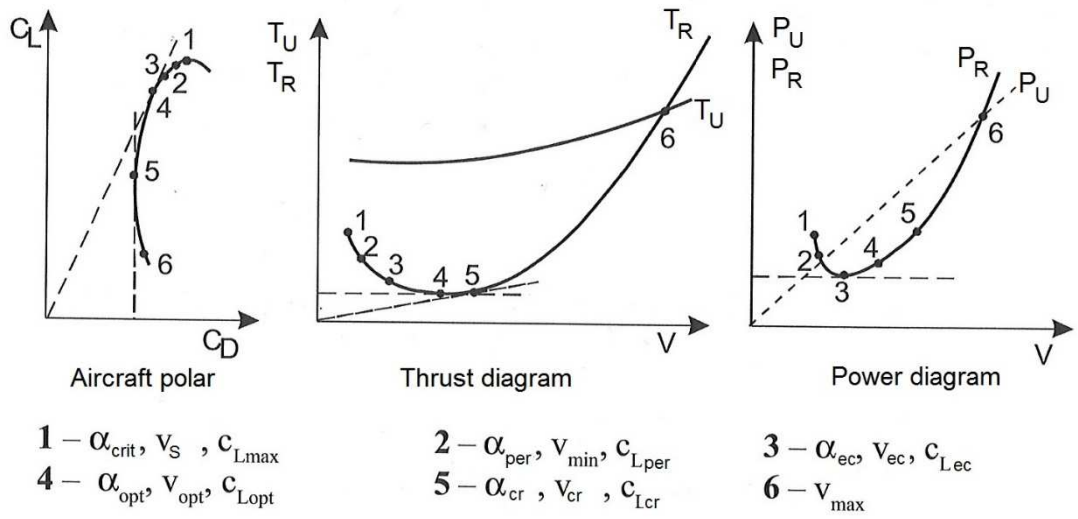

Fig. 6.4 Characteristic speeds of horizontal flight [5]

Economic flight speed is defined as speed of horizontal flight at which minimum power is required.

$$V_{ec} = 13{,}40\ m \cdot s^{-1}$$

Important flight regime is the horizontal flight at optimum speed. During the flight at this speed, minimal thrust is required.

$$V_{opt} = 17{,}40\ m \cdot s^{-1}$$

Cruise speed is speed corresponding to the minimum drag at UAV polar. This speed can be also defined as tangent to the required thrust curve, which passes through required thrust curve graph origin.

$$V_{cr} = 22{,}20\ m \cdot s^{-1}$$

Maximum speed in horizontal flight could be determined as solution of equation 6.8.

$$P_U(V_{max}) - P_V(V_{max}) = 0 \tag{6.8}$$

Maximum flight speed is than:

$$V_{max} = 30{,}95\ m \cdot s^{-1}$$

6.2 Climbing flight

Forces acting on the aircraft in climbing flight could be seen in the figure 6.5 below.

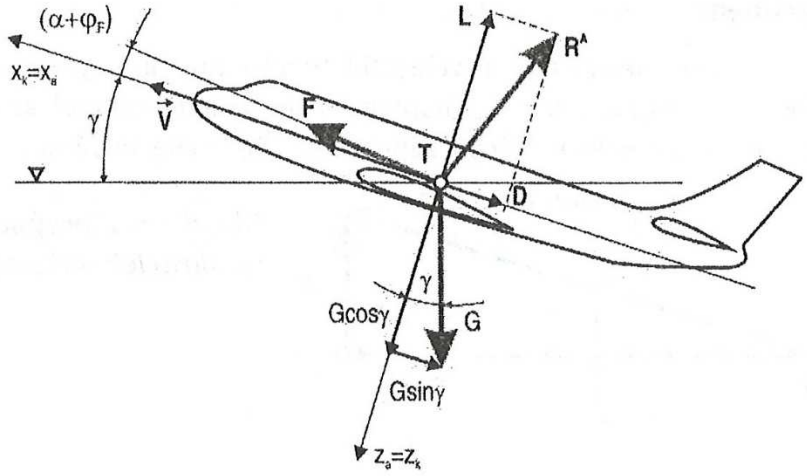

Fig. 6.5 Force equilibrium in steady climb [2]

When simplification, the same as in the chapter 6.1 is taken into account, resulting equations of force equilibrium have following form.

$$F - D - G \cdot \sin\gamma = 0 \tag{2} (6.9)$$

$$-L + G \cdot \cos\gamma = 0 \tag{2} (6.10)$$

After adjustments made to equation 6.9 resulting equation for climb speed is:

$$w = \frac{(F-D)V}{G} = \frac{\Delta F \cdot V}{G} = \frac{\Delta P}{G} \tag{2} (6.11)$$

The table of climb speed calculated for speed range from 11 to 30,5 m/s is included in appendix A.4, table A4.5. The graph of climb speed dependence on flight speed can be seen in the figure 6.6 on the next page.

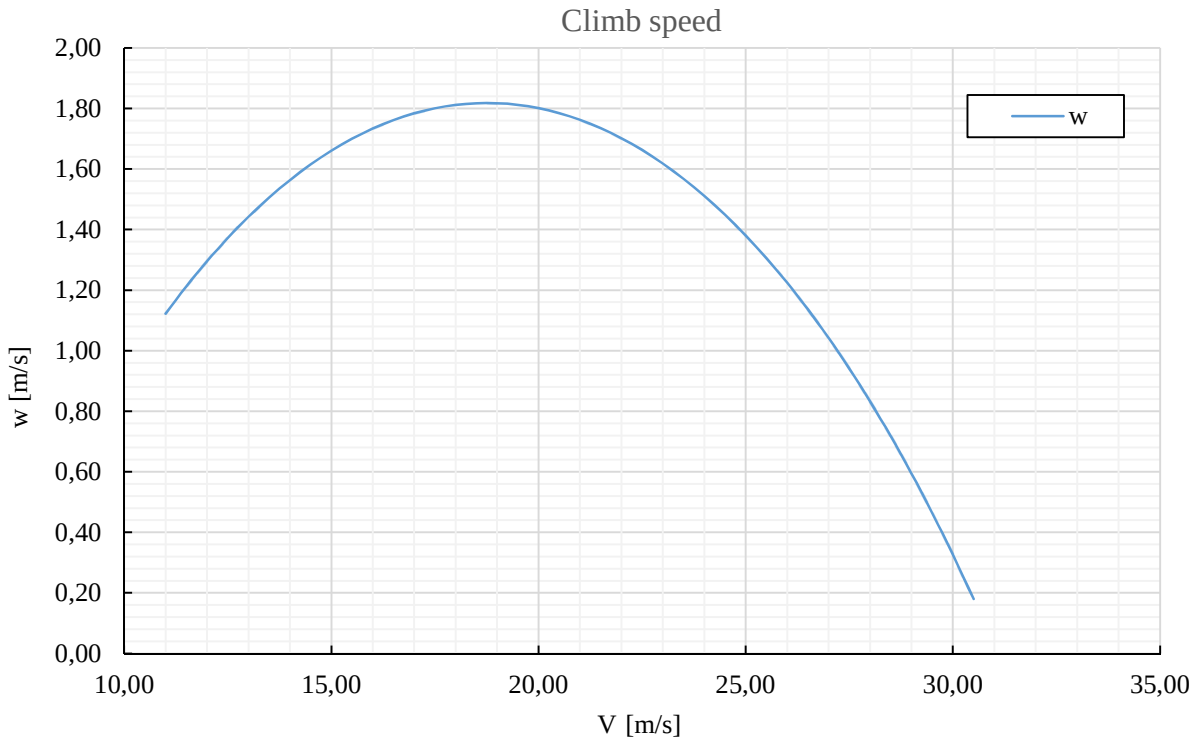

Fig. 6.6 Climb speed dependence on flight speed

Maximum climb speed is 1,82 m/s and is achieved at the flight speed of 18,75 m/s.

$$V_{w_{max}} = 18{,}75\ m \cdot s^{-1}$$

$$w_{max} = 1{,}82\ m \cdot s^{-1}$$

The angle of climb can be calculated using equation 6.12, which was created expressing angle of climb from equation 6.9.

$$\gamma = \arcsin\left(\frac{\Delta F}{G}\right) \qquad [2]\ (6.12)$$

Table of the angle of climb calculated for speed range from 11 to 30,5 m/s are included in appendix A.4, table A4.6. The graph of climb speed dependence on flight speed can be seen in the figure 6.7 on the following page.

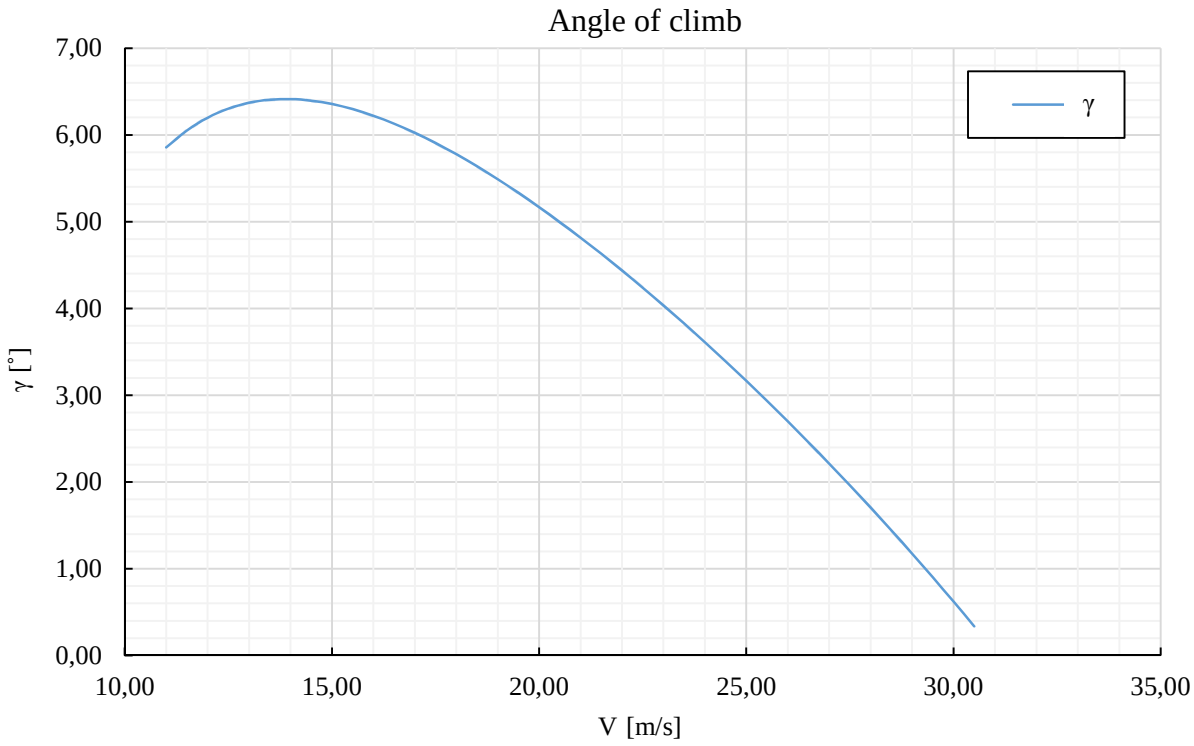

Fig. 6.7 Angle of climb dependence on flight speed

Maximum angle of climb is 6,41˚ and is achieved at the flight speed of 13,9 m/s.

$$V_{\gamma max} = 13{,}90\ m \cdot s^{-1}$$

$$\gamma_{max} = 6{,}41°$$

6.3 Turning flight

Forces acting on the aircraft in turning flight could be seen in the figure 6.8 below.

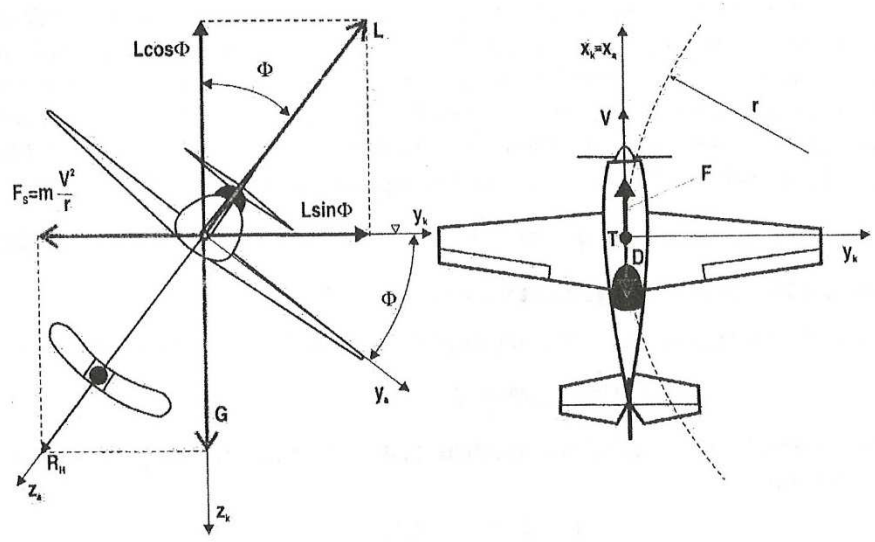

Fig. 6.8 Force equilibrium in steady turn [2]

When simplification, same as in the chapter 6.1 is taken into account, resulting equations of force equilibrium have following form.

$$F - D = 0 \qquad \text{[2] (6.13)}$$

$$L \cdot \sin \Phi - m \cdot \frac{V^2}{r} = 0 \qquad \text{[2] (6.14)}$$

$$-L \cdot \cos \Phi + G = 0 \qquad \text{[2] (6.15)}$$

It is necessary to determine limit turns diagram. Approximate shape of limit turns diagram could be seen in figure 6.9 below. There are three main limitations in turning flight.

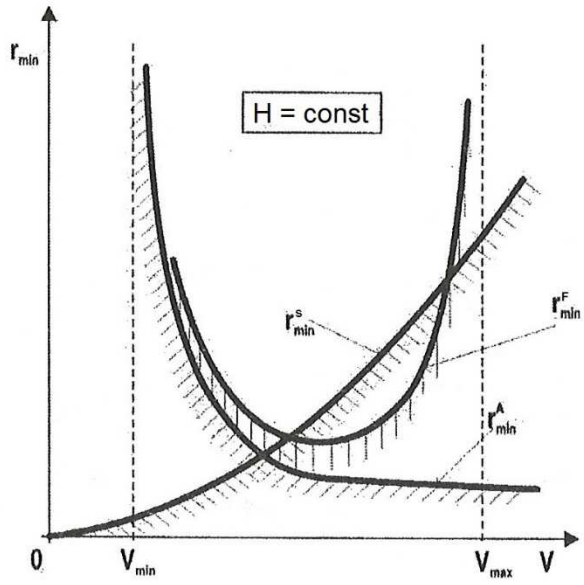

Fig. 6.9 Limit turns minimal radius diagram [2]

a) Structural limitation – limitation due to the maximum operational load factor
b) Aerodynamical limitation – limitation due to the maximal lift coefficient
c) Propulsion limitation – limitation due to the maximal usable thrust [2]

Structural limit turns:

Load factor n^S_{max}, which is equal to the maximal operational load factor is substituted to equations for limit turn parameters.

Maximal bank angle:

$$\Phi^S_{max} = \arccos\left(\frac{1}{n^S_{max}}\right) \qquad \text{[2] (6.16)}$$

Minimum turn radius:

$$r^S_{min} = \frac{V^2}{g \cdot \sqrt{(n^S_{max})^2 - 1}} \qquad \text{[2] (6.17)}$$

Minimum 360˚ turn time:

$$t_{min}^{S} = \frac{2 \cdot \pi \cdot V^2}{g \cdot \sqrt{(n_{max}^{S})^2 - 1}} \quad \text{[2] (6.18)}$$

Aerodynamical limit turns:

Load factor n_{max}^{A}, which is dependent on the actual flight speed and can be calculated using equation 7.19.

$$n_{max}^{A} = \frac{L_{max}}{G} = \frac{\frac{1}{2} \cdot \rho \cdot V^2 \cdot S_w \cdot C_{L_{max}}}{\frac{1}{2} \cdot \rho \cdot V_S^2 \cdot S_w \cdot C_{L_{max}}} = \left(\frac{V}{V_S}\right)^2 \quad \text{[2] (6.19)}$$

Maximal bank angle:

$$\Phi_{max}^{A} = \arccos\left(\frac{1}{n_{max}^{A}}\right) = \arccos\left(\frac{V_S}{V}\right)^2 \quad \text{[2] (6.20)}$$

Minimum turn radius:

$$r_{min}^{A} = \frac{V^2}{g \cdot \sqrt{(n_{max}^{A})^2 - 1}} = \frac{V^2}{g \cdot \sqrt{\left(\frac{V}{V_S}\right)^4 - 1}} \quad \text{[2] (6.21)}$$

Minimum 360˚ turn time:

$$t_{min}^{A} = \frac{2 \cdot \pi \cdot V^2}{g \cdot \sqrt{(n_{max}^{S})^2 - 1}} = \frac{2 \cdot \pi \cdot V^2}{g \cdot \sqrt{\left(\frac{V}{V_S}\right)^4 - 1}} \quad \text{[2] (6.22)}$$

Propulsion limit turns:

Load factor n_{max}^{F}, which is dependent on the actual flight speed and can be calculated using equation 6.23. However, the procedure for obtaining lift coefficient appropriate to thrust of propulsion system at given speed is slightly more difficult. The first step is to find thrust at given speed from usable thrust curve. The second step is to find drag coefficient for speed, for which the usable thrust value was found. This could be done from equilibrium between drag and thrust. Final step is to find the lift coefficient C_L^F associated to calculated drag coefficient. This could be done using UAV polar. [2]

$$n_{max}^{F} = \frac{L^F}{G} = \frac{C_L^F \cdot \frac{1}{2} \cdot \rho \cdot V^2 \cdot S_W}{G} \quad \text{[2] (6.23)}$$

Maximal bank angle:

$$\Phi_{max}^{F} = \arccos\left(\frac{1}{n_{max}^{F}}\right) \quad \text{[2] (6.24)}$$

Minimum turn radius:

$$r_{min}^{F} = \frac{V^2}{g \cdot \sqrt{(n_{max}^{F})^2 - 1}} \quad \text{[2] (6.25)}$$

Minimum 360˚ turn time:

$$t_{min}^{F} = \frac{2 \cdot \pi \cdot V^2}{g \cdot \sqrt{(n_{max}^{F})^2 - 1}} \qquad [2] \ (6.26)$$

All above mentioned limit turns parameters were calculated and could be seen in appendix A.4, tables A4.7 to A4.9. The graph of the minimum turn radius in dependence to the flight speed can be seen in figure 6.10. Minimum time to perform 360 degrees turn in dependence to flight speed can be seen in figure 6.11.

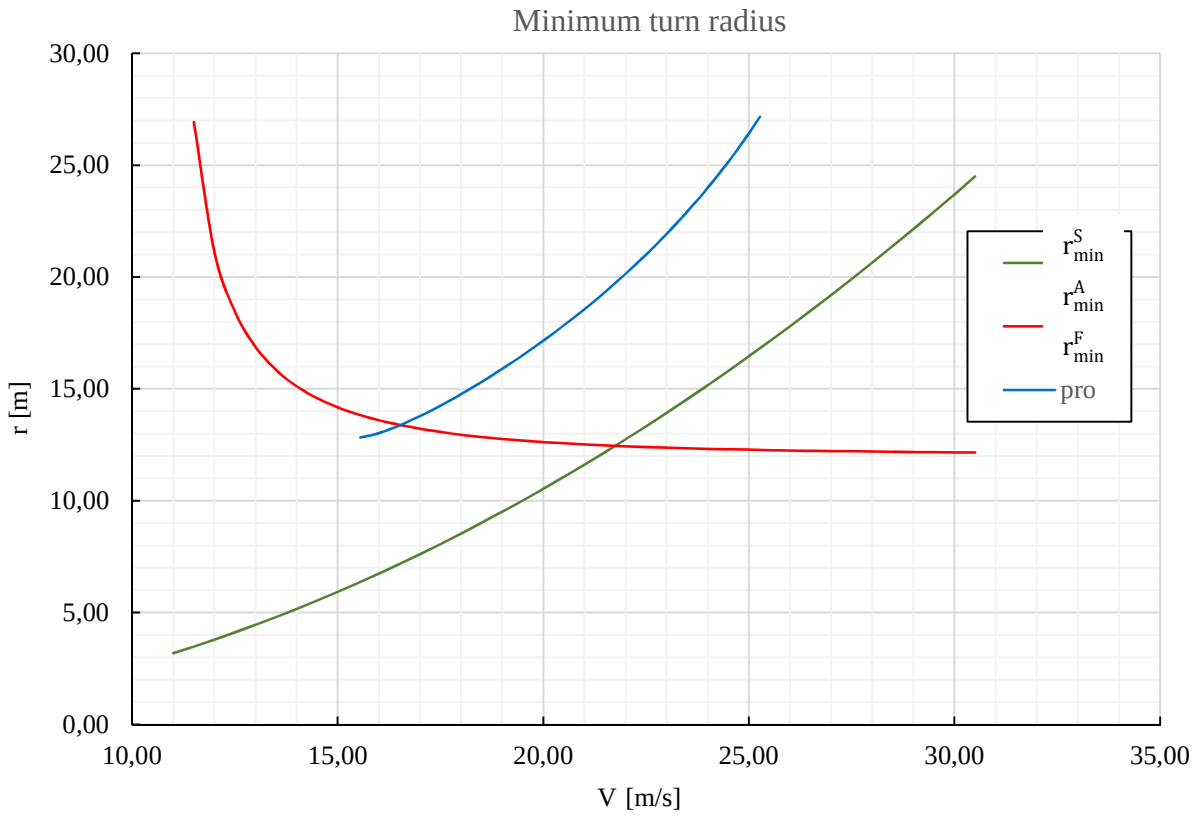

Fig. 6.10 Minimum turn radius

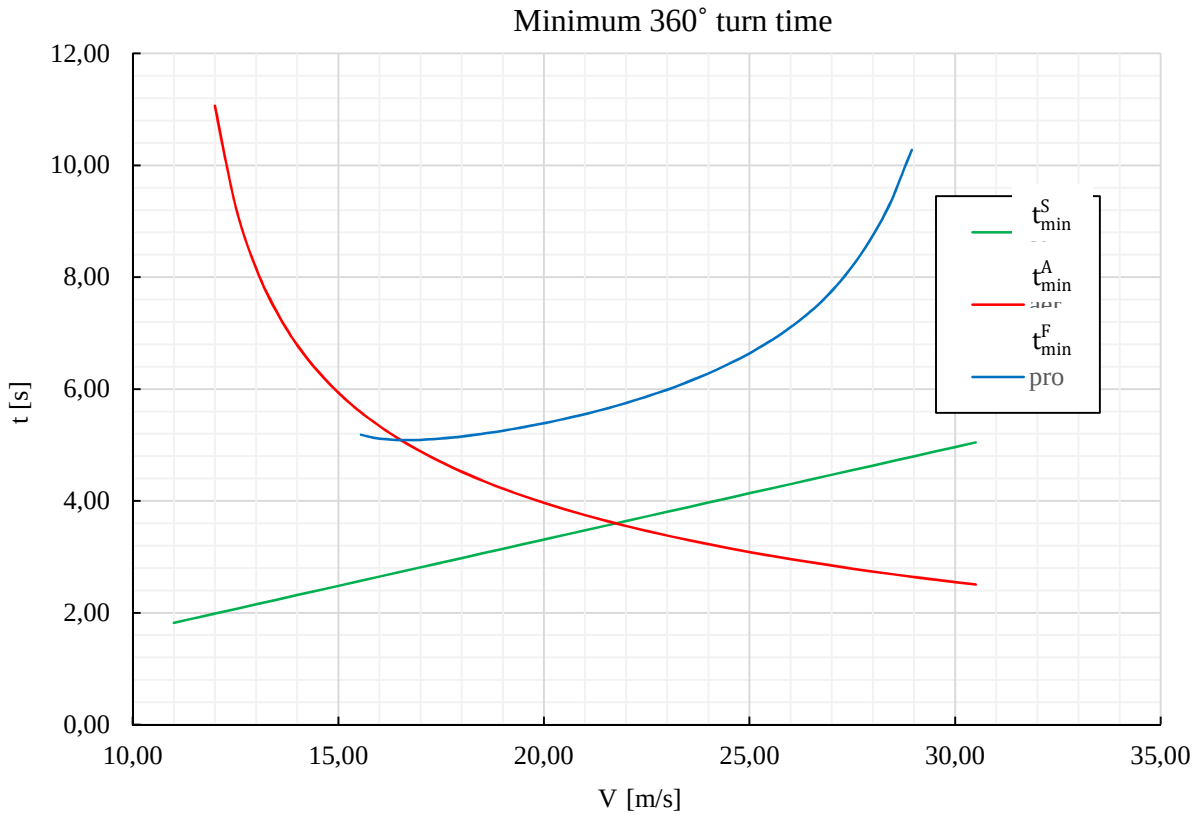

Fig. 6.11 Minimum time to perform 360 degrees turn

6.4 Ground roll start phase

The analysis of the ground roll distance was performed using equation 6.27 and aerodynamic polar, which was determined by the procedure mentioned in section 5.6 and was created with ground effect taken into account.

$$s_G = \frac{1}{g} \cdot \int_0^{V_{LOF}} \frac{V dV}{\frac{F_U}{G} - f - (C_D - f \cdot C_L)\frac{\rho \cdot V^2 \cdot S_W}{2 \cdot G}} \qquad \text{[2] (6.27)}$$

Analysis of ground-roll time was performed using equation 6.28.

$$t_G = \frac{1}{g} \cdot \int_0^{V_{LOF}} \frac{dV}{\frac{F_U}{G} - f - (C_D - f \cdot C_L)\frac{\rho \cdot V^2 \cdot S_W}{2 \cdot G}} \qquad \text{[2] (6.28)}$$

Speed V_{LOF}:

$$V_{LOF} = 1{,}15 \cdot V_S = 12{,}506\ m \cdot s^{-1}$$

Friction coefficient f, which is friction coefficient of landing gear was set to the value of 0,02, which corresponds to the surface of hard runway (concrete, asphalt) [2].

$$f = 0{,}02$$

The member of equation designated F stands for thrust of propulsion system. However, thrust of propulsion system is dependent on the flight speed. The dependence of usable thrust on flight speed was determined by fitting of usable thrust curve by polynomial function of fourth degree.

$$F_U = (-4{,}867966 \cdot 10^{-6}) \cdot V^4 + (5{,}084267 \cdot 10^{-4}) \cdot V^3 - (2{,}245088 \cdot 10^{-2}) \cdot V^2 + (2{,}365060 \cdot 10^{-2}) \cdot V + 1{,}806309 \cdot 10^{1} \quad (6.29)$$

Optimal lift coefficient C_L and drag coefficient C_D during ground roll phase had to be found. This was done from UAV polar with ground effect and from the condition of optimal lift coefficient (eq. 6.30).

$$\frac{\partial C_D}{\partial C_L} = f \quad [2] \ (6.30)$$

This could be seen in the figure 6.12 below.

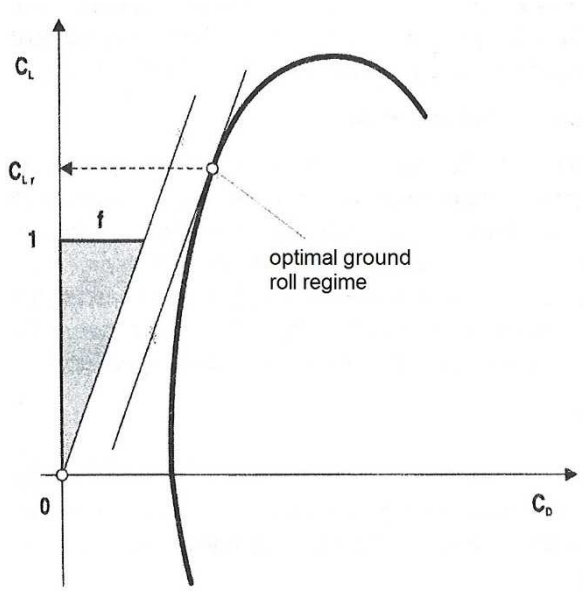

Fig. 6.12 Optimal ground roll regime [2]

After analysis of UAV polar with ground effect (see appendix A.3, Fig. A3.1) optimal lift and drag coefficient are.

$$C_L = 0{,}24$$
$$C_D = 0{,}0201$$

Finally after integration of equations 7.27 and 7.28 results are:

$$s_G = 51{,}888\ m$$
$$t_G = 7{,}966\ s$$

7 MASS AND BALANCE

Chapter brings a closer look at the calculation of weight and centre of gravity of the UAV.

7.1 Mass analysis

The tabular data below represents the weight of individual parts of the UAV and include their centre of gravity position and will be later used to determine the position of the centre of gravity of entire UAV. Zero X coordinate was placed at the front surface of the motor partition.

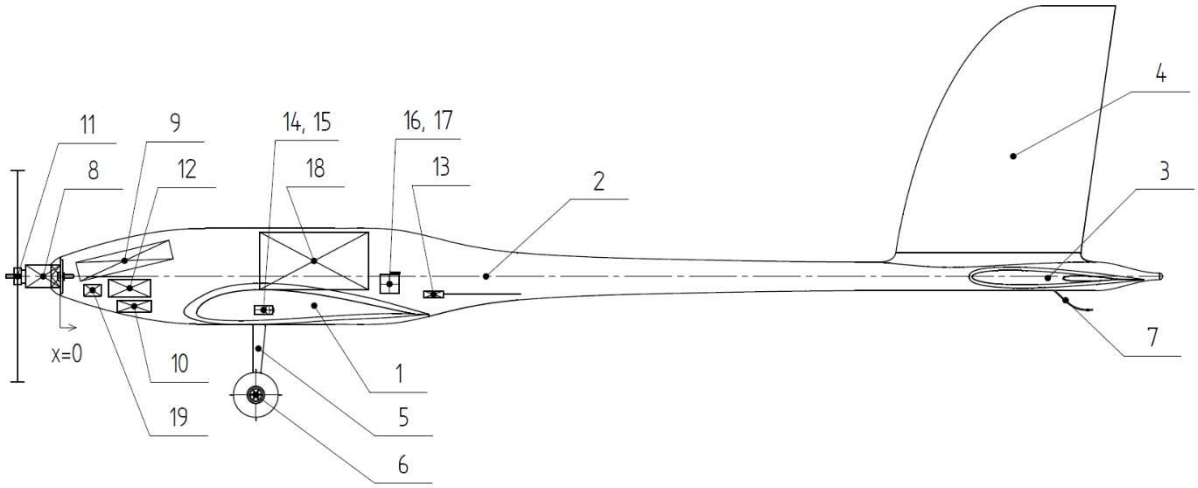

Fig. 7.1 Positions of individual masses

Position	Part	m [g]	x_{CG} [mm]	m· x_{CG} [g·mm]
1	Wing	988	396,8	392038,4
2	Fuselage	225	664,1	149422,5
3	Horizontal tail	159	1540,9	245003,1
4	Vertical tail	103	1487,0	153161,0

Tab. 7.1 Airframe mass group

Position	Part	m [g]	x_{CG} [mm]	m· x_{CG} [g·mm]
5	Shock absorber	20	308,9	6178,0
6	Wheels	52	304,8	15849,6
7	Tail skid	2	1568,6	3137,2

Tab. 7.2 Landing gear mass group

Position	Part	m [g]	x_{CG} [mm]	m· x_{CG} [g·mm]
8	Electric motor	181	-27,0	-4887,0
9	Motor battery	482	100,0	48200,0
10	Motor regulator	56	115,0	6440,0
11	Propeller	48	-67,0	-3216,0

Tab. 7.3 Propulsion unit mass group

Position	Part	m [g]	x_{CG} [mm]	m· x_{CG} [g·mm]
12	RX battery	165	108	17820,0
13	Receiver	6	582,0	3492,0
14	Left aileron servo motor	22	353,6	7779,2
15	Right aileron servo motor	22	353,6	7779,2
16	Elevator servo motor	22	513,5	11297,0
17	Rudder servo motor	22	513,5	11297,0

Tab. 7.4 Electronics mass group

Position	Part	m [g]	x_{CG} [mm]	m· x_{CG} [g·mm]
18	Payload	6775	395,67	2680664,3
19	Balance mass	150	50	7500,0

Tab. 7.5 Payload mass group

Empty weight of the UAV was calculated to be:

$$m_{oew} = 2{,}725\ kg$$

Maximum take-off weight:

$$m_{mtow} = 9{,}500\ kg$$

Payload weight:

$$m_{pld} = 6{,}775\ kg$$

7.2 Determination of centre of gravity

The position of UAV centre of gravity was calculated using equation 7.1.

$$x_{CG} = \frac{\sum_{i=1}^{i=17} m_i \cdot x_{CGi}}{\sum_{i=1}^{i=17} m_i} \tag{7.1}$$

After substitution into above mentioned equation:

$$x_{CG} = 395{,}7\ mm$$

Wing MAC has its most forward point at coordinate:

$$x_{fMAC} = 246{,}6\ mm$$

The difference between centre of gravity coordinate and MAC forward point coordinate, divided by MAC length is relative position of CG at MAC.

$$\overline{x_{CG}} = \frac{x_{CG} - x_{fMAC}}{c_{MAC}} \tag{7.2}$$

And finally after substitution:

$$\overline{x_{CG}} = 0{,}487765$$

This value is close to the value of UAV centre of gravity desired position on wing MAC, as defined in chapter 5.7. The difference is $4{,}1 \cdot 10^{-5}$. However, the centre of gravity position of UAV could be adjusted by moving the balance weight forward or backward or by changes in the balance weight mass if needed.

8 STRUCTURAL DESIGN

In this chapter, the structural design of UAV will be described. The main objective is the description of individual parts composition and creation of comprehensive view of the UAV structure. In the figure 8.1 below, UAV structure could be seen. In next chapters, individual subassemblies will be described.

Fig. 8.1 UAV internal structure

In table 8.1, the materials used in the UAV structure are described.

Material designation	Surface density [g/m^2]	Volume density [kg/m^3]	Material type	Material style	Material thickness [mm]
Style 458-1	55	-	Carbon	Linen	0,10
Style 447	160	-	Carbon	Linen	0,27
Style 405	375		Carbon	Linen	0,63
UD CS 600	600	-	Carbon	Two grids	0,75
UD CS 200	200	-	Carbon	Two grids	0,30
EE 23 P	23	-	Glass	Linen	0,032
RHC.51	-	52	ROHACELL	Foam	1-70
RHC.71	-	75	ROHACEL	Foam	3-60
LG 285	-	-	Epoxy resin	-	-
HG 285	-	-	Hardener	-	-

Tab. 8.1 Description of materials used [15]

8.1 Wing design

The wing structure composes of a front main wing spar, a back auxiliary wing spar (without flanges) and wing ribs. The wing cover is of a sandwich type. In the back part of the wing central segment is located partition with holes for screws, which are intended for the wing attachment to the fuselage. In front part of the wing central segment is located front wing to fuselage attachment. This joint is intended as two pins in two holes. The two pins are a part of the wing structure and fits into the holes made in the fuselage partition. The wing is attached to the fuselage by inserting the pins into the holes in fuselage partition and securing wing by the rear screw joint. The composition of individual wing parts is described under figure 8.2.

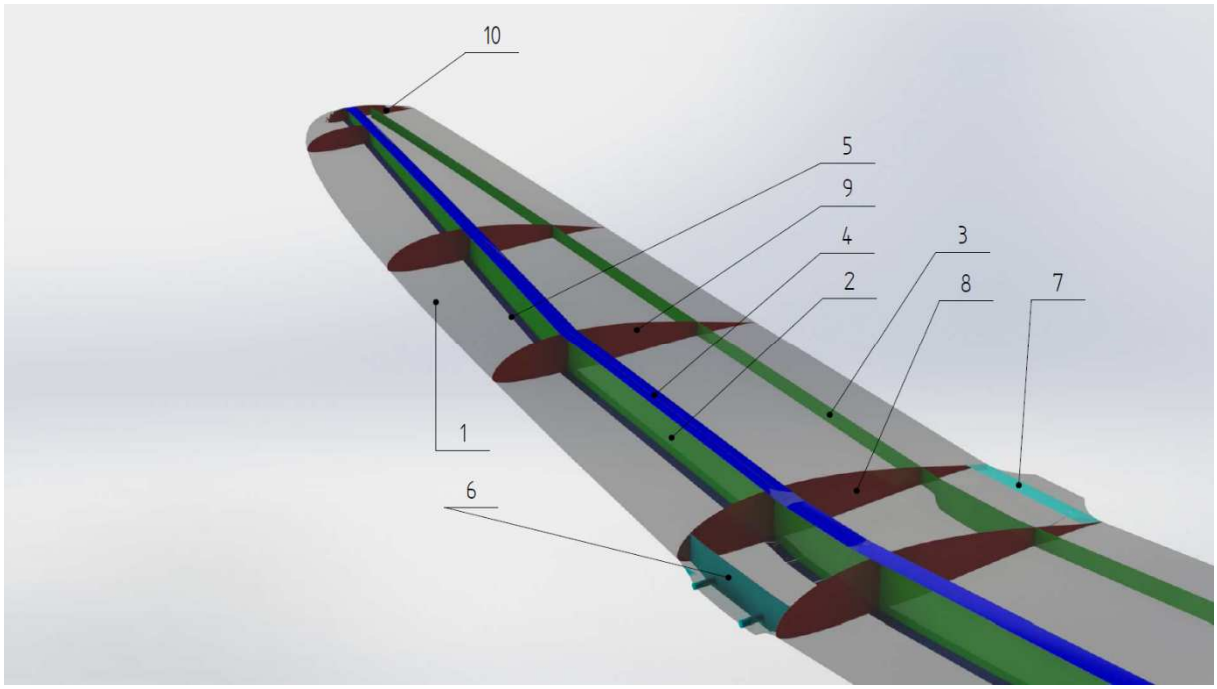

Fig. 8.2 Wing internal structure

Position	Part description
1	Wing covering
2	Wing main spar web
3	Wing auxiliary spar web
4	Wing main spar upper flange
5	Wing main spar lower flange
6	Front wing to fuselage attachment partition (wing part)
7	Rear wing to fuselage attachment (wing part)
8	Strengthened wing rib
9	Wing rib
10	Rib at the end of auxiliary wing spar

Tab. 8.2 Description of wing parts

Position	Layer 1	Layer 2	Layer 3	Layer 4	Layer 5
1	EE 23 P	Style 458-1	RHC.51 (2mm)	Style 458-1	-
2	Style 458-1	RHC.71 (3mm)	Style 458-1	-	-
3	Style 458-1	RHC.71 (3,0mm)	Style 458-1	-	-
4	UD CS 600	UD CS 600	-	-	-
5	UD CS 600	UD CS 600	-	-	-
6	Style 458-1	UD CS 600	UD CS 600	Style 458-1	-
7	Style 458-1	UD CS 600	UD CS 600	Style 458-1	-
8	Style 458-1	Style 458-1	RHC.71 (3,0 mm)	Style 458-1	Style 458-1
9	Style 458-1	RHC.51 (1,5 mm)	Style 458-1	-	-
10	Style 458-1	RHC.51 (1,5 mm)	Style 458-1	-	-

Tab. 8.3 Composition of individual wing parts

8.2 Fuselage design

The fuselage (Fig. 8.3, Fig. 8.4) structure is of a thin shell type. Inside the fuselage front part, a motor partition is placed. At the back part of the fuselage, partitions are placed to reinforce fuselage structure it the place of horizontal tail connection. Also a payload box is attached to the fuselage inner surface. In front of the fuselage, an engine partition is located. The fuselage is divided into two separate parts because of limited dimensions of the transportation box. The fuselage front part to the rear part connection is designed as tube on tube connection. This joint is secured against rotation by pin. The vertical stabiliser is an integral part of the fuselage back part structure. Inside the vertical stabiliser, the main and auxiliary spars are located. Both of them without flanges, only web. The vertical stabiliser covering is of the same type as the wing covering.

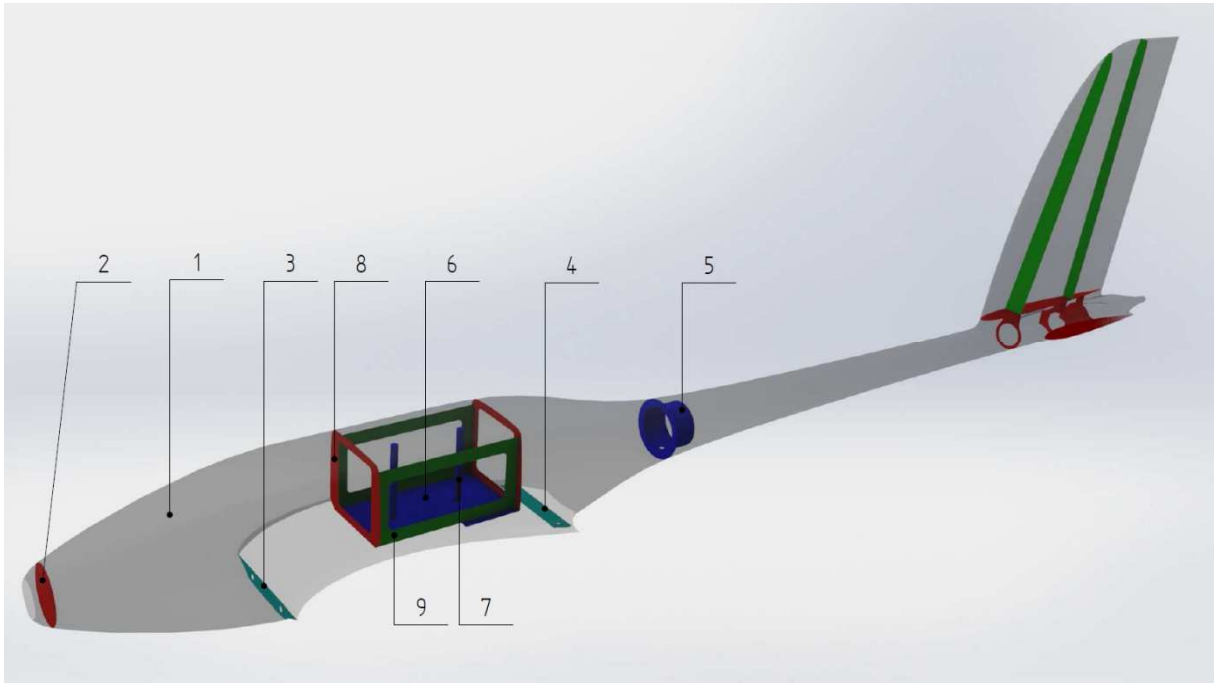

Fig. 8.3 Front fuselage segment

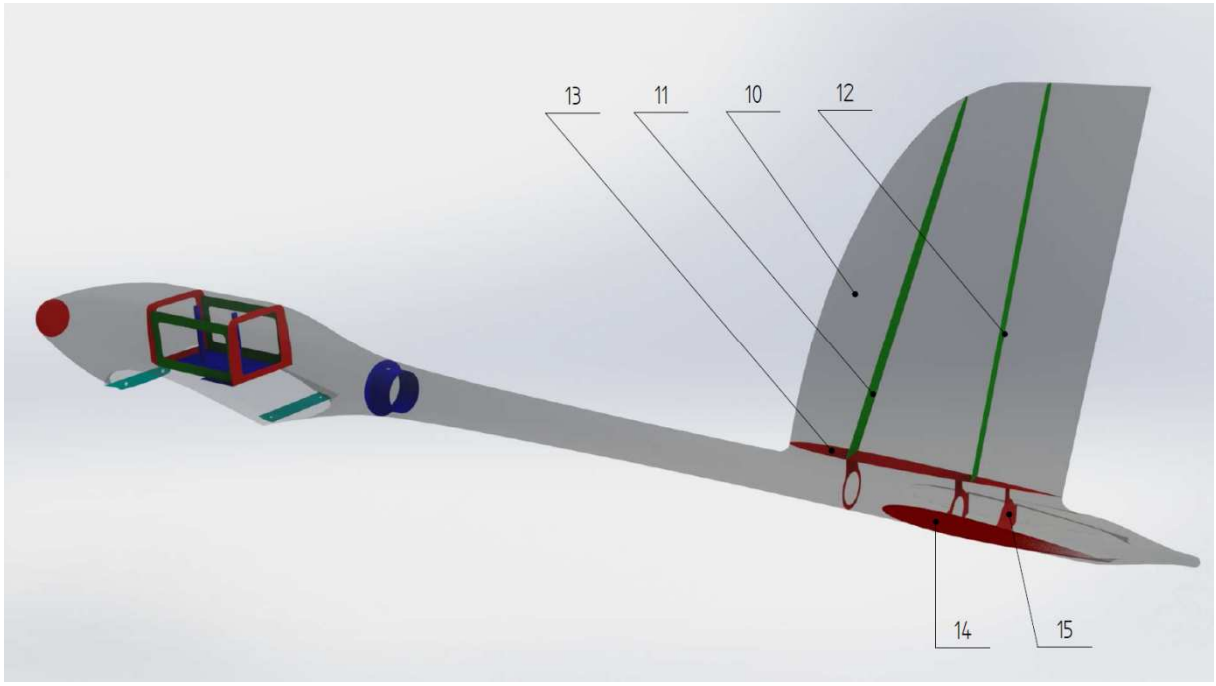

Fig. 8.4 Rear fuselage segment

Position	Part description
1	Fuselage covering
2	Electric motor partition
3	Front wing to fuselage attachment partition (fuselage part)
4	Rear wing to fuselage attachment (fuselage part)
5	Rear fuselage to front fuselage segment attachment
6	Payload box floor
7	Payload supports (pins)
8	Payload box partitions
9	Payload box ribs
10	Vertical stabiliser covering
11	Vertical stabilisers front spar (web only)
12	Vertical stabilisers rear spar (web only)
13	Vertical stabilisers strengthened rib
14	Fuselage to horizontal stabiliser rib
15	Back fuselage partitions

Tab. 8.4 Description of fuselage parts

Position	Layer 1	Layer 2	Layer 3	Layer 4	Layer 5
1	EE 23 P	Style 458-1	Style 458-1	Style 458-1	-
2	Style 458-1	UD CS 600	UD CS 600	Style 458-1	-
3	Style 458-1	UD CS 600	UD CS 600	Style 458-1	-
4	Style 458-1	UD CS 600	UD CS 600	Style 458-1	-
5	Style 458-1	UD CS 200	UD CS 200	UD CS 200	Style 458-1
6	Style 458-1	UD CS 600	UD CS 600	Style 458-1	-
7	Style 447	Style 447	Style 447	-	-
8	Style 458-1	RHC.51 (2,0mm)	Style 458-1	-	-
9	Style 458-1	RHC.51 (2,0mm)	Style 458-1	-	-
10	EE 23 P	Style 458-1	RHC.51 (2mm)	Style 458-1	-
11	Style 458-1	RHC.71 (3mm)	Style 458-1	-	-
12	Style 458-1	RHC.71 (3mm)	Style 458-1	-	-

13	Style 458-1	RHC.71 (3,0mm)	Style 458-1	-	-
14	Style 458-1	RHC.71 (3mm)	Style 458-1	-	-
15	Style 458-1	RHC.71 (3mm)	Style 458-1	-	-

Tab. 8.5 Composition of individual fuselage parts

8.3 Horizontal stabiliser

The horizontal stabiliser (Fig. 8.5) is of all flying type. The internal structure consist of inner, outer and two internal ribs connected by a spar with flanges. Covering of the horizontal stabiliser is of a similar type as the wing and vertical stabiliser covering. The horizontal stabiliser is intended to be attached to the fuselage by tube on tube type connection secured by the pin.

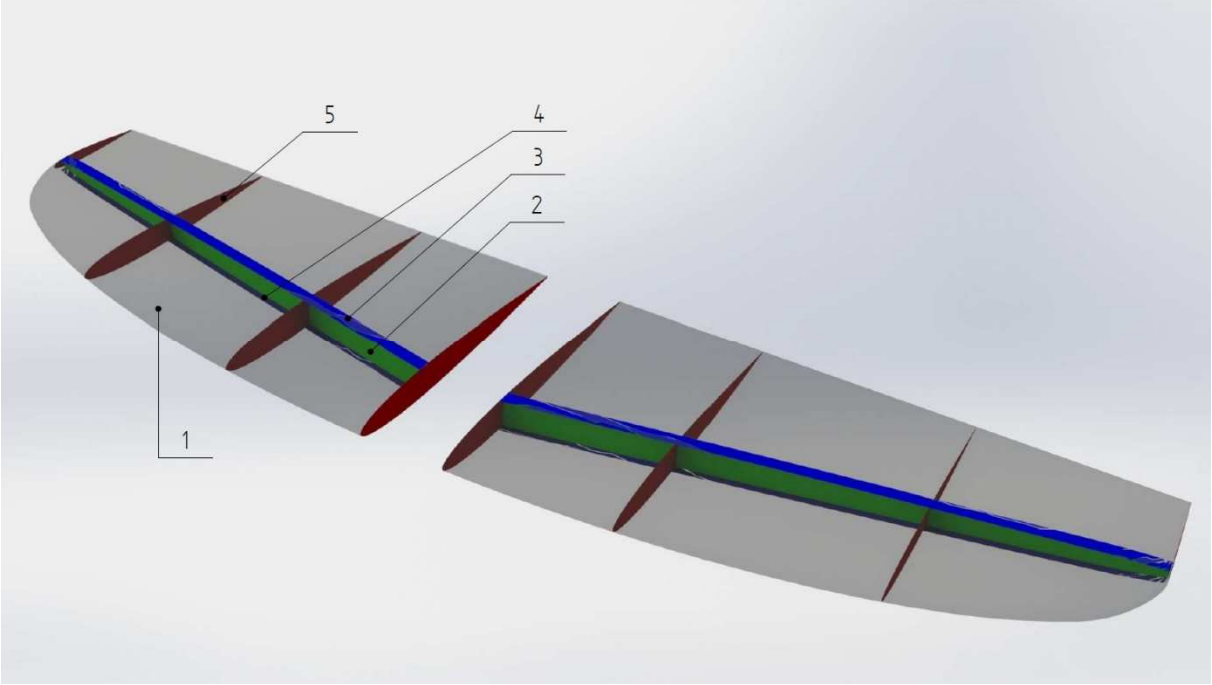

Fig. 8.5 Horizontal stabiliser internal structure

Position	Part description
1	Horizontal stabiliser covering
2	Horizontal stabiliser spar web
3	Horizontal stabiliser spar upper flange
4	Horizontal stabiliser spar lower flange
5	Horizontal stabiliser ribs

Tab. 8.6 Description of fuselage parts

Position	Layer 1	Layer 2	Layer 3	Layer 4	Layer 5
1	EE 23 P	Style 458-1	RHC.51 (2 mm)	Style 458-1	-
2	Style 458-1	RHC.71 (3,0 mm)	Style 458-1	-	-
3	UD CS 600	UD CS 600	UD CS 600	-	-
4	UD CS 600	UD CS 600	UD CS 600	-	-
5	Style 458-1	RHC.51 (1,5mm)	Style 458-1	-	-

Tab. 8.7 Composition of individual horizontal stabiliser parts

8.4 Landing gear

The landing gear consist of a solid spring type main landing gear (Fig. 8.6) and a tail skid (Fig. 8.7). Wheels are actually of a factory type, but there is possibility to change them by custom-made wheels with lower weight. A solid spring type shock absorber will be made of carbon fibres reinforced composite and attached to the wing spar using screws. The tail skid is also intended to be made of carbon fibre reinforced composite and to be attached to the fuselage rear partition.

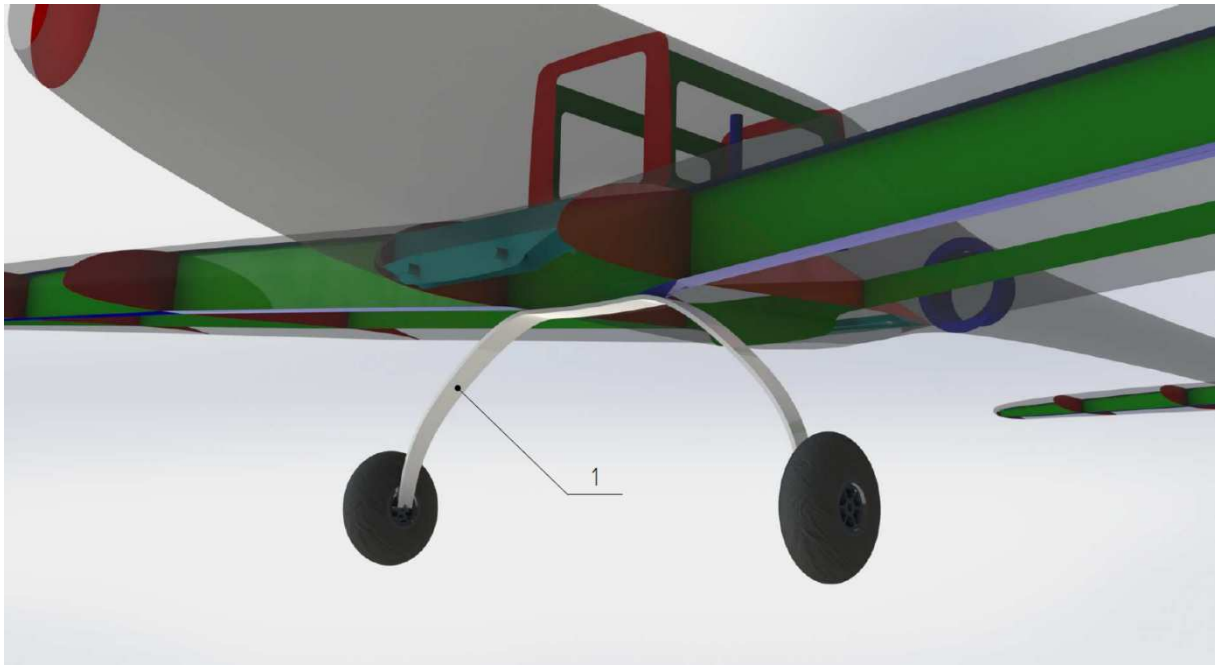

Fig. 8.6 Main landing gear shock absorber

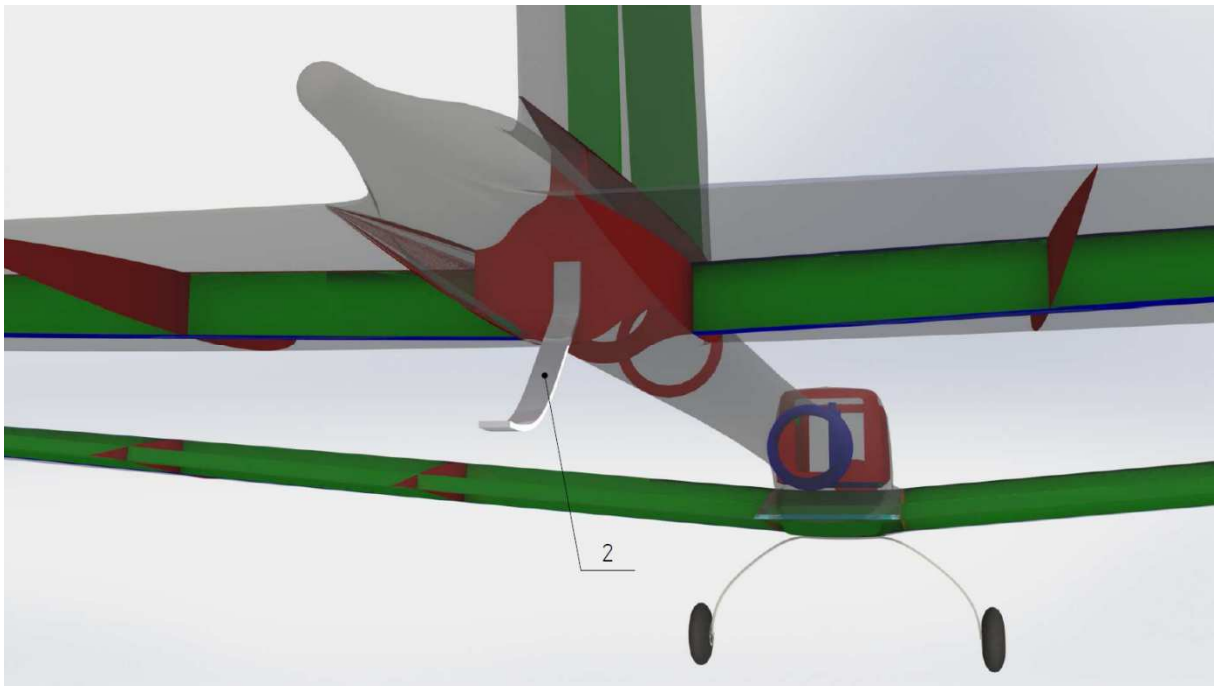

Fig. 8.7 Tail skid

Position	Layer 1	Layer 2	Layer 3	Layer 4	Layer 5
1	Style 458-1	Style 405	Style 405	Style 405	Style 458-1
2	Style 458-1	Style 405	Style 405	Style 458-1	-

Tab. 8.8 Composition of landing gear parts

9 PAYLOAD PREDICTION

The payload weight is based on the empty weight and MTOW of the UAV. Firstly, the MTOW dependence on the air density had to be found. Ground roll start phase mustn't be longer than 60 m. Because of that, payload dependence on the air density was defined by fixing ground roll length and calculation of MTOW for second value of air density. The first value was 1,130 kg·m^{-3} and the second one was defined to be 1,225 kg·m^{-3}. By calculation of MTOW for these two air density values, the linear dependence of payload on air density can be set.

The calculation of ground roll parameters was performed using UAV polar for start with ground effect (see appendix A.3, Fig A3.1) taken into account and usable thrust curve established for air density of 1,225 kg·m^{-3} (see appendix A.4, Tab. A4.1).

Usable thrust curve is defined by the polynomial:

$$F_U = (-5{,}357824 \cdot 10^{-6}) \cdot V^4 + (5{,}595891 \cdot 10^{-4}) \cdot V^3 - (2{,}471009 \cdot 10^{-2}) \cdot V^2 + (2{,}603053 \cdot 10^{-2}) \cdot V + 1{,}988076 \cdot 10^{1} \quad (9.1)$$

Using the same procedure as in chapter 7.4, following parameters of ground roll for air density of 1,225 kg·m^{-3} was calculated (Tab. 9.1).

Parameter	Designation	Value	Unit
Maximum take-off weight	MTOW	10,568	kg
Stall speed	V_S	11,016	m/s
Lift off speed	V_{LOF}	12,668	m/s
Friction coefficient	f	0,020	-
Lift coefficient	C_L	0,240	-
Drag coefficient	C_D	0,201	-
Ground roll distance	s_g	51,883	m
Ground roll time	t_g	7,965	s

Tab. 9.1 Take-off ground roll parameters for air density 1,225 kg·m^{-3}

In the following table 9.2, parameters needed for payload prediction dependence on air density are mentioned. Value of MTOW and payload for air density of 1,320 kg·m^{-3} was determined using linear function (eq. 9.2) to define payload and MTOW for air density value range of 1,225±0,095 kg·m^{-3}. For ACC 2015 competition, it is mandatory to define the payload weight prediction in form of linear function.

MTOW [kg]	Empty weight [kg]	Payload weight [kg]	Air density [kg·m^{-3}]
9,500	2,725	6,775	1,130
10,568	2,725	7,843	1,225
11,636	2,725	8,911	1,320

Tab. 9.2 Take-off ground roll parameters for air density

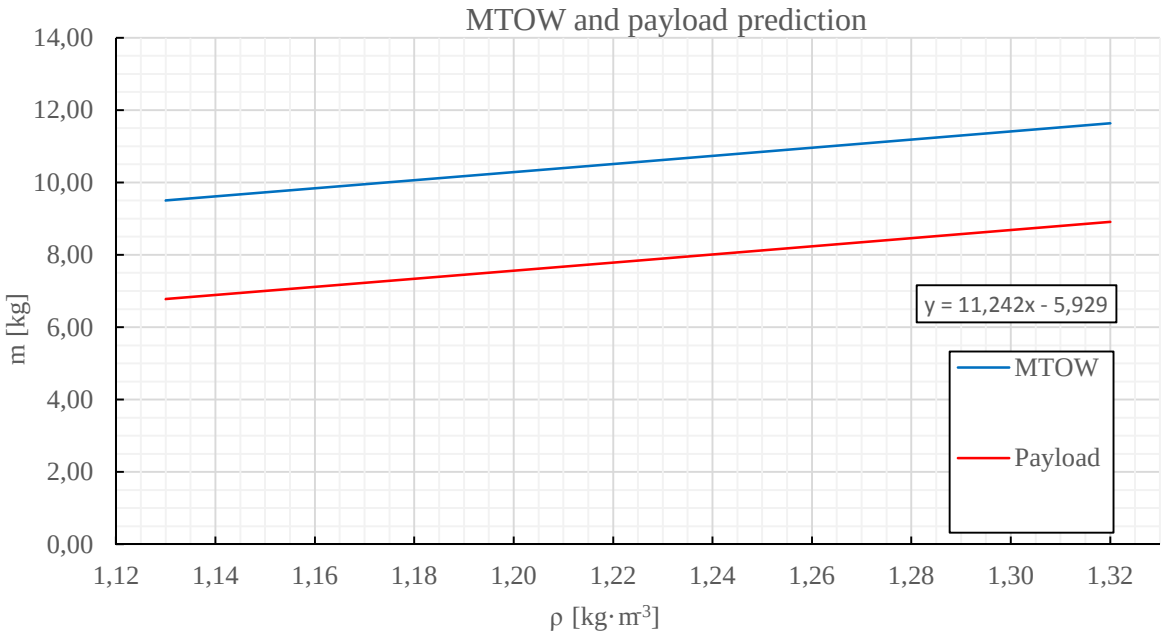

Fig. 9.1 Maximum take-off and payload weight dependence on air density

As shown in the figure 9.1 on the previous page, the payload is predicted to depend on air density in form of linear function:

$$m_{pld} = 11{,}242 \cdot \rho - 5{,}929 \tag{9.2}$$

10 CONCLUSION

In this bachelor's thesis, the conceptual design of a small UAV was performed. UAV, which was finally named FabricK, was designed to meet all requirements of the Air Cargo Challenge 2015 competition and to exceed this requirements mainly in the field of flight performance. From the beginning of the design process, the design was focused on creating an aircraft with the highest possible flight speed and at the same time capable of carrying a payload of at least 6 kg. This goal, which was set by the design team, was achieved by the maximum effort to minimize drag and empty weight of aircraft.

The specific of the FabricK aircraft is a flapless wing and the use of all flying elevator type. A flapless wing was chosen because of its lower weight compared to the wing with flaps. The decision of using of all flying elevator type was based on the requirement of high maneuverability, which will be helpful in the turning flight.

FabricK was designed to have wingspan of 3 meters, empty weight of 2,725 kg and maximum take-off weight of 9,5 kg.

Engine manufacturer recommends the maximum take-off weight of airplane models using AXI 2826/10 to be 3 kg. [17]

Even the maximum take-off weight of FabricK is three times higher, preliminary calculations shows that airplane will be able to lift-off after 51,9 meter long ground roll at speed of 12,5 m/s. Preliminary design calculations also suggest, that FabricK will be capable of steady climb with climb speed of 1,82 m/s while flight speed is 18,75 m/s. Maximum climb angle of 6,41˚ will be achieved at the flight speed of 13,9 m/s. Maximum speed calculated is 30,95 m/s and cruise speed has value of 22,2 m/s.

Last details of the design should be finalized until the end of the first half of June 2015. During the final improvements of the design, there will be intensive negotiations with sponsors of the project. At the same time, moulds for the parts construction will be prepared in form of 3D CAD models and further forwarded to the sponsors with machining capabilities. After finalisation of moulds, the actual construction of individual parts will begin.

Above mentioned flight performance and design parameters suggest that FabricK will be a strong competitor in the battle for victory in the Air Cargo Challenge 2015 competition.

BIBLIOGRAPHY

[1] BROŽ, Václav, DANĚK, Vladimír, FILAKOVSKÝ, Karol. *Základy aerodynamiky: učební texty dle předpisu JAR-66 studijní modul 8.* Brno: Akademické nakladatelství CERM, 2004. 163 p. ISBN 80-7204-316-1.

[2] DANĚK, Vladimír. *Mechanika letu I: letové výkony.* Vydání první. Brno: Akademické nakladatelství CERM, 2009. 293 p. ISBN 978-80-7204-659-1.

[3] DANĚK, Vladimír. *Mechanika letu II: letové vlastnosti.* Vydání první. Brno: Akademické nakladatelství CERM, 2011. 334 p. ISBN 978-80-7204-761-1.

[4] HOŘENÍ, Bohumír, LNĚNIČKA, Jaroslav. *Letecké modelářství a aerodynamika.* První vydání. Praha: Naše vojsko, 1977. 296 p.

[5] KELLER, Ladislav, et al. *Učebnice pilota 2006: pro žáky a piloty letounů a sportovních létajících zařízení, provozujících létání jako svou zájmovou činnost.* Vydání první. Cheb: Svět křídel, 2006. 696 p. ISBN 80-86808-28-9.

[6] LYON, Christopher A. *Summary of low-speed airfoil data: volume 3.* First printing. Virginia Beach, SoarTech Publications, 1997. 418 p. ISBN 0-9646747-3-4.

[7] MIKULA, Jan. *Konstrukce a projektování letadel II.* Vydání první. Praha: Nakladatelství ČVUT, 2005. 264 p. ISBN 80-01-03338-4.

[8] SEILIG, Michael S. *Summary of low-speed airfoil data: volume 1.* First printing. Virginia Beach, SoarTech Publications, 1995. 292 p. ISBN 0-9646747-1-8.

[9] SLAVÍK, Svatomír, et al. *Aerodynamika, konstrukce a systémy letadel: učební texty dle předpisu JAR-66 studijní modul 13.* Brno: Akademické nakladatelství CERM, 2005. 450 p. ISBN 80-7204-395-1.

[10] SLAVÍK, Svatomír, et al. *Aerodynamika, konstrukce a systémy letounů: učební texty dle předpisu JAR-66 studijní modul 11.* Brno: Akademické nakladatelství CERM, 2005. 600 p. ISBN 80-7204-367-6.

[11] JANOVEC, Jan, LNĚNIČKA, Jaroslav. Ocasní plochy letadel: i jejich modelů. *Akademie letectví* [online]. Published: 31.8.2008, 2008, 5, revised: 5.5.2008 [cit. 2015-04-18]. Available from: < http://www.airspace.cz/akademie/rocnik/2008/05/ocasni_plochy.php>.

[12] *acc2013.ubi.pt* [online]. 2015 [cit. 2015-05-12]. Available from: < http://acc2013.ubi.pt/>

[13] *Aerodynamika* [online]. [cit. 2015-04-15]. Available from: <http://lu.fme.vutbr.cz/ucebnice/opory/aerodynamics.php>.

[14] *Electric engines power small Unmanned Aerial Vehicles | Embedded content form Electronic Design* [online]. 4/2010 [cit. 2015-05-12]. Available from: <http://electronicdesign.com/embedded/uavs-conquer-skies>

[15] *Grm-systems.cz* [online]. 2015 [cit. 2015-05-02]. Available from: < http://www.grm-systems.cz/>.

[16] *Internet shop for Chargers (Pulsar), Planes, Pilots, Propellers, etc.* [online]. [cit. 2015-05-12]. Available from: <http://www.pp-rc.de/?shop=pp-rc_en>

[17] *Model motors s.r.o. – modelářské elektromotory AXI, Mini AC, VM* [online]. 2006 [cit. 2015-04-13]. Available from: <http://www.modelmotors.cz/>.

[18] *RC Rubekon 4376-k22 explorer 1500 motor glider kit* [online]. 2009 [cit. 2015-05-12]. Available from: < http://www.ruberkon.com/4367k22-explorer-1500-motor-glider.html >

[19] *Regulations for the Air Cargo Challenge 2015 in Stuttgart: European edition* [online]. Version 1.00, 2014-10-20 [cit. 2015-04-21]. 35 p. (PDF). Available from: < http://www.acc2015.com/inhalt/regulations/ACC2015_Regulations_V1_00.pdf>.

[20] SLAVĚTÍNSKÝ, Dušan. *O letadlech – Dušan Slavětínský starší – obecná geometrie křídla* [online]. 12/2010 [cit. 2015-04-15]. Available from: < http://www.slavetind.cz/stavba/konstrukce/kridlo/Kridlo-obecnageometrie.aspx>.

[21] *Staufenbiel Modellbau Shop – R/C Modellbau günstick online kaufen* [online]. [cit. 2015-05-12]. Available from: <http://www.modellhobby.de/>

[22] *TOP modeltechnik | The flying experience….* [online]. [cit. 2015-05-12] Available from: < http://topmodeltehnik.com/ >

[23] *Weather Forecast & Reports – Long Range &Local | Wunderground | Weather Underground* [online]. 2015 [cit. 2015-05-12]. Available from: <http://www.wunderground.com/>

[24] SILVAGNI, Mario. *AXI 2826-10 GOLD – Test Results – 090704.* 2009-07-04. 3 p. (PDF).

LIST OF FIGURES

LIST OF TABLES

LIST OF SYMBOLS AND ACRONYMS

Symbol	Description	Unit
$\overline{S_V}$	Vertical tailplane relative area	-
$\overline{S_H}$	Horizontal tailplane relative area	-
$\overline{b_{0H}}$	Relative root airfoil thickness of horizontal tailplane	%
$\overline{b_{TH}}$	Relative tip airfoil thickness of horizontal tailplane	%
$\overline{b_{HMAC}}$	Vertical tailplane relative thickness at place of mean aerodynamic chord	%
$\overline{S_A}$	Aileron relative area	-
$\overline{S_E}$	Relative elevator area	-
$\overline{d_F}$	Relative diameter of fuselage	-
$\overline{x_F}$	Relative position of UAV aerodynamic centre	-
$\overline{x_{SM}}$	Relative value of static margin	-
$\overline{x_{CG}}$	Relative position of the UAV centre of gravity	-
μ	Dynamic viscosity	$Pa \cdot s$
a	Speed of sound	$m \cdot s^{-1}$
a	UAV lift curve slope	rad^{-1}
A.C.	Aerodynamic centre	-
A_{ax}	Position of aileron axis in % of wing mean aerodynamic chord	%
A_H	Horizontal tail volume	-
a_H	Horizontal tail lift curve slope	rad^{-1}
AR	Aspect ratio	-
AR_H	Horizontal tailplane aspect ratio	-
AR_V	Vertical tailplane aspect ratio	-
AR_W	Wing aspect ratio	-
A_V	Vertical tail volume	-
a_W	Wing lift curve slope	rad^{-1}
c	Chord length	mm
c_{0H}	Horizontal tailplane root chord	mm
c_{0V}	Vertical tailplane root chord	mm
c_{0W}	Wing root chord length	mm
c_A	Aileron depth	mm
C_D	Drag coefficient	-

C_{DF}	Fuselage drag coefficient	-
C_{DH}	Horizontal tail drag coefficient	-
C_{DP}	Parasite drag coefficient	-
C_{DSa}	Shock absorber drag coefficient	-
C_{DV}	Vertical tail drag coefficient	-
C_{DW}	Wing drag coefficient	-
C_{DWh}	Wheel drag coefficient	-
c_{HMAC}	Horizontal tail mean aerodynamic chord length	mm
C_L	Lift coefficient	-
C_{LH}	Horizontal tail lift coefficient	-
C_{Lmax}	Maximum lift coefficient	-
C_{LW}	Wing lift coefficient	-
c_{MAC}	Mean aerodynamic chord length	mm
c_R	Depth of rudder	mm
C_R	Drag coefficient of flat plate	-
c_{TH}	Horizontal tailplane tip chord	mm
c_{TV}	Vertical tailplane tip chord	mm
c_{TW}	Wing tip chord length	mm
c_{VMAC}	Vertical tail mean aerodynamic chord length	mm
D	Factor of washout angle dependence on angle of attack	-
D	Drag force	N
d_{Fmax}	Maximum diameter of fuselage	mm
E_{ax}	Position of elevator axis in % of vertical tailplane mean aerodynamic chord	%
F	Thrust force	N
f	Start strip friction coefficient	-
F_i	Interference drag correction factor	-
F_R	Required thrust force	N
F_U	Usable thrust force	N
g	Acceleration of gravity	$m \cdot s^{-2}$
G	UAV force of gravity	N
L	Lift force	N
l_A	Length of aileron	mm
l_E	Elevator length	mm
l_F	Fuselage length	mm
L_H	Horizontal tailplane arm	m
l_H	Horizontal tailplane span	mm

l_R	Length of rudder	mm
l_V	Vertical tailplane span	mm
L_V	Vertical tailplane arm	m
l_W	Wingspan	m
l_{Wmt}	Maximum theoretical wingspan	m
m	mass	kg
MAC	Mean aerodynamic chord	-
m_{MTOW}	Maximum take-off weight	kg
m_{oew}	Operational empty weight	kg
m_{pld}	Payload weight	kg
MTOW	Maximum take-off weight	-
M_x	Banking moment	N·m
m_{z0W}	Wing moment coefficient around its quarter MAC point	-
n^A_{max}	Aerodynamical limited load factor	-
n^F_{max}	Propulsion limited load factor	-
n^S_{max}	Structural limited load factor	-
P_R	Required power	W
P_U	Usable power	W
r^A_{min}	Minimal radius of aerodynamical limited turn	m
R_{ax}	Position of rudder axis in % of vertical tailplane mean aerodynamic chord	%
Re_F	Fuselage Reynolds number	-
r^F_{min}	Minimal radius of propulsion limited turn	m
r^S_{min}	Minimal radius of structural limited turn	m
S	Area	m^2
S_A	Aileron area	mm^2
S_{DF}	Fuselage wetted area	m^2
S_{DSa}	Shock absorber wetted area	m^2
S_{DWh}	Wheel frontal area	m^2
S_E	Elevator area	mm^2
s_G	Ground roll distance	m
S_H	Horizontal tailplane area	m^2
S_R	Rudder area	mm^2
S_V	Vertical tailplane area	m^2
S_W	Wing area	m^2
t^A_{min}	Minimal time to perform 360˚ aerodynamical limited turn	m
t^F_{min}	Minimal time to perform 360˚ limited turn	m

t_G	Ground roll time	s
t^S_{min}	Minimal time to perform 360˚ structural limited turn	m
UAV	Unmanned aerial vehicle	-
V	Flight speed	$m \cdot s^{-1}$
V_{ao}	Resulting speed on wing in lateral direction	$m \cdot s^{-1}$
V_{cr}	Cruise speed	$m \cdot s^{-1}$
V_{ec}	Economic flight speed	$m \cdot s^{-1}$
V_H	Horizontal component of speed	$m \cdot s^{-1}$
V_{inf}	Speed of the stream unaffected by the UAV	$m \cdot s^{-1}$
V_{LOF}	Lift-off speed	$m \cdot s^{-1}$
V_{max}	Maximum flight speed	$m \cdot s^{-1}$
V_{min}	Minimum flight speed	$m \cdot s^{-1}$
V_{opt}	Optimum flight speed	$m \cdot s^{-1}$
V_S	Stall speed	$m \cdot s^{-1}$
V_V	Vertical component of speed	$m \cdot s^{-1}$
V_{Wmax}	Flight speed for maximum climb speed	$m \cdot s^{-1}$
$V_{\gamma max}$	Flight speed for maximum angle of climb	$m \cdot s^{-1}$
w	Climb speed	$m \cdot s^{-1}$
w_{max}	Maximum climb speed	$m \cdot s^{-1}$
x	Leading edge longitudinal coordinate	mm
x_{CG}	Centre of gravity x coordinate	mm
x_{fMAC}	Most forward point of wing MAC x coordinate	mm
x_{HMAC}	Horizontal tail mean aerodynamic chord leading edge point position	mm
x_{MAC}	Mean aerodynamic chord leading edge point position	mm
x_{VMAC}	Vertical tail mean aerodynamic chord leading edge point position	mm
y	Spanwise coordinate	mm
y_{HMAC}	Horizontal tail mean aerodynamic chord spanwise position	mm
y_{MAC}	Mean aerodynamic chord spanwise position	mm
y_{VMAC}	Vertical tail mean aerodynamic chord spanwise position	mm
α	Angle of attack	˚
α_{cr}	Cruise angle of attack	˚
α_{crit}	Critical angle of attack	˚
α_{ec}	Economic angle of attack	˚
α_H	Horizontal tail angle of attack	˚
α_{opt}	Optimal angle of attack	˚
α_{per}	Permitted angle of attack	˚

α_W	Wing angle of attack	°
Γ	Dihedral angle	°
γ	Angle of climb	°
Γ_H	Horizontal tailplane dihedral angle	°
γ_{max}	Maximum angle of climb	°
Γ_W	Wing dihedral angle	°
δ	Angle of deflection	°
$\Delta\overline{x_{FH}}$	Change of the UAV aerodynamic centre due to influence of horizontal tailplane	-
δ_A	Aileron deflection	°
ΔC_{LW}	Wing lift coefficient deviation	-
δ_E	Elevator deflection	°
ΔF	Thrust surplus	N
ΔL_H	Increment of horizontal tail lift	N
ΔL_W	Increment of wing lift	N
ΔP	Power surplus	W
δ_R	Rudder deflection	°
ε	Washout angle	°
ε_w	Washout angle	°
Λ	Angle of sweep	°
ν	Kinematic viscosity	$m^2 \cdot s^{-1}$
ρ	Air density	$kg \cdot m^{-3}$
τ	Factor of wing planform shape	-
φ	Adjustment angle	°
Φ	Bank angle	°
Φ^A_{max}	Maximum bank angle in aerodynamical limited load factor	°
Φ^F_{max}	Maximum bank angle in propulsion limited load factor	°
φ_H	Horizontal tailplane angle of incidence	°
Φ^S_{max}	Maximum bank angle in structural limited load factor	°
φ_W	Wing angle of incidence	°
ω_x	Angular velocity of banking	$rad \cdot s^{-1}$

LIST OF APPENDICES

APPENDICES

A.1 Conceptual design figures

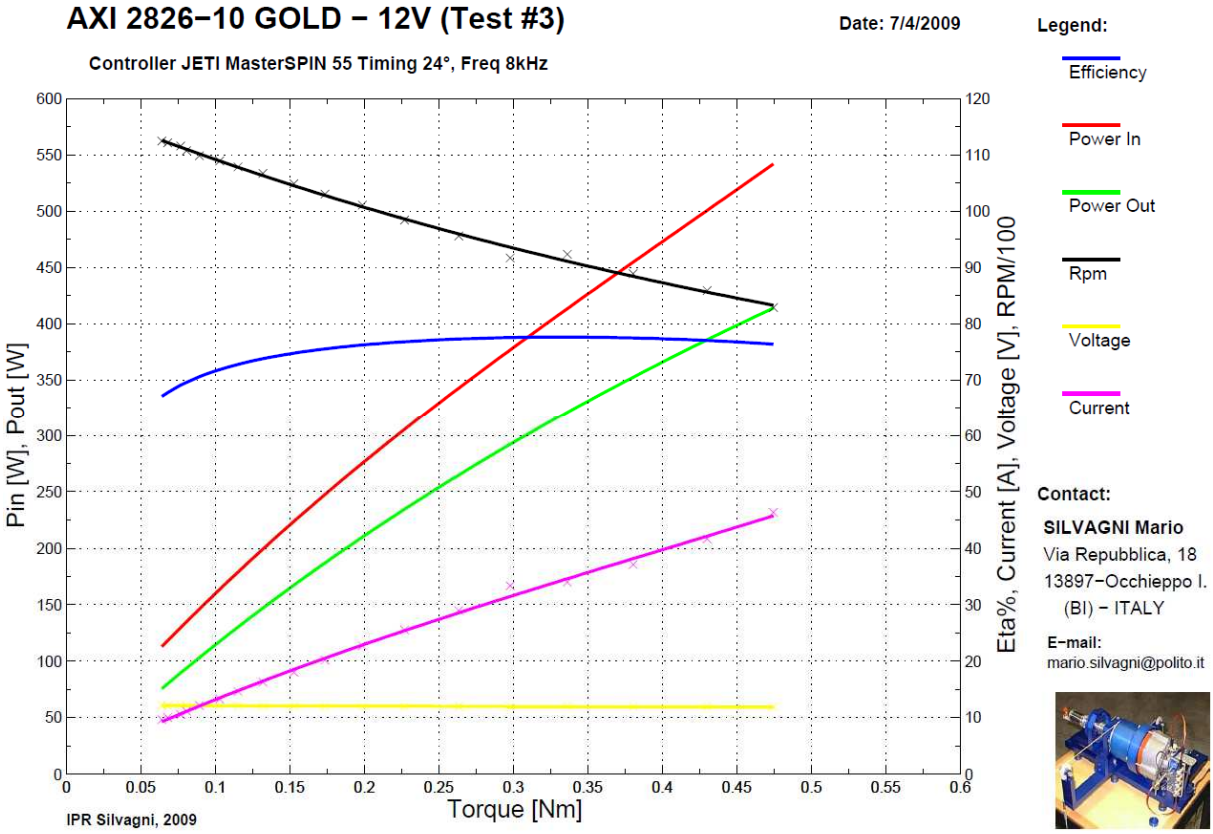

Fig. A1.1 AXI 2826/10 Electric motor characteristics [24]

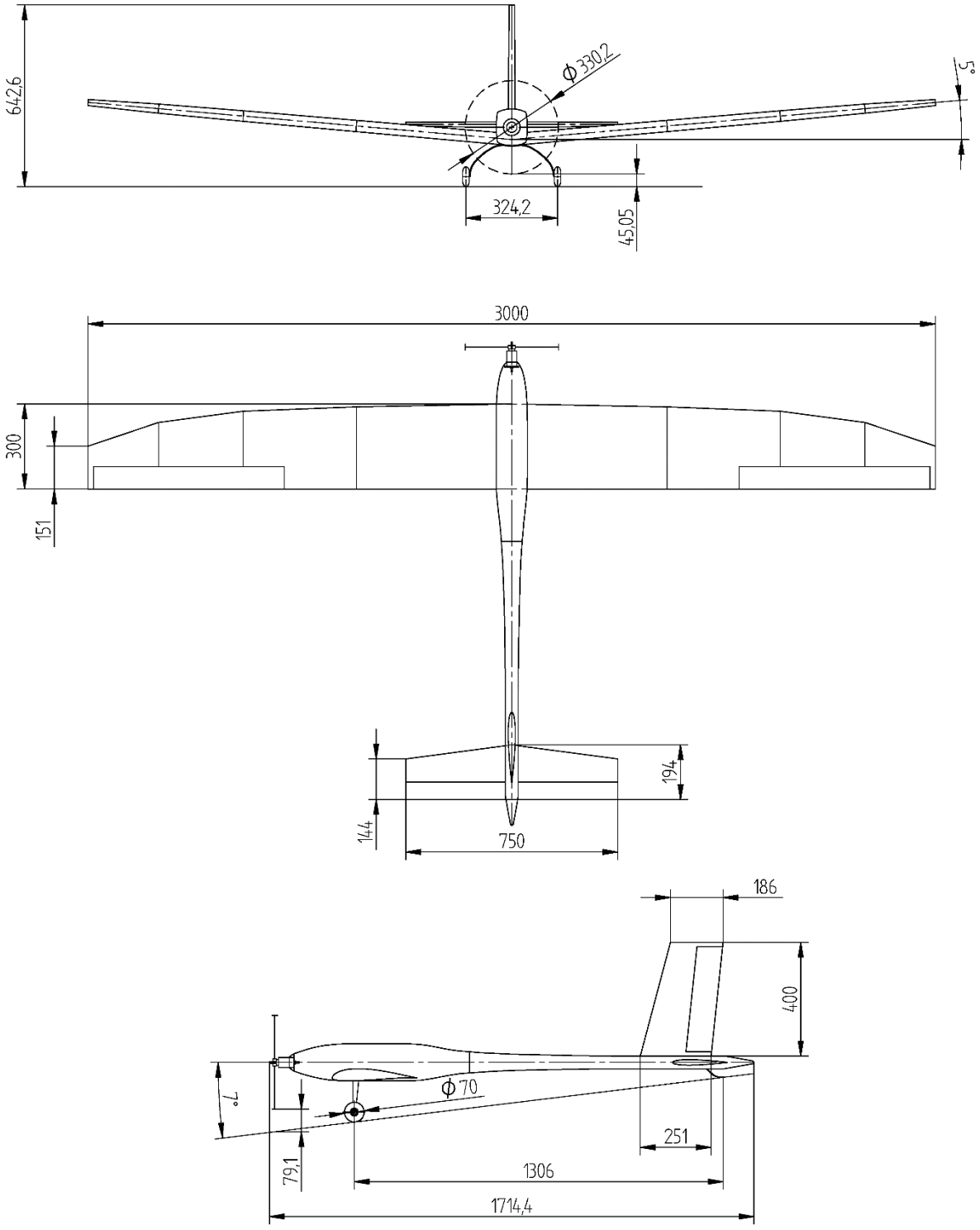

Fig. A1.2 Concept sketch of FabricK UAV

A.2 Aerodynamic coefficients

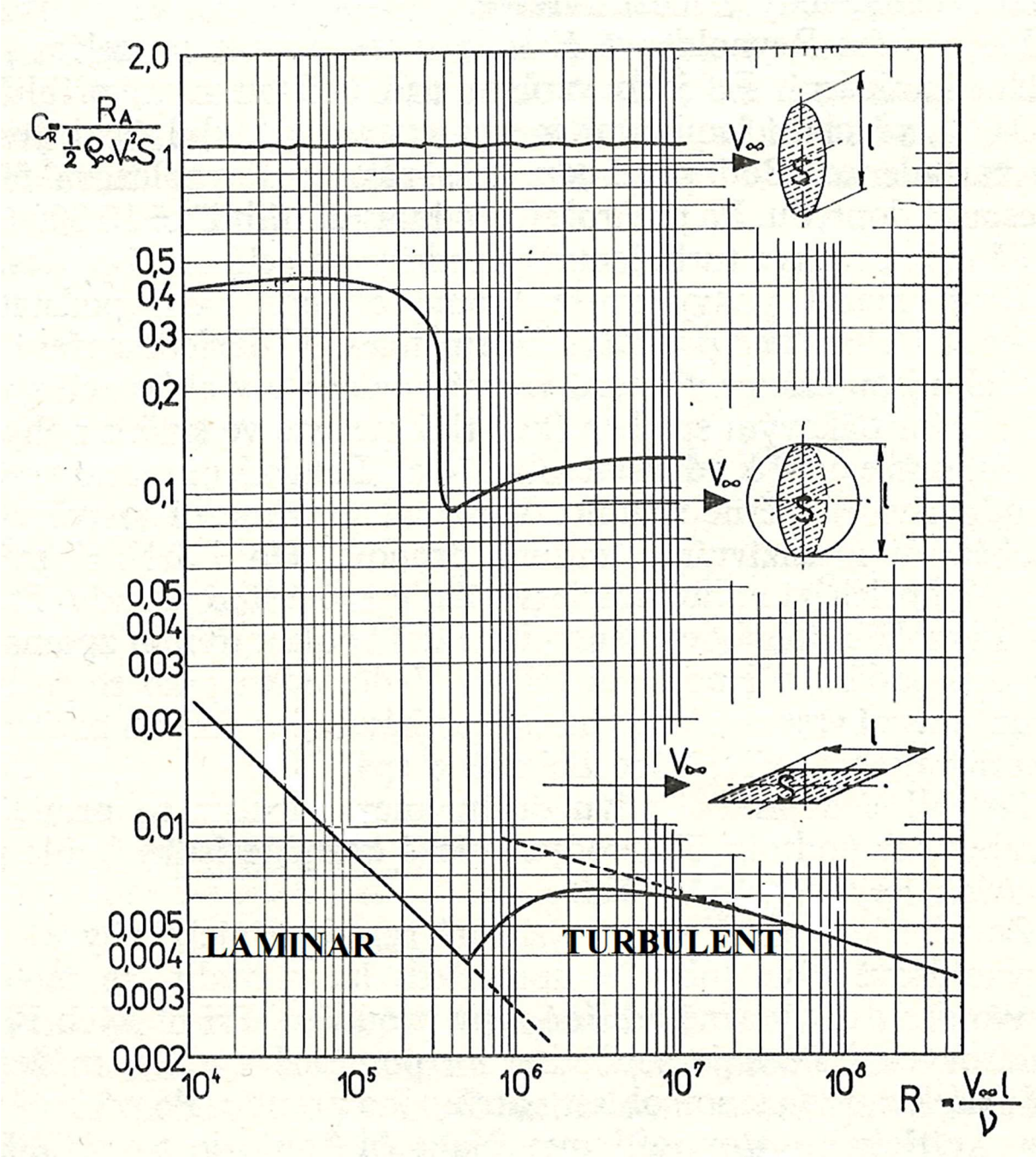

Fig. A2.1 Aerodynamic coefficients of three simple bodies [4]

A.3 Aerodynamic data

Wing AOA α_W [˚]	Wing lift coefficient C_{LW} [-]	Horizontal stab. AOA α_H [˚]	Horizontal stab. Lift coefficient C_{LH} [-]
0,0	0,2749937	0,0	-6,84E-17
0,4	0,3105017	0,4	0,02705925
0,8	0,3460275	0,8	0,05418271
1,2	0,3815461	1,2	0,08141177
1,6	0,4170323	1,6	0,1087602
2,0	0,4524585	2,0	0,1362309
2,4	0,4877816	2,4	0,1638222
2,8	0,5229515	2,8	0,1915308
3,2	0,5582332	3,2	0,2193531
3,6	0,593508	3,6	0,2472853
4,0	0,6287042	4,0	0,275324
4,4	0,6638738	4,4	0,3034664
4,8	0,6990257	4,8	0,3317095
5,2	0,7341625	5,2	0,3600511
5,6	0,7693119	5,6	0,3884888
6,0	0,8044862	6,0	0,4170208
6,4	0,8396608	6,4	0,445645
6,8	0,8748846	6,8	0,4743598
7,2	0,9101094	7,2	0,5031634
7,6	0,9453804	7,6	0,5320542
8,0	0,9806645	8,0	0,5610307
8,4	1,015978	8,4	0,5900913
8,8	1,051321	8,8	0,6192347
9,2	1,086676	9,2	0,6484594
9,6	1,122064	9,6	0,677764
10,0	1,157469	10,0	0,7071472

Tab. A3.1 Wing and horizontal stabiliser lift curves data

Wing AOA α_W [˚]	Wing moment coefficient m_{z0W} [-]	Wing AOA α_W [˚]	Wing moment coefficient m_{z0W} [-]
-5,0	-0,094748	3,0	-0,093664
-4,6	-0,092859	3,4	-0,095302
-4,2	-0,091192	3,8	-0,097036
-3,8	-0,089723	4,2	-0,098866
-3,4	-0,088456	4,6	-0,100801
-3,0	-0,087386	5,0	-0,102844
-2,6	-0,086517	5,4	-0,105001
-2,2	-0,085855	5,8	-0,107257
-1,8	-0,085405	6,2	-0,109620
-1,4	-0,085160	6,6	-0,112080
-1,0	-0,085121	7,0	-0,114633
-0,6	-0,085282	7,4	-0,117273
-0,2	-0,085630	7,8	-0,119993
0,2	-0,086150	8,2	-0,122785
0,6	-0,086831	8,6	-0,125643
1,0	-0,087664	9,0	-0,128559
1,4	-0,088638	9,4	-0,131525
1,8	-0,089739	9,8	-0,134534
2,2	-0,090951	10,2	-0,137577
2,6	-0,092251		

Tab. A3.2 Wing moment coefficient data

Plane AOA α [˚]	Horizontal flight C_L [-]	Horizontal flight C_D [-]	Turning flight C_L [-]	Turning flight C_D [-]
-5,0	-	-	-0,231671	0,024256
-4,6	-	-	-0,192538	0,022779
-4,2	-	-	-0,153459	0,021507
-3,8	-	-	-0,114433	0,020408
-3,4	-	-	-0,075453	0,019489
-3,0	-	-	-0,036511	0,018753
-2,6	0,000000	0,002704	0,002402	0,018164
-2,2	0,041301	0,014697	0,041301	0,017635
-1,8	0,080203	0,015242	0,080203	0,017198
-1,4	0,119125	0,015581	0,119125	0,016924
-1,0	0,158078	0,015883	0,158078	0,016783
-0,6	0,197067	0,016228	0,197067	0,016776
-0,2	0,236084	0,016672	0,236084	0,016936
0,2	0,275126	0,017283	0,275126	0,017280
0,6	0,314209	0,017629	0,314209	0,017364
1,0	0,352963	0,019038	0,352963	0,018519
1,4	0,392482	0,020078	0,392482	0,019309
1,8	0,431550	0,021282	0,431550	0,020287
2,2	0,471043	0,022596	0,471043	0,021384
2,6	0,510191	0,023946	0,510191	0,022543
3,0	0,549297	0,025438	0,549297	0,023861
3,4	0,588576	0,027078	0,588576	0,025297
3,8	0,627814	0,028887	0,627814	0,026860
4,2	0,667026	0,030835	0,667026	0,028590
4,6	0,706238	0,032913	0,706238	0,030468
5,0	0,745477	0,035113	0,745477	0,032479
5,4	0,784770	0,037439	0,784770	0,034626
5,8	0,824085	0,039880	0,824085	0,036900
6,2	0,863476	0,042451	0,863476	0,039302
6,6	0,902905	0,045139	0,902905	0,041831
7,0	0,942408	0,047945	0,942408	0,044483
7,4	0,981956	0,050885	0,981956	0,047258
7,8	1,021582	0,053962	1,021582	0,050159
8,2	1,061249	0,057177	1,061249	0,053183
8,6	1,100993	0,060538	1,100993	0,056341
9,0	1,140783	0,064040	1,140783	0,059629
9,4	1,180630	0,067694	1,180630	0,063051
9,8	1,220538	0,071508	1,220538	0,066612
10,2	1,260491	0,075486	1,260491	0,070315

Tab. A3.3 UAV Polars data for horizontal and turning flight

Plane AOA α [°]	Start C_L [-]	Start C_D [-]
-5,0	-0,262255	0,038623
-4,6	-0,217775	0,032318
-4,2	-0,173399	0,029080
-3,8	-0,129121	0,027405
-3,4	-0,084934	0,025269
-3,0	-0,040829	0,024092
-2,6	0,003208	0,023019
-2,2	0,047195	0,021958
-1,8	0,091152	0,021189
-1,4	0,135101	0,020615
-1,0	0,179058	0,020256
-0,6	0,223029	0,020113
-0,2	0,267011	0,020167
0,2	0,311002	0,020392
0,6	0,355050	0,020616
1,0	0,398630	0,021226
1,4	0,443229	0,021819
1,8	0,487197	0,022530
2,2	0,531789	0,023354
2,6	0,575925	0,024168
3,0	0,619993	0,025186
3,4	0,664205	0,026327
3,8	0,708374	0,027559
4,2	0,752524	0,028885
4,6	0,796690	0,030300
5,0	0,840917	0,031818
5,4	0,885247	0,033456
5,8	0,929666	0,035203
6,2	0,974255	0,037067
6,6	1,019002	0,039045
7,0	1,063983	0,041156
7,4	1,109214	0,043440
7,8	1,154790	0,045913
8,2	1,200753	0,048524
8,6	1,247246	0,051288
9,0	1,294387	0,054267
9,4	1,342387	0,057577

Tab. A3.4 UAV Polar data for start (with ground effect at h=0,25 m)

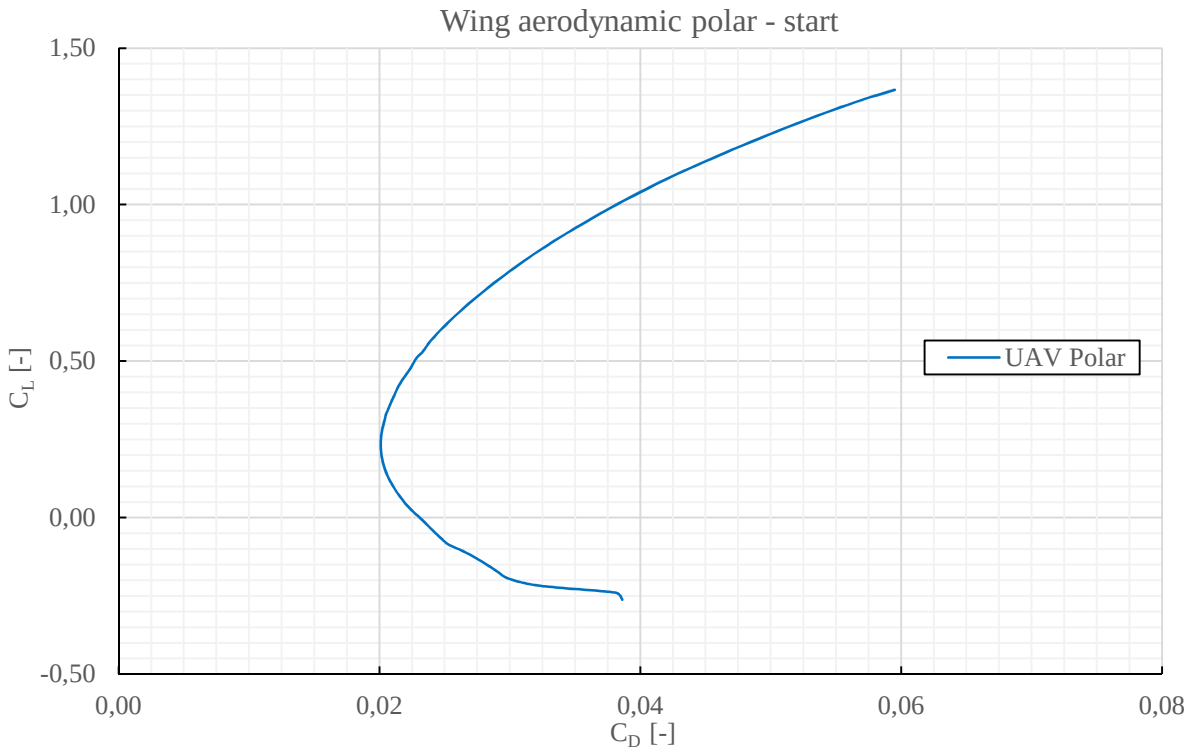

Fig. A3.1 UAV Polar graph for start (with ground effect at h=0,25 m)

A.4 Flight performance data

Flight speed V [m/s]	Flight speed V [km/h]	Usable thrust (ρ=1,113 kg/m^3) F_U [N]	Usable thrust (ρ=1,225 kg/m^3) F_U [N]
0,000	0,000	18,017	19,830
1,051	3,784	17,987	19,797
2,067	7,440	17,950	19,756
3,121	11,236	17,887	19,687
4,135	14,884	17,809	19,602
5,199	18,715	17,704	19,485
6,271	22,577	17,564	19,331
7,317	26,342	17,366	19,113
8,405	30,259	17,109	18,831
9,477	34,116	16,815	18,507
10,586	38,111	16,444	18,099
11,715	42,174	16,046	17,660
12,821	46,157	15,612	17,183
14,005	50,417	15,140	16,664
15,210	54,754	14,617	16,088
16,472	59,301	14,058	15,472
17,788	64,035	13,509	14,869
19,179	69,045	12,939	14,241
20,669	74,407	12,372	13,617
22,199	79,916	11,761	12,944
23,786	85,630	11,149	12,271
27,606	99,381	9,933	10,932
28,582	102,895	9,367	10,310
29,564	106,430	8,821	9,709
30,532	109,914	8,290	9,124
31,433	113,157	7,785	8,568
32,236	116,050	7,332	8,070
33,157	119,364	6,838	7,526
33,981	122,333	6,372	7,013
34,846	125,446	5,902	6,496
35,670	128,411	5,445	5,993
36,133	130,080	5,068	5,578
37,348	134,451	4,518	4,973
38,179	137,445	4,063	4,472
39,015	140,454	3,607	3,970
39,836	143,408	3,159	3,477
40,687	146,474	2,688	2,958
41,519	149,468	2,223	2,447
42,382	152,576	1,733	1,907
43,254	155,714	1,225	1,349
44,142	158,912	0,707	0,778
44,999	161,996	0,191	0,211

Tab. A4.1 Usable thrust data

Flight speed V [m/s]	Required thrust (ρ=1,113 kg/m^3, m = 9,5 kg) F_R [N]	Flight speed V [m/s]	Required thrust (ρ=1,113 kg/m^3, m = 9,5 kg) F_R [N]
10,630	7,437	14,570	4,580
10,697	7,360	14,739	4,543
10,765	7,059	14,914	4,508
10,834	6,862	15,095	4,475
10,905	6,713	15,283	4,445
10,976	6,588	15,478	4,415
11,050	6,478	15,680	4,388
11,125	6,378	15,891	4,364
11,201	6,286	16,110	4,342
11,279	6,201	16,338	4,323
11,358	6,121	16,577	4,307
11,439	6,045	16,826	4,295
11,522	5,973	17,087	4,287
11,607	5,903	17,360	4,284
11,693	5,836	17,647	4,286
11,781	5,769	17,949	4,297
11,872	5,705	18,267	4,314
11,964	5,641	18,601	4,339
12,059	5,579	18,954	4,373
12,155	5,518	19,328	4,415
12,254	5,458	19,726	4,469
12,356	5,400	20,152	4,517
12,460	5,342	20,609	4,594
12,566	5,285	21,087	4,672
12,676	5,230	21,610	4,766
12,788	5,176	22,180	4,884
12,903	5,123	22,788	5,025
13,021	5,070	23,440	5,175
13,142	5,019	24,152	5,227
13,267	4,969	24,941	5,570
13,395	4,921	25,811	5,852
13,527	4,874	26,779	6,181
13,662	4,828	27,864	6,579
13,802	4,783	29,092	7,067
13,946	4,740	30,497	7,672
14,095	4,698	32,128	8,421
14,248	4,658	34,051	9,361
14,406	4,618	36,366	10,574

Tab. A4.2 Required thrust data

Flight speed V [m/s]	Flight speed V [km/h]	Usable power (ρ=1,113 kg/m^3) P_U [N]	Usable power (ρ=1,225 kg/m^3) P_U [N]
0,000	0,000	0,000	0,000
1,051	3,784	18,906	20,808
2,067	7,440	37,097	40,830
3,121	11,236	55,827	61,444
4,135	14,884	73,635	81,044
5,199	18,715	92,036	101,298
6,271	22,577	110,147	121,231
7,317	26,342	127,069	139,856
8,405	30,259	143,810	158,281
9,477	34,116	159,354	175,389
10,586	38,111	174,086	191,604
11,715	42,174	187,975	206,891
12,821	46,157	200,171	220,314
14,005	50,417	212,038	233,375
15,210	54,754	222,313	244,684
16,472	59,301	231,564	254,867
17,788	64,035	240,296	264,477
19,179	69,045	248,167	273,139
20,669	74,407	255,707	281,438
22,199	79,916	261,072	287,343
23,786	85,630	265,188	291,873
27,606	99,381	274,206	301,799
28,582	102,895	267,727	294,668
29,564	106,430	260,793	287,036
30,532	109,914	253,109	278,579
31,433	113,157	244,687	269,310
32,236	116,050	236,370	260,156
33,157	119,364	226,735	249,551
33,981	122,333	216,534	238,323
34,846	125,446	205,651	226,345
35,670	128,411	194,209	213,752
36,133	130,080	183,109	201,535
37,348	134,451	168,752	185,733
38,179	137,445	155,128	170,739
39,015	140,454	140,735	154,897
39,836	143,408	125,827	138,488
40,687	146,474	109,357	120,361
41,519	149,468	92,316	101,605
42,382	152,576	73,450	80,841
43,254	155,714	53,007	58,341
44,142	158,912	31,217	34,358
44,999	161,996	8,615	9,482

Tab. A4.3 Usable power data

Flight speed V [m/s]	Required power (ρ=1,113 kg/m^3, m = 9,5 kg) P_R [W]	Flight speed V [m/s]	Required power (ρ=1,113 kg/m^3, m = 9,5 kg) P_R [W]
10,630	79,058	14,570	66,731
10,697	78,730	14,739	66,961
10,765	75,992	14,914	67,238
10,834	74,339	15,095	67,554
10,905	73,206	15,283	67,924
10,976	72,310	15,478	68,334
11,050	71,575	15,680	68,807
11,125	70,952	15,891	69,340
11,201	70,413	16,110	69,945
11,279	69,939	16,338	70,623
11,358	69,522	16,577	71,391
11,439	69,153	16,826	72,265
11,522	68,820	17,087	73,244
11,607	68,518	17,360	74,363
11,693	68,235	17,647	75,636
11,781	67,971	17,949	77,117
11,872	67,726	18,267	78,811
11,964	67,492	18,601	80,717
12,059	67,278	18,954	82,880
12,155	67,074	19,328	85,341
12,254	66,887	19,726	88,157
12,356	66,718	20,152	91,029
12,460	66,557	20,609	94,685
12,566	66,419	21,087	98,527
12,676	66,292	21,610	102,993
12,788	66,185	22,180	108,319
12,903	66,095	22,788	114,510
13,021	66,019	23,440	121,291
13,142	65,965	24,152	126,245
13,267	65,927	24,941	138,922
13,395	65,916	25,811	151,056
13,527	65,925	26,779	165,517
13,662	65,958	27,864	183,317
13,802	66,018	29,092	205,600
13,946	66,100	30,497	233,970
14,095	66,214	32,128	270,564
14,248	66,360	34,051	318,743
14,406	66,526	36,366	384,515

Tab. A4.4 Required power data

Flight speed V [m/s]	Climb speed (ρ=1,113 kg/m^3, m = 9,5 kg) w [m/s]	Flight speed V [m/s]	Climb speed (ρ=1,113 kg/m^3, m = 9,5 kg) w [m/s]
11,000	1,122	21,000	1,763
11,500	1,212	21,500	1,735
12,000	1,296	22,000	1,702
12,500	1,372	22,500	1,663
13,000	1,442	23,000	1,618
13,500	1,506	23,500	1,568
14,000	1,564	24,000	1,511
14,500	1,615	24,500	1,449
15,000	1,661	25,000	1,380
15,500	1,700	25,500	1,305
16,000	1,734	26,000	1,224
16,500	1,762	26,500	1,137
17,000	1,784	27,000	1,042
17,500	1,801	27,500	0,941
18,000	1,812	28,000	0,833
18,500	1,817	28,500	0,717
19,000	1,818	29,000	0,595
19,500	1,812	29,500	0,464
20,000	1,801	30,000	0,326
20,500	1,785	30,500	0,180

Tab. A4.5 Climb speed data

Flight speed V [m/s]	Climb angle (ρ=1,113 kg/m^3, m = 9,5 kg) γ [˚]	Flight speed V [m/s]	Climb angle (ρ=1,113 kg/m^3, m = 9,5 kg) γ [˚]
11,000	5,855	21,000	4,815
11,500	6,051	21,500	4,629
12,000	6,198	22,000	4,436
12,500	6,302	22,500	4,238
13,000	6,370	23,000	4,034
13,500	6,405	23,500	3,825
14,000	6,413	24,000	3,610
14,500	6,395	24,500	3,390
15,000	6,356	25,000	3,165
15,500	6,297	25,500	2,935
16,000	6,221	26,000	2,699
16,500	6,129	26,500	2,458
17,000	6,024	27,000	2,212
17,500	5,906	27,500	1,961
18,000	5,777	28,000	1,705
18,500	5,638	28,500	1,443
19,000	5,489	29,000	1,175
19,500	5,332	29,500	0,902
20,000	5,167	30,000	0,623
20,500	4,994	30,500	0,338

Tab. A4.6 Climb angle data

Structural limit turns			
Flight speed V [m/s]	Maximum bank angle Φ^{S}_{max} [°]	Minimum turn radius r^{S}_{min} [m]	Minimum time to perform 360˚ turn t^{S}_{min} [s]
11,000	75,522	3,186	1,820
11,500	75,522	3,482	1,902
12,000	75,522	3,791	1,985
12,500	75,522	4,114	2,068
13,000	75,522	4,450	2,151
13,500	75,522	4,798	2,233
14,000	75,522	5,160	2,316
14,500	75,522	5,536	2,399
15,000	75,522	5,924	2,481
15,500	75,522	6,326	2,564
16,000	75,522	6,740	2,647
16,500	75,522	7,168	2,730
17,000	75,522	7,609	2,812
17,500	75,522	8,063	2,895
18,000	75,522	8,531	2,978
18,500	75,522	9,011	3,060
19,000	75,522	9,505	3,143
19,500	75,522	10,012	3,226
20,000	75,522	10,532	3,309
20,500	75,522	11,065	3,391
21,000	75,522	11,611	3,474
21,500	75,522	12,171	3,557
22,000	75,522	12,743	3,639
22,500	75,522	13,329	3,722
23,000	75,522	13,928	3,805
23,500	75,522	14,540	3,888
24,000	75,522	15,165	3,970
24,500	75,522	15,804	4,053
25,000	75,522	16,456	4,136
25,500	75,522	17,120	4,218
26,000	75,522	17,798	4,301
26,500	75,522	18,490	4,384
27,000	75,522	19,194	4,467
27,500	75,522	19,911	4,549
28,000	75,522	20,642	4,632
28,500	75,522	21,386	4,715
29,000	75,522	22,143	4,797
29,500	75,522	22,913	4,880
30,000	75,522	23,696	4,963
30,500	75,522	24,493	5,046

Tab. A4.7 Structural limit turns data

Aerodynamical limit turns			
Flight speed V [m/s]	Maximum bank angle Φ^{A}_{max} [°]	Minimum turn radius r^{A}_{min} [m]	Minimum time to perform 360˚ turn t^{A}_{min} [s]
11,000	12,233	56,910	32,507
11,500	26,599	26,931	14,714
12,000	34,795	21,131	11,064
12,500	40,816	18,448	9,273
13,000	45,596	16,879	8,158
13,500	49,545	15,847	7,376
14,000	52,891	15,120	6,786
14,500	55,775	14,584	6,319
15,000	58,294	14,174	5,937
15,500	60,514	13,853	5,615
16,000	62,489	13,596	5,339
16,500	64,256	13,387	5,098
17,000	65,847	13,215	4,884
17,500	67,286	13,072	4,693
18,000	68,594	12,952	4,521
18,500	69,787	12,850	4,364
19,000	70,879	12,763	4,220
19,500	71,881	12,688	4,088
20,000	72,805	12,623	3,966
20,500	73,657	12,566	3,851
21,000	74,446	12,517	3,745
21,500	75,178	12,473	3,645
22,000	75,858	12,435	3,552
22,500	76,492	12,401	3,463
23,000	77,083	12,371	3,380
23,500	77,636	12,345	3,301
24,000	78,153	12,321	3,226
24,500	78,638	12,299	3,154
25,000	79,094	12,280	3,086
25,500	79,522	12,263	3,022
26,000	79,925	12,247	2,960
26,500	80,306	12,233	2,900
27,000	80,665	12,220	2,844
27,500	81,004	12,209	2,789
28,000	81,325	12,198	2,737
28,500	81,629	12,188	2,687
29,000	81,917	12,179	2,639
29,500	82,190	12,171	2,592
30,000	82,450	12,164	2,548
30,500	82,697	12,157	2,504

Tab. A4.8 Aerodynamical limit turns data

Propulsion limit turns			
Flight speed V [m/s]	Maximum bank angle Φ^{F}_{max} [°]	Minimum turn radius r^{F}_{min} [m]	Minimum time to perform 360˚ turn t^{F}_{min} [s]
15,552	62,518	12,829	5,183
16,020	63,523	13,035	5,112
16,415	64,176	13,297	5,090
16,968	64,908	13,748	5,091
17,510	65,487	14,257	5,116
18,057	65,973	14,822	5,157
18,619	66,397	15,446	5,212
19,005	66,653	15,898	5,256
19,603	66,996	16,636	5,332
20,015	67,198	17,173	5,391
20,653	67,458	18,054	5,493
21,094	67,603	18,699	5,570
21,545	67,718	19,396	5,656
22,008	67,805	20,151	5,753
22,483	67,861	20,972	5,861
22,968	67,878	21,867	5,982
23,466	67,859	22,848	6,118
23,972	67,789	23,926	6,271
24,488	67,668	25,119	6,445
25,009	67,479	26,445	6,644
25,534	67,213	27,929	6,873
26,059	66,852	29,604	7,138
26,580	66,376	31,510	7,449
27,083	65,741	33,707	7,820
27,571	64,925	36,269	8,265
28,047	63,905	39,289	8,802
28,502	62,621	42,900	9,457
28,948	61,014	47,339	10,275
29,545	57,656	56,367	11,987
30,053	52,531	70,591	14,758
30,533	39,718	114,433	23,548

Tab. A4.9 Propulsion limit turns data

A.5 3 view drawing

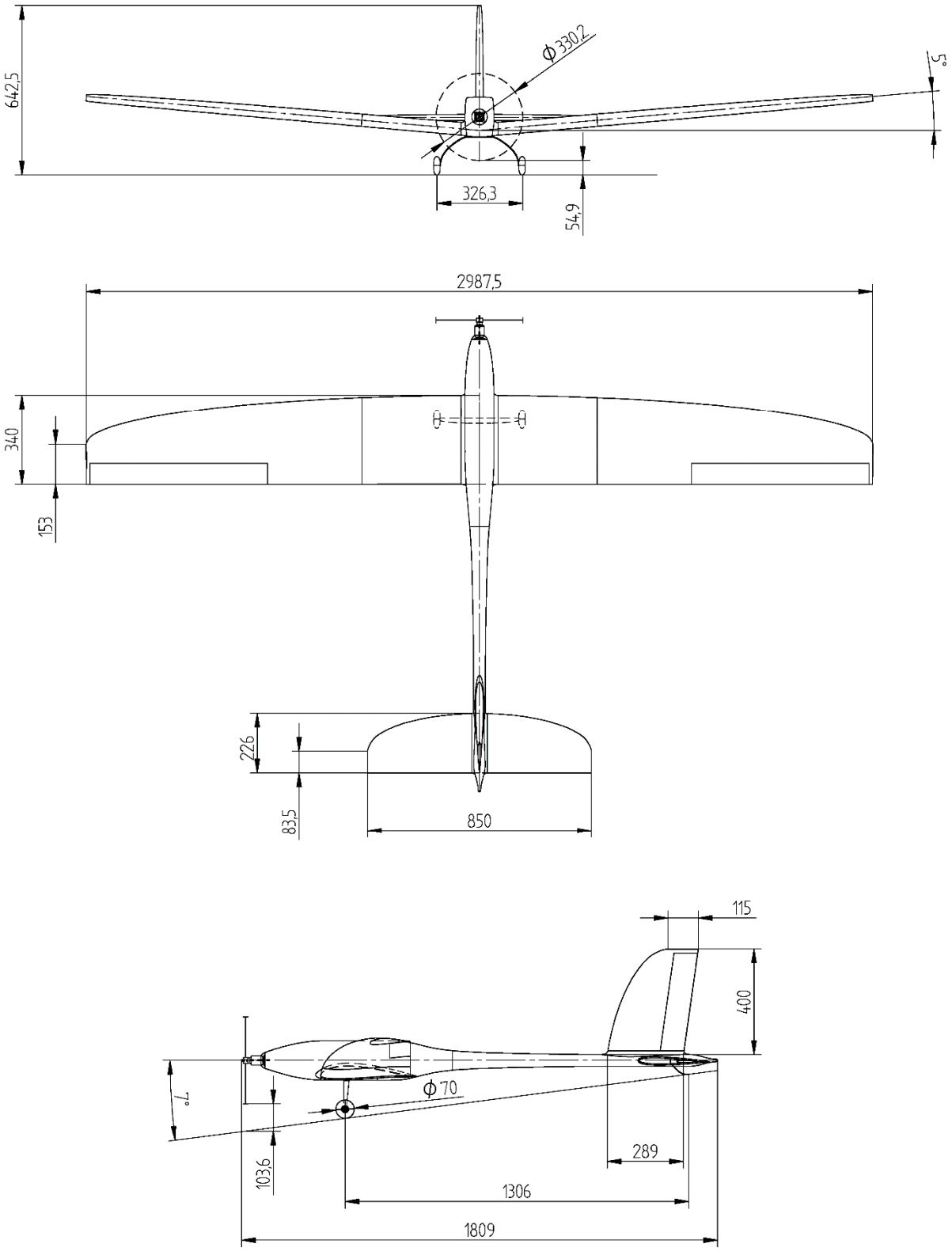

Fig. A5.1 3 view drawing of FabricK UAV

A.6 Contents of CD with electronic form of bachelor’s thesis

1) PDF version of bachelor’s thesis

2) CAD model of FabricK UAV

3) Simulation file of XFLR5 Software